On the Performance Analysis of Cooperative Vehicular Communication

by

Mohamed Fathy Mohamed Feteiha

A thesis
presented to the University of Waterloo
in fulfillment of the
thesis requirement for the degree of
Doctor of Philosophy
in
Electrical and Computer Engineering

Waterloo, Ontario, Canada, 2012

I hereby declare that I am the sole author of this thesis. This is a true copy of the thesis, including any required final revisions, as accepted by my examiners.

I understand that my thesis may be made electronically available to the public.

Abstract

Vehicular networking is envisioned to be a key technology area for significant growth in the coming years. Although the expectations for this emerging technology are set very high, many practical aspects remain still unsolved for a vast deployment of vehicular networks. This dissertation addresses the enabling physical layer techniques to meet the challenges in vehicular networks operating in mobile wireless environments. Considering the infrastructure-less nature of vehicular networks, we envision *cooperative diversity* well-positioned to meet the demanding requirements of vehicular networks with their underlying distributed structure.

Cooperative diversity has been proposed as a powerful means to enhance the performance of high-rate communications over wireless fading channels. It realizes spatial diversity advantages in a distributed manner where a node uses others antennas to relay its message creating a virtual antenna array. Although cooperative diversity has garnered much attention recently, it has not yet been fully explored in the context of vehicular networks considering the unique characteristics of vehicular networks, this dissertation provides an error performance analysis study of cooperative transmission schemes for various deployment and traffic scenarios.

In the first part of this dissertation, we investigate the performance of a cooperative vehicle-to-vehicle (V2V) system with amplify-and-forward relaying for typical traffic scenarios under city/urban settings and a highway area. We derive pairwise error probability (PEP) expressions and demonstrate the achievable diversity gains. The effect of imperfect channel state information (CSI) is also studied through an asymptotical PEP analysis. We present Monte-Carlo simulations to confirm the analytical derivations and present the error rate performance of the vehicular scheme with perfect and imperfect-CSI.

In the second part, we consider road-to-vehicle (R2V) communications in which roadside access points use cooperating vehicles as relaying terminals. Under the assumption of decode-and-forward relaying, we derive PEP expressions for single-relay and multi-relay scenarios.

In the third part, we consider a cooperative multi-hop V2V system in which direct transmission is not possible and investigate its performance through the PEP derivation and diversity gain analysis. Monte-Carlo simulations are further provided to confirm the analytical derivations and provide insight into the error rate performance improvement.

Acknowledgements

I am thankful to ALLAH, the most merciful and most compassionate for blessing me with the strength to seek knowledge and complete this work.

I would like to express my deepest gratitude to my adviser, prof. Murat Uysal, who has provided me with a continuous support, assistance, and motivation. I am grateful for his insightful suggestions, valuable discussions and advices. My sincere thankfulness to prof. Mohamed Oussama Damen for his precious guidance and suggestions. It is my pleasure to thank my doctoral thesis committee members prof. Weihua Zhuang, prof. Guang Gong, prof. Sarbast Rasheed and prof. Kemal Tepe for taking the time to evaluate and examin my research work and provide me with their magnificent feedback and suggestions.

I am very thankful to my research group colleagues for their valuable help and useful discussions during my PhD study especially, Suhail Al-Dharrab, Dr. Salama Ikki and Dr. Walid Abediseid. Special "thank you" to Dr. Osama Amin my dear brother, friend and colleague for providing me with his appreciable knowledge and support from day "one" of my PhD journey.

A special recognition for the Egyptian Ministry of Higher Education, Egyptian Cultural and Educational Bureau in Canada, and the "City of Scientific Researches and Technological Applications" in Egypt for offering me this PhD scholarship.

Dedication

To my wife Eman, my two baby boys Eyad and Aser, and my parents Fathy and Nadia.

Table of Contents

List of Tables

List of Figures

List of Notations

$\lvert . \rvert$	Absolute value
$\mathbb{E}\left[. \right]$	Expectation
$\otimes$	Kronecker product
$(.)^{\mathrm{T}}$	Transpose
$(.)^{*}$	Conjugate
$(.)^{\mathrm{H}}$	Hermitian operations
$\mathrm{tr}\left(. \right)$	Trace of a square matrix
$\lceil . \rceil$	Integer ceil
$\lfloor . \rfloor$	Integer floor
$[\mathbf{H}]_{k,m}$	The $(k,m)^{\mathrm{th}}$ entry of matrix $\mathbf{H}$
$\mathbf{I}_N$	$N \times N$-size identity matrix
$\mathbf{1}$	All-ones matrix with proper dimensions
$\mathbf{0}$	All-zeros matrix with proper dimensions
σ^2	Channel variance
$G_{(.)}$	Relative geometrical gains
$\mathcal{M}_{(.)}$	STBC matrix
γ	Signal-to-noise ratio (SNR)

$F(.)$	Cumulative distribution function (CDF) for a given random variable
$f(.)$	Probability density function (pdf) for a given random variable
Bold	letters denote the matrices and vectors

List of Abbreviations

AF	Amplify-and-forward
AWGN	Additive white Gaussian noise
BEM	Basis Expansion Model
BER	Bit-error rate
C-CE	Cascaded channel estimation
CDF	Cumulative distribution function
CSI	Channel state information
D-CE	Disintegrated channel estimation
DF	Decode-and-forward
DPS	Digital phase sweeping
FFT	Fast Fourier transform
GPS	Global positioning system
IBI	Inter-block interference
I-CSI	Imperfect channel state information
IFFT	Inverse fast Fourier transform
i.i.d	Independent identically distributed
i.n.i.d	Independent non-identically distributed

ISI	Inter-symbol interference
ITS	Intelligent transportation system
IVC	Inter-vehicular communications
LOS	Line-of-sight
LTV	Linear time variant filter
MIMO	Multiple-input multiple-output
ML	Maximum likelihood
MMSE	Minimum mean square estimation
M-QAM	M-ary quadrature amplitude modulation
OFDM	Orthogonal frequency division multiplexing
PACE	Pilot assisted channel estimation
P-CSI	Perfect channel state information
pdf	Probability density function
PEP	Pairwise error probability
PSD	Power spectral density
QoS	Quality of Service
R2V	Road-to-vehicle
RD	Receive diversity protocol
SIMO	Single-input multiple-output
SISO	Single-input single-output
SNR	Signal-to-noise ratio
STBC	Space-time block coding

STD	Simplified transmit diversity protocol
TD	Transmit diversity protocol
TDMA	Time division multiple access
V2R	Vehicle-to-road
V2V	Vehicle-to-vehicle
VAA	virtual antenna array
VANET	Vehicular ad-hoc networks
WAVE	Wireless access in vehicular environments

Chapter 1

Introduction

Intelligent transportation systems (ITSs) [1] involve the application of advanced information processing, communications, sensor, and control technologies in an integrated manner to improve the functioning of the transportation system. Vehicular ad-hoc networks (VANETs) are a crucial component of the ITSs and involve vehicle-to-vehicle (V2V) and vehicle-to-road (V2R) communications [2] enabling a vehicle to communicate with other vehicles and sensors/access-points installed along the road.

The introduction of on-board sensor systems in vehicles and the progressive diffusion of on-board localization systems (e.g., global positioning system (GPS)) along with the investment for roadside access points in various countries make vehicular networking suitable for the development of various applications. Most of the applications aim to help improve road traffic safety and efficiency. These provide drivers with timely information on road and traffic conditions including collisions, incidents, congestion, etc., thereby substantially improve the comfort of daily road travel. Besides these main navigation safety functionalities, potential in-vehicle "infotainment" applications (i.e., information + entertainment) have

recently emerged including audio/video streaming, high-speed internet access, cooperative downloading, multiplayer gaming, mobile commerce and roadside advertising [2, 3].

Major research projects in North America, Europe and Japan such as ADAS and European CarTALK2000 [4–6], FleetNet [4], the Japanese AHS and ASV [6], the USA VSC and VII [6], and the Canadian-USA ATLANTIC [6], have been investigating this emerging topic. Standardization of vehicular communications is also underway by major standardization bodies such as IEEE, IETF, ETSI, ISO, SAE, ASTM. For example, in 2010, the IEEE introduced the 802.11p standard known as *Wireless Access in Vehicular Environments (WAVE)*. This standard focuses on physical and link layers to provide the required robustness for vehicular communications. On the other hand, the ISO developed a set of standards referred to as *Continuous Air-Interface for Long Medium Range Telecommunications (CALM)*. The CALM standard builds on the idea that future vehicles will be equipped with more than one wireless technology. It offers a set of protocol standards that will allow routing data over the available wireless technology at that time, based upon the QoS requirements for the deployed application and the real-time performance of the available communications media [2, 7, 8].

The current literature in VANETs has mainly focused on networking aspects, but has not yet fully explored physical layer issues which inherently differ from well-studied traditional cellular or wireless local area network (WLAN) applications. The main challenge facing the deployment of VANETs indeed manifests itself in their main advantage, i.e., the lack of infrastructure. This makes the recently proposed cooperative transmission [9] an ideal physical layer solution for vehicular networks. In the following, we first summarize the concept of cooperative transmission. Then, we provide an overview of the vehicular fading channels and discuss the available literature on *cooperative vehicular* transmission.

1.1 Cooperative Communication

Diversity techniques are of crucial importance in wireless communication systems to ensure a reliable performance on fading channels. Diversity techniques involve the transmission of multiple replicas of the same information signal over independent fading channels. Diversity can be mainly obtained through time, frequency, and/or spatial dimensions. In the last decade, spatial diversity that involves the deployment of multiple antennas has received much attention. Multiple-Input-Multiple-Output (MIMO) communication systems lead to improvements in link reliability and/or spectral efficiency (see e.g., [10–15]). With their appealing features, they have already become a part of the wireless standards. Unfortunately, the use of multiple antennas might not be practical at mobile devices due to size and power constraints. This limitation motivates the concept of cooperative diversity where nodes help each other relay each others message.

Cooperative diversity [16–20] exploits the broadcast nature of wireless transmission and creates a virtual (distributed) antenna array through cooperating nodes to extract spatial diversity. The source node and its nearby relaying nodes share their antennas and send the same message through independent fading paths. Based on the relaying mode, cooperative transmission can be categorized into two main groups [16, 17]. The first one is *amplify-and-forward* (AF) relaying which is also known as non-regenerative relaying. In this type of relaying, relay node receives an attenuated version of the transmitted signal and retransmits it after scaling the received signal to meet the average power constraint. On the other hand, in *decode-and-forward* (DF) relaying, the relay needs to first detect the signal and then re-encodes it for transmission to the destination. This type of relaying is also known as regenerative relaying.

Either AF or DF relaying can be combined with various cooperation protocols. In their pioneering work [17], Laneman et al. consider a multi-relay cooperation scenario where the source signal is transmitted to a destination terminal through a number of half-duplex terminals and demonstrate that the receiver achieves full spatial diversity. Their proposed user cooperation protocol is built upon a two-phase transmission scheme. In the first transmission phase (i.e., broadcasting phase), the source broadcasts to the destination and relay terminals. In the second transmission phase (i.e., relaying phase), the relays transmit processed version of their received signals to the destination using either orthogonal subchannels (repetition based cooperative diversity) or the same subchannel (space-time coded cooperative diversity).

Since in its introduction, cooperative diversity has attracted much attention within the academic and industrial circles for various applications and there has been already a rich literature on the cooperative diversity techniques. The current results, however, are not directly applicable to vehicular networks due to their underlying assumption of quasi-static Rayleigh fading channel model. Rayleigh distribution is commonly used to characterize the envelope of a fading signal in cellular radio systems. This statistical model typically assumes a wireless communication scenario with a stationary base station antenna above roof-top level and a mobile station at street level. On the other hand, in V2V communication systems, both the transmitter and receiver are in motion and their antennas are relatively at lower elevations invalidating the quasi-static Rayleigh fading assumption. Realizing the full potentials of cooperative diversity in VANETs requires an in-depth investigation of performance limits under realistic vehicular channel models and development of enabling techniques to support broadband vehicular applications.

1.2 Overview of Vehicular Fading Channels

In this section, we introduce the theoretical material on understanding the vehicular channel models that will be used in the later parts of the dissertation. In an effort to emphasize the difference from the conventional models, we first summarize the commonly used Jakes model.

In wireless communication systems, the transmitted signals are subject to multipath propagation that results in variations of the received signal strength as a function of transceiver location and frequency. Due to reflection and refraction, the received signal is a superposition of the delayed, attenuated, and phase-shifted versions of the transmitted signal. These signals may add constructively or destructively, causing severe fluctuations in the received signal strength (with respect to its average power) known as fading.

If the transmitter and/or receiver are in motion, the effect of Doppler shift should be further taken into account. The Doppler shift is the amount of the change in the observed frequency due to the vehicles relative mobility. Ignoring the additive noise, the band-pass received signal can be written as [21]

$$\mathcal{Y}(t) = \mathrm{Re}\left\{ \sum_{n=1}^{\mathcal{N}(t)} \alpha_n(t)\, s_l(t - \tau_n(t))\, e^{j2\pi f_c (t-\tau_n(t))} \right\} \tag{1.1}$$

where $\mathcal{N}(t)$ is the number of resolvable multipath components, $\alpha_n(t)$ is the attenuation factor of the n^{th} path, $s_l(t)$ is the equivalent low-pass signal, $\tau_n(t)$ is the delay associated with the n^{th} path, and f_c is the carrier frequency. The impulse response of a linear time

variant filter (LTV) to model this channel can be therefore written as [21]

$$h(\tau,t)=\sum_{n=1}^{\mathcal{N}(t)}\alpha_n(t)\,e^{-j2\pi f_c\tau_n(t)}\delta(\tau-\tau_n(t)) \tag{1.2}$$

If the transmitter and/or receiver are in motion, the effect of Doppler shift should be further taken into account. This yield [22, 23]

$$\mathcal{Y}(t)=\mathrm{Re}\left\{\sum_{n=1}^{\mathcal{N}(t)}\alpha_n(t)\,s_l(t-\tau_n(t))\,e^{j(2\pi f_c+\omega_{D_n}(t))(t-\tau_n(t))}\right\} \tag{1.3}$$

or, equivalently, the impulse response as

$$h(\tau,t)=\sum_{n=1}^{\mathcal{N}(t)}\alpha_n(t)\,e^{j((\omega_{D_n}(t))(t-\tau_n(t))+2\pi f_c\tau_n(t))}\delta(\tau-\tau_n(t)) \tag{1.4}$$

In the above, $\omega_{D_n}(t)$ is the Doppler phase shift associated with the n^{th} path due to the mobility. It is given by

$$\omega_D(t)=2\pi f_D(t)=\frac{2\pi}{\lambda}v(t).\cos(\vartheta) \tag{1.5}$$

where ϑ is the angle of incidence of the signal on the vehicle, $v(t)$ is the vehicle velocity, λ is the wavelength of the carrier, and $f_D(t)$ is the Doppler shift. The difference between the Doppler shifts in various signal components (contributing to a single fading channel tap) forms the Doppler spread of the channel and is given by $f_d=1/T_d$, where T_d is the coherence time of the channel.

The well known Jakes model assumes an isotropic rich scattering around the mobile

receiver antenna and builds upon a *single-ring model* (see Figure 1.1). In this model, the angles of arrival ϑ of the waves arriving at the receiving antenna are uniformly distributed in the interval of $[-\pi, \pi)$. This single ring model is generally used for cellular systems that typically involve a stationary base station antenna above roof-top level unobstructed by the local scatterers.

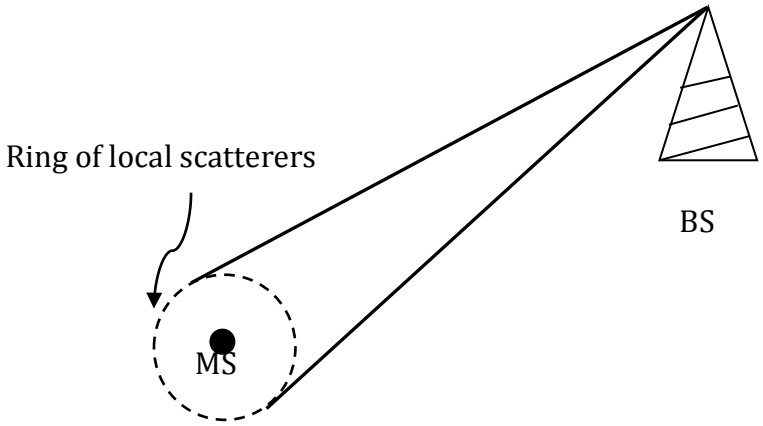

Figure 1.1: The single ring model.

In highly scattered areas, there are a large number of paths along with the absence of a dominating line-of-sight (LOS) path. Central Limit Theorem suggests that the complex fading coefficient can be modeled as zero-mean complex Gaussian. Therefore, the envelope of the channel follows a Rayleigh distribution while the phase is uniformly distributed [21,24,25]. Under the well-known Jakes model, the channel autocorrelation function follows [22]

$$C(\tau) = \sigma^2 J_0(2\pi f_{D_m} \tau) \tag{1.6}$$

where $J_0(.)$ is the zero order Bessel function, σ^2 is the channel variance, and f_{D_m} is the maximum Doppler shift. The corresponding normalized Doppler power spectral density

(PSD), illustrated in Figure 1.2, is given by

$$S(f) = \sigma^2 \left(\pi f_{D_m} \sqrt{1 - (f/f_{D_m})^2} \right)^{-1} \tag{1.7}$$

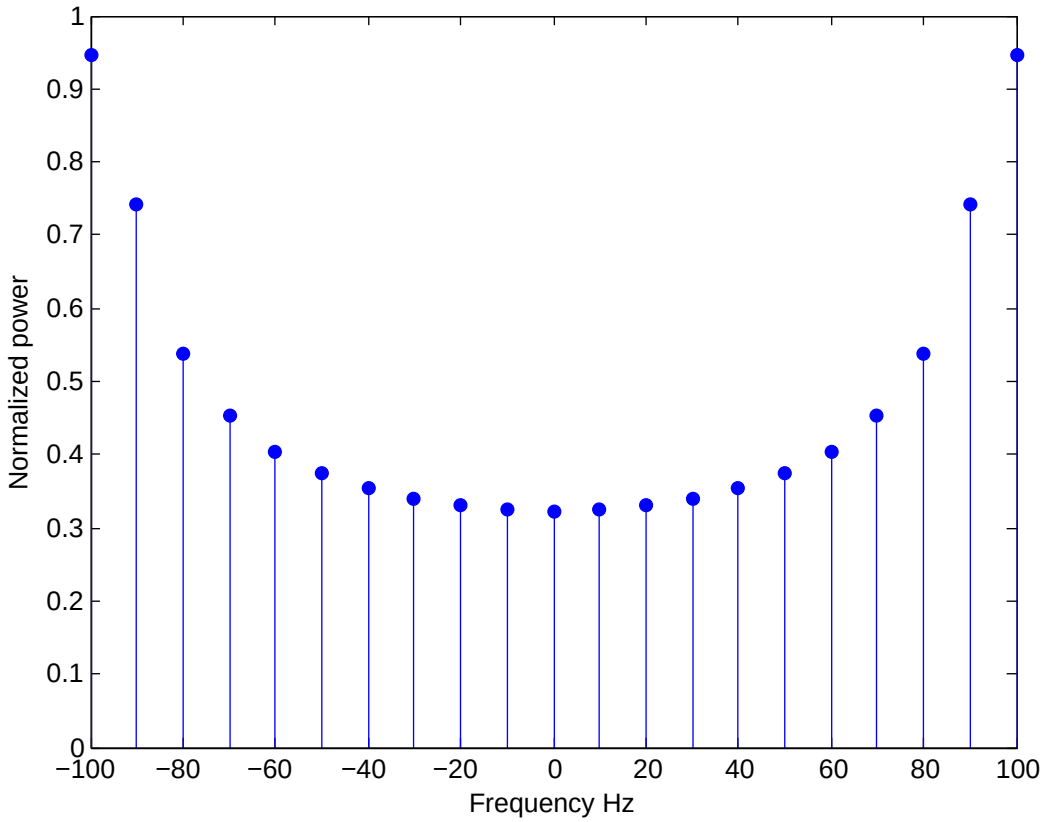

Figure 1.2: Jakes Doppler PSD ($f_{D_m} = 100$Hz).

In contrast to a cellular scenario, the inter-vehicular communication (IVC) has both transmitter and receiver antennas close to the ground level (1.5-2.5m), and mostly dynamic with random speed and variation. This requires considering the local scattering around both transmitters and receivers.

In [26], Akki and Haber consider a scattering model surrounding the mobile terminals with omni-directional antennas. They assume that two communicating terminals moving with velocities v_1 and v_2. For this double-mobility scenario, each path will be subject to separate Doppler shifts yielding to the impulse response [23, 26]

$$h(\tau,t)=\sum_{n=1}^{\mathcal{N}(t)}\alpha_n(t)\,e^{j((\omega_{D1_n}(t)+\omega_{D2_n}(t))(t-\tau_n(t))+2\pi f_c\tau_n(t))}\delta(\tau-\tau_n(t)) \tag{1.8}$$

where $\omega_{D1_n}(t)$ and $\omega_{D2_n}(t)$ are the Doppler phase shifts introduced by the two mobile vehicles. Here, the delay term can be expressed as

$$\tau_n(t)=\tau_i+\delta_{\tau_n}(t) \tag{1.9}$$

where τ_i is the mean value of multipath time delay, $\delta_{\tau_n}(t)$ is the time delay difference for the n^{th} path measured from that mean value. We can then express (1.9) as

$$h(\tau,t)=\sum_{n=1}^{\mathcal{N}(t)}\alpha_n(t)\,e^{j((\omega_{D1_n}(t)+\omega_{D2_n}(t))(t-\tau_i)+2\pi f_c\tau_i+\phi_n)}\delta(\tau-\tau_i-\delta_{\tau_n}(t)) \tag{1.10}$$

in (1.10), $\phi_n=(2\pi f_c+\omega_{D1_n}(t)+\omega_{D2_n}(t))\,\delta_{\tau_n}(t)$ is uniformly distributed in $[0,2\pi)$. The time correlation function is given by

$$C(\Delta t)=\sigma^2 J_0\left(\frac{2\pi}{\lambda}v_2\Delta t\right)J_0\left(\frac{2\pi}{\lambda}v_1\Delta t\right) \tag{1.11}$$

with t_1 and t_2 refer to the two different time instants, we have $\Delta t=t_2-t_1$. The power spectrum of the complex envelope is given by (see Figure 1.3)

$$S(f) = \frac{\sigma^2}{\pi^2 f_{D1_m}\sqrt{\eta}} \mathrm{K}\left[\frac{(1+\eta)}{2\sqrt{\eta}}\sqrt{1-\left(\frac{f}{(1+\eta)\, f_{D1_m}}\right)^2}\right] \tag{1.12}$$

where $\eta = v_2/v_1$, and f_{D1_m} is the maximum Doppler shift due to the motion of the transmitter, and $\mathrm{K}[.]$ is the complete elliptic integral of the first kind. For $\eta = 0$ (i.e., $v_2 = 0$), the power spectrum and time correlation functions reduce back to Jakes model.

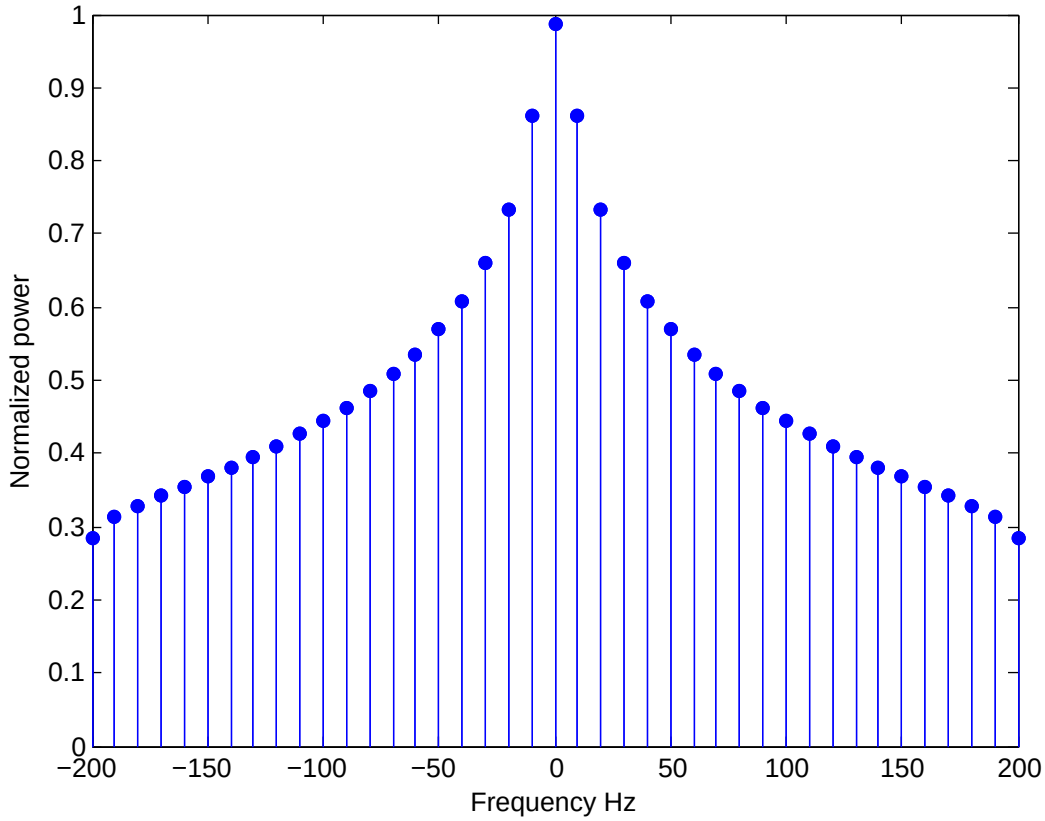

Figure 1.3: Akki and Habers Doppler PSD ($\eta = 1$).

In [23], Patel et al. introduce the *double-ring model* which assumes uniformly distributed ring of local scatterers over two rings around the mobile terminals (See Figure 1.4). In such a model, a sufficiently large distance exists that allows each of them to be

independently surrounded by different rings of local scatterers [27]. Under frequency-flat assumption, the impulse response of the LTV filter for this channel model

$$h(\tau, t) = \sum_{n=1}^{\mathcal{N}(t)} \sum_{m=1}^{\mathcal{M}(t)} \alpha_{nm}(t)\, e^{j((\omega_{D1nm}(t)+\omega_{D2nm}(t))t+\phi_{nm})} \delta(\tau) \tag{1.13}$$

where $\mathcal{N}(t)$ is the number of resolvable multipath components due to the scatterers located in the transmitter ring and $\mathcal{M}(t)$ is the number of resolvable multipath components due to the scatterers located in the receiver ring.

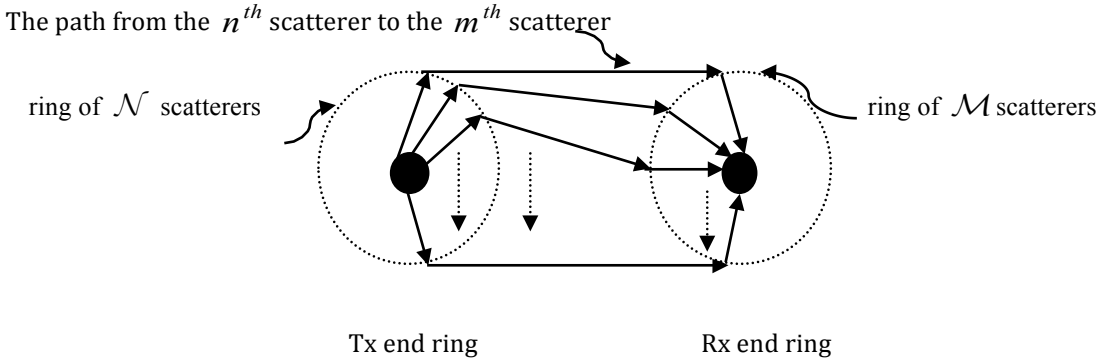

Figure 1.4: The double ring model.

A general form shown in Figure 1.5, to introduce the scatterers and mobility order is further introduced in [28, 29]

$$H = \mathcal{C} + H_1 + \alpha H_2 H_3 + \beta H_4 H_5 H_6 + \ldots \tag{1.14}$$

where H is the cumulative transfer function after multiple layers of scattering, $\mathcal{C}$ is the Rician factor, and H_i with $i = 1, 2, ...$ are complex, independent Gaussian fading processes. This model includes single-Rayleigh and cascaded-Rayleigh [27, 29–31] fading as special cases.

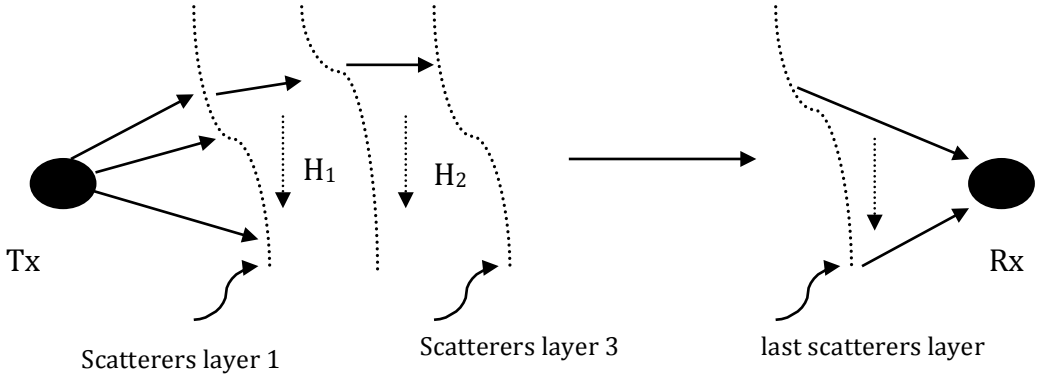

Figure 1.5: Multiple scattering layers.

In [29], Andersen proposes the so-called cascaded *(double) Rayleigh-double Doppler* model where the channel complex envelope is given by

$$h(t) = \sum_{n=1}^{\mathcal{N}(t)} \alpha_n(t)\, e^{j((\omega_{D1_n}(t))t+\phi_n)} \sum_{m=1}^{\mathcal{M}(t)} \alpha_m(t)\, e^{j((\omega_{D2_m}(t))t+\phi_m)} \tag{1.15}$$

This model can be justified in a scenario as illustrated in Figure 1.6. Here, two Dopplers are due to the dual mobility, while the double Rayleigh assumption is due to the fact that different independent scatterers independently surround the two mobile terminals. This differs from the double-ring model in the sense that the distance between the two scatterers rings is much larger than the radius of the ring [27].

If there are common scatterers around both of the two mobile terminals (See Figure 1.7), the corresponding channel model is known as *single Rayleigh-double Doppler* model and the channel complex envelope is given by [26]

$$h(t) = \sum_{n=1}^{\mathcal{N}(t)} \alpha_n(t)\, e^{j((\omega_{D1_n}(t)+\omega_{D2_n}(t))t+\phi_n)} \tag{1.16}$$

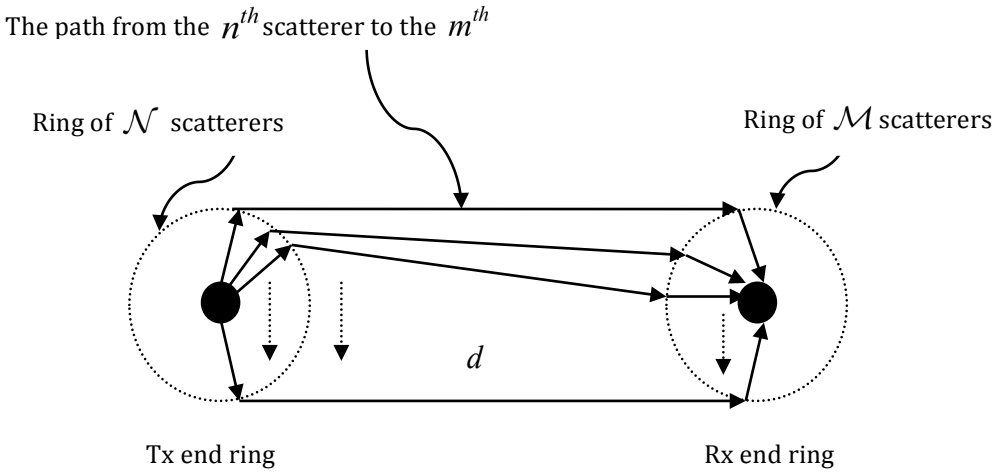

Figure 1.6: Double Rayleigh-double Doppler model.

The single Rayleigh-double Doppler model will have the autocorrelation function and the power spectrum of the complex envelope given by (1.11) and (1.12) respectively [23, 26].

1.3 Related Literature, Dissertation Motivation and Contribution

A decentralization of wireless networks to reduce the dependence on fixed infrastructures has become the hot topic in the past few years. However, decentralization gives rise to various network setup and management issues. The vision for future communication systems need to be builds over more robust networks in the wake of unforeseen situations. We envision future communication networks to be self-organizing and intelligent. The evolution to integrated networks is expected to permit new services and usage models with higher efficiency network to be used in roaming and communicating the network anytime, anywhere and with any technology. To support wide applications that requires higher and

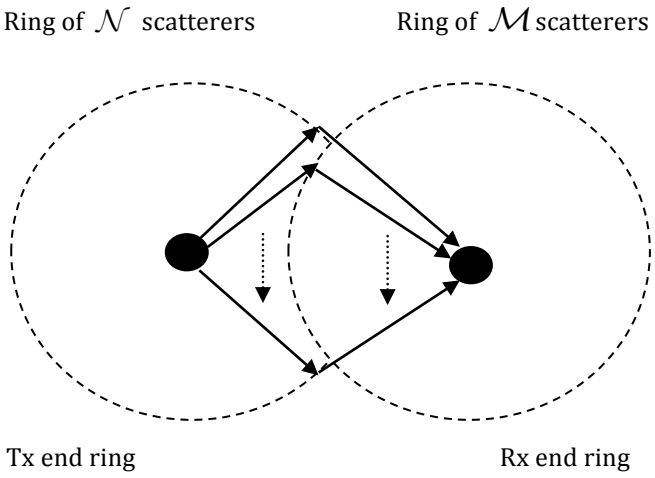

Figure 1.7: Single Rayleigh-double Doppler model.

reliable data rate, wireless communication system designers need to optimize the network performance to meet some challenging parameters such as better link reliability, higher data rates, fewer dropped connections and longer battery life. As a matter of fact, we can make the most of the vehicles on roads by forming a network that relays information from one vehicle to another. In other words, by deploying cooperative techniques in IVC networks we can benefit from both systems similar to the case of mobile terminals in ad hoc as well as wireless sensor networks [27].

Characteristic advantages of IVC networks are; 1) the abundant energy and computing power (including both storage and processing), hence the operating vehicles can afford significant computing, communication and sensing capabilities. 2) Unlike general mobile ad hoc networks, vehicles can have very predictable movement that is in the most common cases limited to roadways. 3) Roadway information is often available from positioning systems and map-based technologies such as GPS. 4) Given the average speed, current speed, and road trajectory, the future position of a vehicle can be predicted. However,

IVC networks physical layer designs have to cope with tremendous challenges that include: extendable network area over the entire road that includes many participants and extremely dynamic environment with a topology that is always changing: e.g., in highways, relative speed of up to 300 km/h may occur, while density of nodes may vary from 1-2 to tens of vehicles per kilometer in busy roads. Due to high-speed movement between vehicles, the topology of vehicular networks is always changing. Due to the same reasons, the connectivity of the vehicular networks could also be changing frequently. Another challenge occurs when the vehicle density is low; it has higher probability that the network is disconnected. In some applications, such as ubiquitous Internet access, the problem needs to be solved. For the most common scenarios, vehicular networks are usually operated in two typical communications environments. The first is the highway traffic scenarios where the environment is relatively simple and straightforward (e.g., constrained one-dimensional movement). The second is the city traffic scenarios where it becomes much more complex. Buildings, trees and other obstacles often separate the streets. Therefore, there isnt always a direct line of communications in the direction of intended data communication.

There has been a growing literature on the networking and application layers in VANETs such as routing, security, or Quality of Service (QoS) [32–38]. However, the relevant literature on the physical layer aspects is sparse. While the existing works on the physical layer of cooperative vehicular networks build upon rather approximate or simplified assumption of narrowband systems in very slow traffic flows such as in rush hours, resulting in frequency-flat and quasi-static fading channels [39–43]. In most practical scenarios, in IVC communication systems, both the transmitter and the receiver are in motion and the elevations of their antennas are relatively lower, invalidating the quasi-static Rayleigh fading channel assumption. Inter-symbol interference (ISI) due to the broadband nature of

the system introduces frequency-selectivity while Doppler spreads result in time-selectivity. For the performance evaluation, conducting field trials are highly expensive and time consuming [24, 25, 43, 44]. Hence, in this dissertation, we aim to find analytical closed form expressions on the performance of vehicular networks and advise possible improvement methods. To assess the performance of vehicular communication systems at the link level, bit error rate (BER), pairwise error probability (PEP) and the diversity gains are used as a performance measures.

In Chapter 2 we investigate the performance of a cooperative vehicular network over a doubly-selective fading channel and double-ring second-order statistics. We consider two vehicular scenarios; in the first scenario we consider a city/urban area where source, relaying and destination vehicles travel with arbitrary velocities and all underlying links experience doubly-selective fading in a highly scattering area. In the second scenario we consider a highway where the source and relaying vehicles typically travel in the same direction with similar speeds and surrounded by scatterers. In this scenario, source-to-destination and relay-to-destination links are modeled by doubly-selective channel. For these two scenarios, under the assumption of AF relaying with orthogonal cooperation protocol, we derive a PEP expression and demonstrate the achievable diversity gains. Via proper linear constellation precoding, we investigate the ability of the cooperative vehicular scheme to extract the maximum available diversity in frequency (through multipath diversity), time (through Doppler diversity) and spatial (through cooperative diversity) dimensions. The effect of imperfect channel state information is also studied through an asymptotical PEP analysis. We further conduct Monte-Carlo simulations to confirm the analytical derivations and present the error rate performance under various mobility conditions and scenarios [45–48].

In Chapter 3, we consider R2V communications in which roadside access points use cooperating vehicles as relaying terminals. This can be particularly useful in suburban or remote areas where the frequent deployment of roadside access points is not either possible or cost-effective. For the doubly-selective vehicular channel under consideration, we employ a precoded cooperative transmission technique to extract the underlying rich multipath-Doppler-spatial diversity. Further we investigate a relay selection scheme to take advantage of the potentially large number of relaying vehicles to extract extra spatial diversity to fully improve the communication performance. Under the assumption of DF relaying, we derive a pairwise error probability expression and demonstrate the achievable diversity gains. We further provide Monte-Carlo simulations to confirm the analytical derivations and provide insight into the error rate performance of infrastructure-to-vehicle cooperative communications [49].

In Chapter 4, we consider a multi-hop broadband communication, for a precoded IVC system using cooperative transmission and DF relaying. Cooperative multi-hop transmission is a way to attain broader coverage by splitting the communication link from the source to the destination into several, possibly shorter hops. It has successfully emerged as a reliable communication model that extends coverage, reliability, scalability, etc. We extend multi-hop relaying into precoded inter-vehicles communication under the doubly-selective realistic assumption. We propose a cooperative scheme that uses vehicles as relaying terminals. A precoded model is used to extract underlying rich diversity gains found in these types of doubly selective channels. Further we investigate relay selection per each hop to take advantage of the potentially large number of relaying vehicles to extract extra spatial diversity to fully improve the communication performance. We investigate the achievable multipath-Doppler diversity gain for the proposed precoded model by deriving a closed

form of the error performance curves. We further conduct numerical and Monte-Carlo simulations to confirm the analytical derivations. Applications for our proposed scheme can be introduced but not limited to connecting two remote urban cities in case of the absence of infrastructure communication network between both of them, relaying emergency messages to infrastructure-less areas in case of accidents or disasters, increasing scalability and reliability for broadcasting traffic and commercial information to IVC networks, etc. Numerical as well as Monte-Carlo simulations are further provided to confirm the analytical derivations and provide insight into the error rate performance [50].

In Chapter 5, we conclude and introduce the future research work.

Chapter 2

Cooperative Vehicle-to-Vehicle Communications

In this chapter, we consider a dual-hop cooperative vehicle-to-vehicle (V2V) transmission over a doubly-selective fading channel. To handle spreading in time and frequency, we investigate a precoded cooperative scheme to exploit delay and Doppler spreads to our advantage. Our transmission model essentially extends the linear constellation precoding technique presented in [51] for conventional SISO direct transmission to a V2V cooperative transmission. For two traffic scenarios under city/urban settings and a highway area, we derive PEP expressions and demonstrate the achievable diversity gains. The effect of imperfect channel state information (CSI) is also studied through an asymptotical PEP analysis. We present Monte-Carlo simulations to confirm the analytical derivations and present the error rate performance of the vehicular scheme with perfect and imperfect CSI.

The chapter is organized as follows: In Section 2.1, we present the precoded cooperative system model along with the vehicular fading channel. In Section 2.2, we provide a

diversity gain analysis through PEP derivation. In Section 2.3, we describe the channel estimation procedure with pilot symbols and investigate the effect of imperfect CSI through an asymptotical PEP analysis in Appendix A. In Section 2.4, we present Monte-Carlo simulation results for the error rate performance. Finally, we conclude in Section 2.5.

2.1 System Model

In this section, we first summarize the channel model along with vehicular scenarios and then present the precoded cooperative SISO and MIMO schemes under consideration.

2.1.1 Traffic Scenarios and Channel Model

We consider two traffic scenarios. In the first scenario (See Figure 2.1), we consider a city/urban area where source, relaying and destination vehicles travel with arbitrary velocities and all underlying links experience doubly-selective fading in a highly scattering area.

In the second scenario (See Figure 2.2), we consider a highway where the source and relaying vehicles typically travel in the same direction with similar speeds and surrounded by scatterers. In this scenario, source-to-destination and relay-to-destination links are modeled by doubly-selective channel. On the other hand, since the relative Doppler frequency of the source and relaying vehicles traveling in the same direction with similar speeds becomes nearly zero, the source-to-relay link can be modeled by time-flat and frequency-flat channel.

To reflect the relay geometry, we consider an aggregate channel model which takes

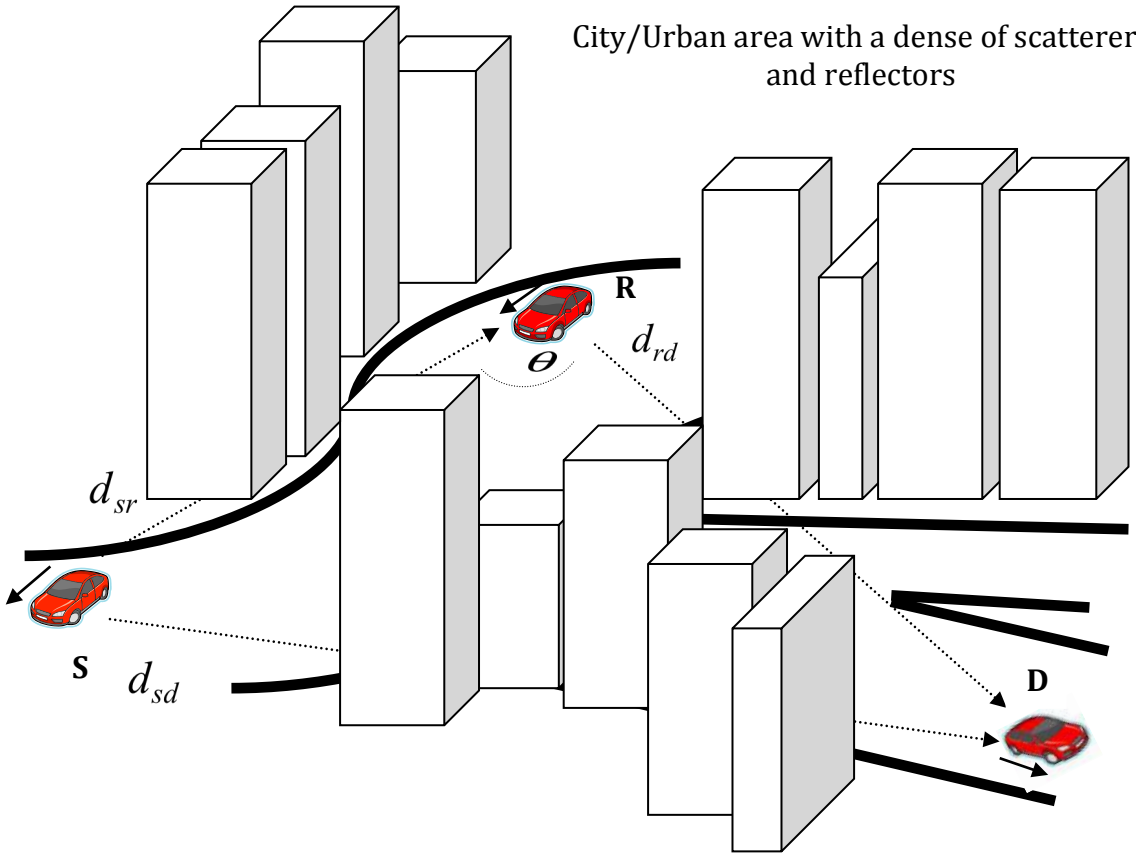

Figure 2.1: Cooperative V2V communication model in a city/urban area.

into account both path-loss and small-scale fading. The path loss is proportional to d^{α} where d is the propagation distance and α is the path loss coefficient. Let d_{sd}, d_{sr} and d_{rd} denote the distances of source-to-destination (S→D), source-to-relay (S→R), and relay-to-destination (R→D) links, respectively, and θ is the angle between lines S→R and R→D. Normalizing the path loss in S→D to be unity, the relative geometrical gains are defined respectively as $G_{sr} = (d_{sd}/d_{sr})^{\alpha}$ and $G_{rd} = (d_{sd}/d_{rd})^{\alpha}$. The ratio G_{sr}/G_{rd} reflects the effect of relay location. More negative this ratio is, more closely the relay is placed to destination terminal.

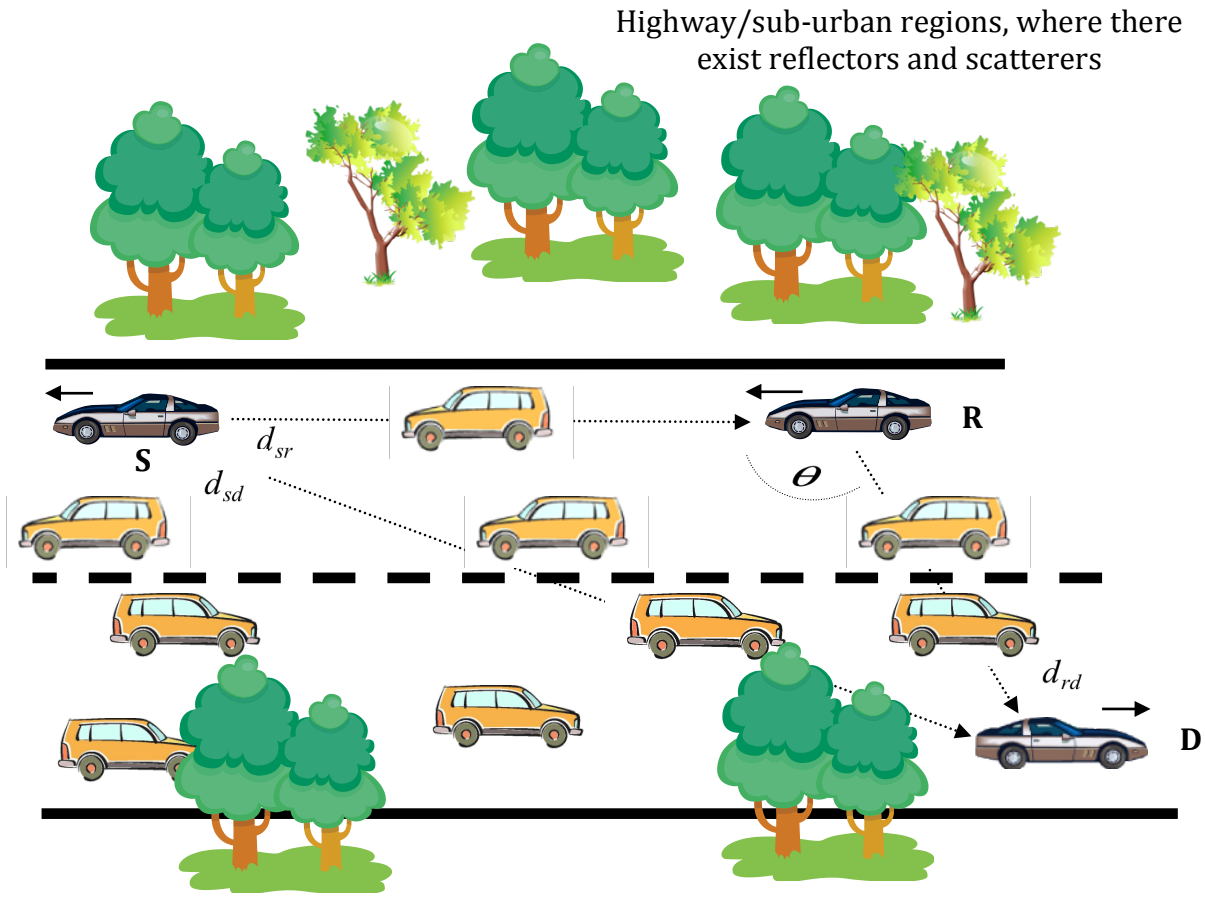

Figure 2.2: Cooperative V2V communication model in a highway/suburban area.

As for the short-term fading model, we adopt the double-ring channel model which is given by the autocorrelation function (1.11) and the corresponding power spectral density in (1.12). The maximum Doppler shift due to the relative motion of the two vehicles is given by $f_{D_m} = [v_1 \cos(\vartheta_1) + v_2 \cos(\vartheta_2)]/\lambda$, where λ is the wavelength of the carrier frequency with ϑ_1 and ϑ_2 representing the angle of incidence of the signal on the first and second vehicles, respectively. Note that in vehicular channel there are several instantaneous velocities due to the acceleration/decelerations. Maximum Doppler shift f_{D_m} is calculated

based on the maximum velocities experienced.

We can further define the delay spread τ, caused by the multiple propagation paths between the transmitter and the receiver, governs the frequency selective nature of the channel. Similarly, the Doppler spread $2f_{D_m}$, caused by the mobility between the transmitter and the receiver, governs the time selectivity. The delay-Doppler spread product $2f_{D_m}\tau$ quantifies the channel variation across time and frequency, and plays an important role in estimating doubly selective channels. For the values of $2f_{D_m}\tau < 1$ the channel is classified as doubly-selective which is a special case of the underspread channel [51], which intuitively speaking, bounds the channels' degrees of freedom and renders channel estimation well posed. Based on the V2V channel model for the traffic densities under consideration, the maximum delay spreads are reported as $\tau_d = 1.113$ μs and 1.773 μs in [44]. In our model, the maximum velocities for source, relay and destination vehicles are assumed to be equal to $\geq$ 50km/h. In line with the IEEE 802.11p standards, we choose an operating frequency of $f_c = 5.9$GHz, resulting in $f_{D_m} = 327.7$Hz. The delay-Doppler spread factor will be equal to $2f_{D_m}\tau \approx 0.0012$ satisfying the doubly-selective underspread condition [51–54].

2.1.2 Model for SISO Cooperative Transmission

Here we assume that source, relay, and destination vehicles are equipped with single antennas. We assume the orthogonal cooperation protocol of [17] and AF relaying. In the broadcasting phase, the source vehicle sends its signal to the relay and the destination vehicles. In the relaying phase, the relay vehicle properly scales its received signal (to avoid power budget violation) and forwards the resulting signal to the destination. The destination makes its decision based on the maximum likelihood (ML) detection of the two

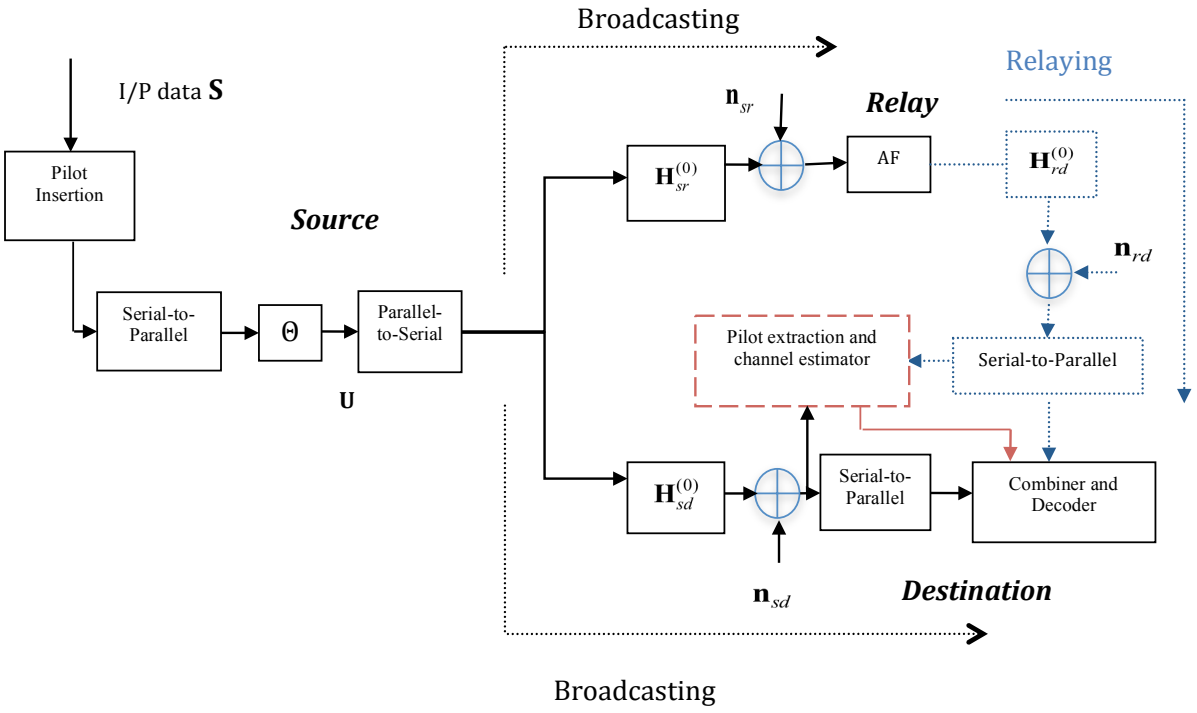

Figure 2.3: SISO cooperative transmission scheme.

received signals.

We consider a precoded cooperative scheme as shown in Figure 2.3. The input data packets (generated from an M-QAM constellation) of length N_t are divided into shorter sub-blocks of length N_s ($N_s \leq N_t$). Let each of these sub-blocks be denoted by $\mathbf{s}(n)$ which will be the input to the linear precoder $\mathbf{\Theta}$ of size $N_s \times N_t$. We use the precoder proposed in [51] which ensures the maximum diversity over doubly-selective channels and eliminates the inter-block interference (IBI) term. It is given by $\mathbf{\Theta} = \mathbf{F}_{P+Q}^{\mathrm{H}} \mathbf{T_1} \otimes \mathbf{T_2}$ where $\mathbf{F}_{P+Q}^{\mathrm{H}}$ is a $(P+Q)$-point IFFT matrix, $\mathbf{T}_1 := [\mathbf{I}_P,\ \mathbf{0}_{P\times Q}]^{\mathrm{T}}$ and $\mathbf{T}_2 := [\mathbf{I}_Z,\ \mathbf{0}_{Z\times L}]^{\mathrm{T}}$. Here, $P \geq 1$ and $Z \geq 1$ are the precoder design parameters such that $N_s = PZ$, $N_t = (P+Q)(Z+L)$. We have $L = \lceil \tau_d / T_s \rceil$ as the number of the resolvable multipath components and the number

of Doppler shifts experienced over the data block is given by $Q = \lceil N_t T_s f_{D_m} \rceil$.

Based on the so-called Basis Expansion Model (BEM), a discrete-time baseband equivalent channel for the doubly-selective channel under consideration is given by

$$h_B(\ell; l) = \sum_{q=0}^{Q} h_q(n; l)\, e^{j w_q \ell}, l \in [0, L] \tag{2.1}$$

where $h_q(n; l)$ is zero-mean complex Gaussian and $w_q = 2\pi(q - Q/2)/N_t$ is the finite Fourier bases that capture the time variation. Here, ℓ denotes the serial index for the input data symbols and the block index is given by $n = \lfloor \ell / N_t \rfloor$. Define $\mathbf{H}_{sd,q}^{(0)}$, $\mathbf{H}_{sr,q}^{(0)}$ and $\mathbf{H}_{rd,q}^{(0)}$ as the lower triangular Toeplitz channel matrices with entries given by (2.1). Let L_{sd}, L_{sr} and L_{rd} denote the channel multipath orders for the S→D, S→R, and R→D links, respectively. Further, let Q_{sd}, Q_{sr} and Q_{rd} denote the number of resolvable Doppler components and define $Q = \max(Q_{sd}, Q_{sr}, Q_{rd})$.

In the broadcasting phase, the received signals at the relay can be expressed in a matrix form as

$$\begin{aligned} \mathbf{y}_{sr}(n) &= \sqrt{G_{sr} E_s} \sum_{q=0}^{Q} \mathbf{D}(w_q) \mathbf{H}_{sr,q}^{(0)}(n)\, \mathbf{u}(n) + \mathbf{n}_{sr}(n) \\ &= \sqrt{G_{sr} E_s} \mathbf{\Phi}(n)\, \mathbf{h}_{sr}(n) + \mathbf{n}_{sr}(n) \end{aligned} \tag{2.2}$$

where $\mathbf{u}(n) = \mathbf{\Theta s}(n)$ is the transmitted data block, E_s is the modulation symbol energy, $\mathbf{D}(w_q) := \text{diag}\,[1, \ \ldots \ , \exp(j w_q (N_t - 1))]$ and $\mathbf{n}_{sr}(n)$ is the additive white Gaussian noise (AWGN) vector with entries of zero mean and $N_0/2$ variance. The second equality follows from the commutativity of products of Toeplitz matrices with vectors where we have further defined the augmented matrices $\mathbf{h}_{sr}(n) = [\mathbf{h}_{sr,0}^{\mathrm{T}}(n), \ \ldots \ , \mathbf{h}_{sr,Q}^{\mathrm{T}}(n)]^{\mathrm{T}}$ and $\mathbf{\Phi}(n) = [\mathbf{D}(w_0)\mathbf{U}(n), \ \ldots \ , \mathbf{D}(w_Q)\mathbf{U}(n)]$, with $\mathbf{U}$ denoting the lower triangular

Toeplitz matrix. Similarly, the received signal at the destination can be written as

$$\mathbf{y}_{sd}(n) = \sqrt{E_s}\mathbf{\Phi}(n)\,\mathbf{h}_{sd}(n) + \mathbf{n}_{sd}(n) \tag{2.3}$$

where $\mathbf{h}_{sd}(n) = [\mathbf{h}_{sd,0}^{\mathrm{T}}(n), \ \ldots \ , \mathbf{h}_{sd,Q}^{\mathrm{T}}(n)]^{\mathrm{T}}$ and $\mathbf{n}_{sd}(n)$ is the AWGN vector with entries of zero mean and $N_0/2$ variance.

The relay scales the received signal $\mathbf{y}_{sr}(n)$ (to ensure that an average output power is maintained) by a factor of $\sqrt{\mathbb{E}_{\mathbf{n}_{sr},\mathbf{\Phi}}[|\mathbf{y}_{sr}(n)|^2]} = (G_{sr}E_s^2)\,\mathrm{tr}\left(\mathbb{E}[\mathbf{\Phi}^{\mathrm{H}}(n)\mathbf{\Phi}(n)]\right) + N_t(N_0/2)$, then forwards the resulting signal to the destination. At the destination, after a proper normalization [55], we have the resulting signal as

$$\mathbf{y}_{rd}(n) = K(n)\sqrt{E_s}\mathbf{\Phi}_{srd}(n)\,\mathbf{h}_{srd}(n) + \mathbf{n}_{srd}(n) \tag{2.4}$$

where

$$K(n) = \sqrt{G_{sr}G_{rd}E_s}\Big/\left(\Omega(n)\,\mathbb{E}_{\mathbf{n}_{sr},\mathbf{\Phi}}\left[|\mathbf{y}_{sr}(n)|^2\right]\right)$$

$$\mathbf{\Phi}_{srd}(n) = \sum\nolimits_{q_2=0}^{Q}\sum\nolimits_{q_3=0}^{Q}\mathbf{D}(w_{q_2})\,\mathbf{D}(w_{q_3})\,\mathbf{U}(n)$$

$$\mathbf{h}_{srd}(n) = \mathbf{H}_{rd,q_3}^{(0)}(n)\,\mathbf{h}_{sr,q_2}(n)$$

and

$$\mathbf{n}_{srd}(n) = \left(\sqrt{G_{rd}E_s}\mathbf{\Phi}(n)\,\mathbf{n}_{sr}(n)\Big/\mathbb{E}_{\mathbf{n}_{sr},\mathbf{\Phi}}\left[|\mathbf{y}_{sr}(n)|^2\right] + \mathbf{n}_{rd}(n)\right)\Big/\Omega(n)$$

with $\Omega(n) = 0.5\sqrt{1 + G_{rd}E_s|\mathbf{\Phi}_{rd}(n)|^2/\mathbb{E}_{\mathbf{n}_{sr},\mathbf{\Phi}}[|\mathbf{y}_{sr}(n)|^2]}$, and $\mathbf{n}_{rd}(n)$ being the AWGN

vector entries of zero mean and $N_0/2$ variance. Arranging (2.3) and (2.4) in a matrix form

$$\mathbf{Y}(n) = \begin{bmatrix} \mathbf{y}_{sd}(n) \\ \mathbf{y}_{rd}(n) \end{bmatrix} = \underbrace{\sqrt{E_s} \begin{bmatrix} \mathbf{\Phi}(n) & 0 \\ 0 & K(n)\,\mathbf{\Phi}_{srd}(n) \end{bmatrix}}_{\mathbf{S}(n)} \underbrace{\begin{bmatrix} \mathbf{h}_{sd}(n) \\ \mathbf{h}_{srd}(n) \end{bmatrix}}_{\mathbf{h}(n)} + \underbrace{\begin{bmatrix} \mathbf{n}_{sd}(n) \\ \mathbf{n}_{srd}(n) \end{bmatrix}}_{\mathbf{n}(n)} \tag{2.5}$$

For the signal detection, coherent reception is preferred for modern communication designs. It is well known that coherent receiver needs more expensive and complex circuits than non-coherent receivers, but in return it achieves a better bit error rate performance [56]. However, because of the rapid advancing of hardware technologies, the cost and complexity issues notably decrease with time, which motivates us to focus on the 'performance' outcome. In a specific study for SISO mobile system with a doubly selective channels and Doppler spread, It was shown thet the coherent receivers needs 5 dB less SNR to achieve the same performance of a non-coherent system [56]. In [57], under the assumption of mismatched coherent systems, the BER performance of coherent system still outperforms the non-coherent one in cooperative system for values of normalized Doppler values $(N_s T_s) f_{D_m} > 0.035$, which is valid for the presented IVC scenarios under consideration.

In the case of imperfect-CSI at the receiver side, a reference signal (RS) can be used to assist in the coherent detection of the data. The adopted channel estimation technique "i.e., Pilot Symbol Assisted Modulation (PSAM)" uses distributed pilot pattern that can be used also in synchronization purpose without additional cost [58–63]. If the channel varies slowly, then it is reasonable to expect performance/efficiency to be close to the perfect-CSI assumption. If the channel varies rapidly, on the other hand, the performance/efficiency might be lower. There is thus an underlying dependence between achievable performance

and velocity (or, more generally, Doppler spectrum) and this dependence is also a function of the effective SNR (signal-to-noise ratio) [60]. Furthermore, in (A.5) of Appendix A, we show that the effective SNR of the imperfect-CSI is a function of the transmitting power and the underlying channel matrix rank "i.e., diversity order". Hence, for coherent detection by increasing the extracted diversity order we expect a closer performance to the perfect-CSI assumption. Extracting the underlying multipath-Doppler-spatial diversity, intends to mitigate the rapid fading which is the central problem in wireless mobile communications since it causes the received signal to exhibit both deep fading and frequency spreading, as quantified by the signal-to-noise ratio (SNR) and maximum Doppler frequency shift parameters, respectively.

The received signals are then fed to an ML detector [1].

2.1.3 Model for MIMO Cooperative Transmission

In this part, we assume that source and destination nodes are equipped with two antennas while the relay node has a single transmit/receive antenna. We assume that Alamouti-type space-time block coding (STBC) [11] is used across the two transmit antennas of the source node [2]. Since time-selectivity will destroy the orthogonality of STBC, we employ digital phase sweeping (DPS) [65] to overcome the degrading effects of time-selectivity. DPS converts space-time time-selective channels into a single faster time-selective channel. Specifically, it shifts the $Q+1$ bases of the associated channel (corresponding to each of the transmit antennas) such that all the bases are consecutive on the FFT grid of complex exponentials.

[1] ML detection requires an exhaustive search with high complexity (exponential in the block length N_t). A relatively less complex near-ML search is provided by the sphere-decoding algorithm [64].

[2] Extension to more than two antennas is straightforward with a more cumbersome notation.

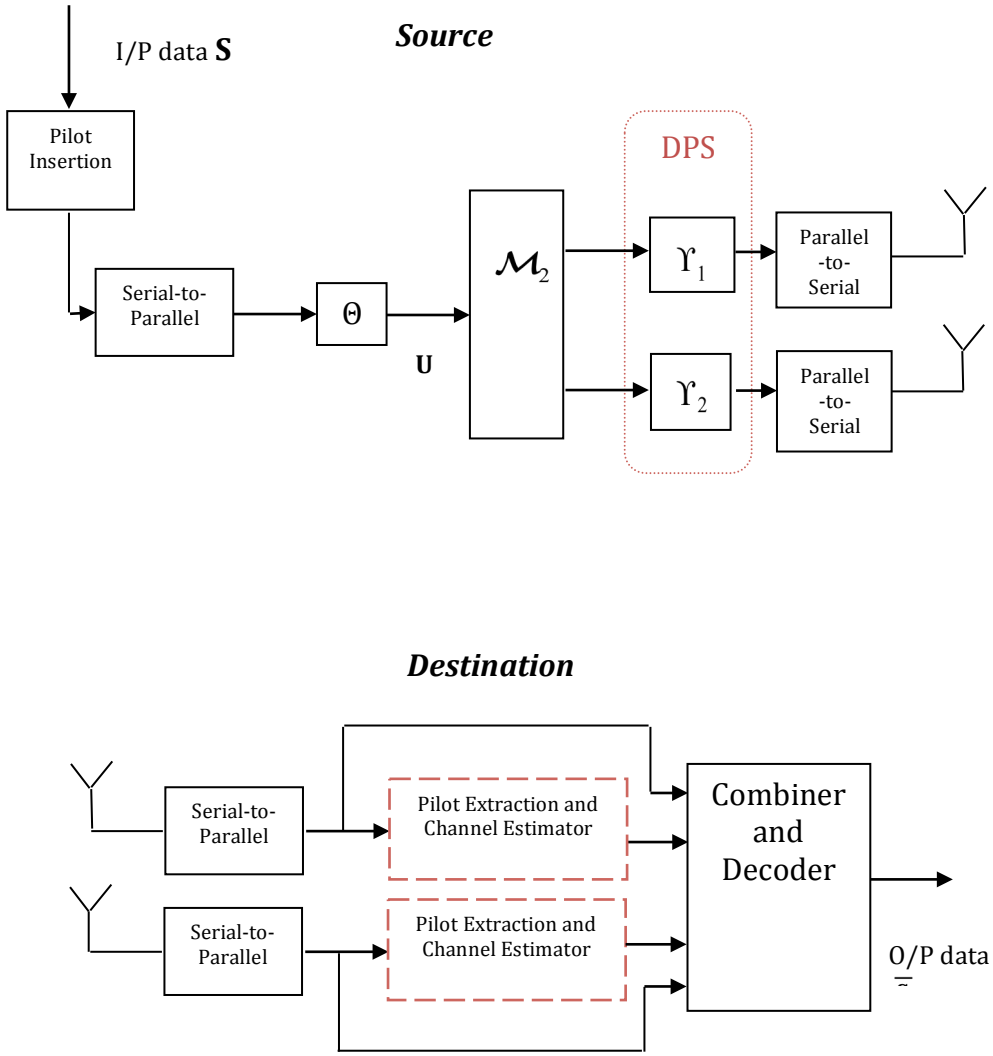

Figure 2.4: Alamouti-code based MIMO cooperative transmission scheme.

Figure 2.4 shows the block diagram for the source and the destination with $\mathcal{M}_2$ denoting the STBC matrix.

As summarized in Table 2.1, we use four transmission phases. During the first transmission phase (broadcasting-1), the source vehicle broadcasts two precoded blocks, i.e., $\mathbf{u}(n-1) = \mathbf{\Theta s}(n-1)$ and $\mathbf{u}(n) = \mathbf{\Theta s}(n)$, from the first and second antennas re-

Table 2.1: Encoding for STBC cooperative transmission.

	Phase 1 (broadcasting-1)	Phase 2 (broadcasting-2)	Phase 3 (relaying-1)	Phase 4 (relaying-2)
Tx antenna-1	transmit $\mathbf{s}(n-1)$	transmit $-\mathbf{s}^*(n)$	*idle*	*idle*
Tx antenna-2	transmit $\mathbf{s}(n)$	transmit $\mathbf{s}^*(n-1)$	*idle*	*idle*
Relay antenna	receive $\mathbf{y}_{sr}(n-1)$	receive $\mathbf{y}_{sr}(n)$	transmit $\bar{\mathbf{y}}_{sr}(n-1)$	transmit $\bar{\mathbf{y}}_{sr}(n)$
Rx antenna-1	receive $\mathbf{y}_{sd,1}(n-1)$	receive $\mathbf{y}_{sd,1}(n)$	receive $\mathbf{y}_{rd,1}(n-1)$	receive $\mathbf{y}_{rd,1}(n)$
Rx antenna-2	receive $\mathbf{y}_{sd,2}(n-1)$	receive $\mathbf{y}_{sd,2}(n)$	receive $\mathbf{y}_{rd,2}(n-1)$	receive $\mathbf{y}_{rd,2}(n)$

spectively. During the second transmission phase (broadcasting-2), the source vehicle broadcasts another version of the two precoded blocks, i.e. $\mathbf{u}^*(n) = -\mathbf{\Theta}\mathbf{s}^*(n)$ and $\mathbf{u}^*(n-1) = \mathbf{\Theta}\mathbf{s}^*(n-1)$, from the first and second antennas respectively. In the third and fourth transmission phases (relaying-1/2), the relay first scales the received signal and then forwards the resulting signal to the destination. Following similar matrix manipulations and proper normalizations in Section 2.1.2, a compact form for the received signal at the destination is given by

$$\mathbf{Y}(n) = \sqrt{\frac{E_s}{2}}\mathbf{S}(n)\,\mathbf{h}(n) + \mathbf{n}(n) \tag{2.6}$$

where we define

$$\mathbf{Y}(n) = \left[\mathbf{y}_{sd,1}(m) \quad \mathbf{y}_{sd,2}(m) \quad \mathbf{y}_{sd,1}(n) \quad \mathbf{y}_{sd,2}(n) \quad \mathbf{y}_{rd,1}(m) \quad \mathbf{y}_{rd,2}(m) \quad \mathbf{y}_{rd,1}(n) \quad \mathbf{y}_{rd,2}(n)\right]^{\mathrm{T}},$$

$$\mathbf{S}(n) = \left[\mathbf{S}_1(n) \quad \mathbf{S}_2(n)\right],$$

$$\mathbf{h}(n) = \begin{bmatrix} \mathbf{h}_1(n) & \mathbf{h}_2(n) \end{bmatrix}^{\mathrm{T}} ,$$

$$\mathbf{n}(n) = \begin{bmatrix} \mathbf{n}_{sd}^{(1)}(m) & \mathbf{n}_{sd}^{(2)}(m) & \mathbf{n}_{sd}^{(1)}(n) & \mathbf{n}_{sd}^{(2)}(n) & \tilde{\mathbf{n}}_{rd}^{(1)}(m) & \tilde{\mathbf{n}}_{rd}^{(2)}(m) & \tilde{\mathbf{n}}_{rd}^{(1)}(n) & \tilde{\mathbf{n}}_{rd}^{(2)}(n) \end{bmatrix}^{\mathrm{T}}$$

The related variables are further defined as follows

$$\mathbf{h}_a(n) = \begin{bmatrix} \mathbf{h}_{sd}^{(a,1)}(m) & \mathbf{h}_{sd}^{(a,2)}(m) & \left(\mathbf{h}_{sd}^{(a,1)}(n)\right)^* & \left(\mathbf{h}_{sd}^{(a,2)}(n)\right)^* & \mathbf{H}_{rd}^{(1,1)}(m)\,\mathbf{h}_{sr}^{(a,1)}(m) \\ \mathbf{H}_{rd}^{(1,2)}(m)\,\mathbf{h}_{sr}^{(a,1)}(m) & \mathbf{H}_{rd}^{(1,1)}(n)\left(\mathbf{h}_{sr}^{(a,1)}(n)\right)^* & \mathbf{H}_{rd}^{(1,2)}(n)\left(\mathbf{h}_{sr}^{(a,1)}(n)\right)^* \end{bmatrix}^{\mathrm{T}} ,$$

$$\mathbf{S}_1(n) = \mathrm{diag}\Big(\sqrt{G_{sd}/2}\mathbf{\Phi}_{sd}^{(1,1)}(m), \sqrt{G_{sd}/2}\mathbf{\Phi}_{sd}^{(1,2)}(m), -\sqrt{G_{sd}/2}\mathbf{\Phi}_{sd}^{(1,1)}(n), -\sqrt{G_{sd}/2}\mathbf{\Phi}_{sd}^{(1,2)}(n), K_1(m)\,\mathbf{\Phi}_{srd}^{(1,1)}(m), K_2(m)\,\mathbf{\Phi}_{srd}^{(1,2)}(m), -K_1(n)\,\mathbf{\Phi}_{srd}^{(1,1)}(n), -K_2(n)\,\mathbf{\Phi}_{srd}^{(1,2)}(n)\Big),$$

$$\mathbf{S}_2(n) = \mathrm{diag}\Big(\sqrt{G_{sd}/2}\mathbf{\Phi}_{sd}^{(2,1)}(n), \sqrt{G_{sd}/2}\mathbf{\Phi}_{sd}^{(2,2)}(n), \sqrt{G_{sd}/2}\mathbf{\Phi}_{sd}^{(2,1)}(m), \sqrt{G_{sd}/2}\mathbf{\Phi}_{sd}^{(2,2)}(m), K_1(m)\,\mathbf{\Phi}_{srd}^{(2,1)}(n), K_2(m)\,\mathbf{\Phi}_{srd}^{(2,2)}(n), K_1(n)\,\mathbf{\Phi}_{srd}^{(2,1)}(n), K_2(n)\,\mathbf{\Phi}_{srd}^{(2,2)}(n)\Big),$$

in the above we define $m = n - 1$

$$\mathbf{\Phi}_{sr}^{(a,b)}(.) = \begin{bmatrix} \mathbf{D}(w_0)\,\mathbf{\Upsilon}_a\mathbf{U}_{sr}^{(a,b)}(.), & \ldots & , \mathbf{D}(w_Q)\,\mathbf{\Upsilon}_a\mathbf{U}_{sr}^{(a,b)}(.) \end{bmatrix} ,$$

$$\mathbf{\Phi}_{srd}^{(a,b)}(.) = \sum\nolimits_{q_2=0}^{Q}\sum\nolimits_{q_3=0}^{Q}\mathbf{D}(w_{q_2})\,\mathbf{D}(w_{q_3})\,\mathbf{\Upsilon}_a\mathbf{U}_{sr}^{(a,b)}(.),$$

$$\boldsymbol{\Upsilon}_a = \mathrm{diag}\left[1, \exp\left(j2\pi\left(a-1\right)\left(Q+1\right)/N_t\right), \ldots, \exp\left(j2\pi\left(a-1\right)\left(Q+1\right)\left(N_t-1\right)/N_t\right)\right]$$

$$K_b\left(.\right) = \sqrt{\frac{G_{sr}G_{rd}}{2\mathbb{E}_{\mathbf{n}_{sr},\boldsymbol{\Phi}}[|\mathbf{y}_{sr,b}\left(.\right)|^2]}\left(\frac{G_{rd}\mathbb{E}\left|\sum_{q=0}^{Q}\mathbf{D}\left(w_q\right)\boldsymbol{\Upsilon}_1\mathbf{H}_{rd,q}^{(1,b)}\left(.\right)\right|^2}{G_{rd}\sqrt{\frac{E_s}{2}}\mathbb{E}\left|\sum_{q=0}^{Q}\mathbf{D}\left(w_q\right)\boldsymbol{\Upsilon}_1\mathbf{H}_{rd,q}^{(1,b)}\left(.\right)\right|^2 + 2\mathbb{E}_{\mathbf{n}_{rd},\boldsymbol{\Phi}}\left[\left|\mathbf{y}_{rd,b}\left(.\right)\right|^2\right]}\right)}$$

$$\tilde{\mathbf{n}}_{rd}^{(b)}\left(.\right) = \sqrt{\frac{G_{rd}\sqrt{\frac{E_s}{2}}\mathbb{E}\left|\sum_{q=0}^{Q}\mathbf{D}\left(w_q\right)\boldsymbol{\Upsilon}_1\mathbf{H}_{rd,q}^{(1,b)}\left(.\right)\right|^2}{G_{rd}\sqrt{\frac{E_s}{2}}\mathbb{E}\left|\sum_{q=0}^{Q}\mathbf{D}\left(w_q\right)\boldsymbol{\Upsilon}_1\mathbf{H}_{rd,q}^{(1,b)}\left(.\right)\right|^2 + 2\mathbb{E}_{\mathbf{n}_{rd},\boldsymbol{\Phi}}\left[\left|\mathbf{y}_{rd}\left(.\right)\right|^2\right]}} \times \left(\frac{\sqrt{G_{rd}}\mathbb{E}\left|\sum_{q=0}^{Q}\mathbf{D}\left(w_q\right)\boldsymbol{\Upsilon}_1\mathbf{H}_{rd,q}^{(1,b)}\left(.\right)\right|^2}{\sqrt{\mathbb{E}_{\mathbf{n}_{sr},\boldsymbol{\Phi}}\left[\left|\mathbf{y}_{sr}\left(.\right)\right|^2\right]}}\mathbf{n}_{sr}\left(.\right) + \mathbf{n}_{rd}^{b}\left(.\right)\right)$$

with $a, b \in \{1, 2\}$.

2.2 PEP Derivation and Diversity Gain Analysis

In this section, we investigate the achievable diversity gain orders for V2V SISO and MIMO cooperative schemes through the derivation of the PEP. We assume perfect-CSI at the receiver side.

2.2.1 SISO Cooperation

Let $\hat{\mathbf{S}}$ represent the erroneously decoded data matrix instead of the originally transmitted $\mathbf{S}$. After dropping the block index n in (2.5) for convenience of the presentation, the conditional PEP is given by [10]

$$P(\mathbf{S} \to \hat{\mathbf{S}} \Big| \mathbf{h}) = Q\left(\sqrt{\frac{1}{2N_0} d^2\left(\mathbf{S}, \hat{\mathbf{S}} \Big| \mathbf{h}\right)}\right) \tag{2.7}$$

which can be upper bounded by

$$P_s\left(\mathbf{S} \to \hat{\mathbf{S}} \Big| \mathbf{h}\right) \leq \exp\left(-\frac{1}{4N_0} d^2\left(\mathbf{S}, \hat{\mathbf{S}} \Big| \mathbf{h}\right)\right) \tag{2.8}$$

In the above, the Euclidean distance conditioned on the fading channel coefficients is $d^2\left(\mathbf{S} \to \hat{\mathbf{S}} \Big| \mathbf{h}\right) = \mathbf{h}^{\mathrm{H}} \boldsymbol{\Delta} \mathbf{h}$ with $\boldsymbol{\Delta} = \left(\mathbf{S} - \hat{\mathbf{S}}\right)^{\mathrm{H}} \left(\mathbf{S} - \hat{\mathbf{S}}\right)$. In the following, we first derive the PEP for the city/urban area scenario in which all underlying links experience doubly-selective fading. Then, we present the PEP for highway/suburban area as a special case of the derived expression.

Defining $\boldsymbol{\chi}_1 = \left(\boldsymbol{\Phi}^{\mathrm{H}} - \hat{\boldsymbol{\Phi}}^{\mathrm{H}}\right)\left(\boldsymbol{\Phi} - \hat{\boldsymbol{\Phi}}\right)$ and $\boldsymbol{\chi}_2 = \left(\boldsymbol{\Phi}_{srd}^{\mathrm{H}} - \hat{\boldsymbol{\Phi}}_{srd}^{\mathrm{H}}\right)\left(\boldsymbol{\Phi}_{srd} - \hat{\boldsymbol{\Phi}}_{srd}\right)$, we can rewrite (2.8) as

$$P_s\left(\mathbf{S} \to \hat{\mathbf{S}} \Big| \mathbf{h}\right) \leq \exp\left(-\left(\mathbf{h}_{sd}^{\mathrm{H}} \boldsymbol{\chi}_1 \mathbf{h}_{sd} + K^2 \mathbf{h}_{srd}^{\mathrm{H}} \boldsymbol{\chi}_2 \mathbf{h}_{srd}\right) \frac{\gamma}{4}\right) \tag{2.9}$$

where $\gamma = E_s/N_0$ is the signal-to-noise ratio (SNR). We need to average (2.9) over $\mathbf{h}_{sd}$. Note that the channel autocorrelation matrix is given by $\mathbf{C}_{h,sd} := \mathbb{E}[\mathbf{h}_{sd}^{\mathrm{H}} \mathbf{h}_{sd}]$ and the channel rank is $r_h := \mathrm{rank}\left(\mathbf{C}_{h,sd}\right) \leq (Q_{sd}+1)(L_{sd}+1)$. Using the eigenvalue decomposition of the autocorrelation matrix, we have $\mathbf{C}_{h,sd} = \mathbf{V}_{h1} \mathbf{D}_{h1} \mathbf{V}_{h1}^{\mathrm{H}}$ where $\mathbf{V}_{h1}^{\mathrm{H}} \mathbf{V}_{h1} = \mathbf{I}_{r_{h1}}$ and

$\mathbf{D}_{h1} := \text{diag}\left(\sigma_0^2, \ \sigma_1^2, \ \ldots \ , \sigma_{r_h-1}^2 \right)$. Let the normalized channel vector be denoted as $\bar{\mathbf{h}}_{sd}$ of size $r_h \times 1$ whose entries are independent and identically distributed (i.i.d.) Gaussian random variables with zero mean and unit variance. We can replace $\mathbf{h}_{sd}$ with $\mathbf{V}_{h1}\mathbf{D}_{h1}^{1/2}\bar{\mathbf{h}}_{sd}$ since both will have identical distribution, so the PEP will remain statistically invariant. Further define $\mathbf{A}_{e1} := \left(\mathbf{V}_{h1}\mathbf{D}_{h1}^{1/2}\right)^{\mathrm{H}} \boldsymbol{\chi}_1 \mathbf{V}_{h1}\mathbf{D}_{h1}^{1/2}$, where $\mathbf{A}_{e1}$ is Hermitian (i.e., $\mathbf{A}_{e1} = \mathbf{A}_{e1}^{\mathrm{H}}$), so there exists a unitary matrix $\mathbf{V}_{e1}$ and a real non-negative definite matrix $\mathbf{D}_{e1}$ such that $\mathbf{V}_{e1}^{\mathrm{H}}\mathbf{A}_{e1}\mathbf{V}_{e1} := \mathbf{D}_{e1}$. The eigenvector of $\mathbf{A}_{e1}$ is $\mathbf{D}_{e1} := \text{diag}\left(\lambda_0, \ \lambda_1, \ \ldots \ , \lambda_{r_h-1} \right)$. Since $\mathbf{V}_{e1}$ is unitary, the vector $\tilde{\mathbf{h}}_{sd} = \mathbf{V}_{e1}\bar{\mathbf{h}}_{sd}$ will have correlation matrix identical to $\bar{\mathbf{h}}_{sd}$, namely we have $\bar{\mathbf{C}} := \mathbb{E}[\tilde{\mathbf{h}}_{sd}^{\mathrm{H}}\tilde{\mathbf{h}}_{sd}] = \mathbb{E}[\mathbf{V}_{e1}^{\mathrm{H}}\bar{\mathbf{h}}_{sd}^{\mathrm{H}}\bar{\mathbf{h}}_{sd}\mathbf{V}_{e1}]$. After these mathematical manipulations, we have

$$P_s\left(\mathbf{S} \to \hat{\mathbf{S}} \middle| \mathbf{h}\right) \leq \exp\left(-\bar{\mathbf{h}}_{sd}^{\mathrm{H}}\mathbf{A}_{e1}\bar{\mathbf{h}}_{sd}\frac{\gamma}{4}\right)\exp\left(-K^2\mathbf{h}_{srd}^{\mathrm{H}}\boldsymbol{\chi}_2\mathbf{h}_{srd}\frac{\gamma}{4}\right) \tag{2.10}$$

Defining $\beta_{p_1}^{sd}$ as the p_1^{th} element of $\bar{\mathbf{h}}_{sd}$, we have $\bar{\mathbf{h}}_{sd}^{\mathrm{H}}\mathbf{A}_{e1}\bar{\mathbf{h}}_{sd} = \sum_{p_1=0}^{r_1-1}\lambda_{p_1}\left|\beta_{p_1}^{sd}\right|^2$ with $r_1 := \text{rank}\left(\mathbf{A}_{e1}\right)$. For a normalized power Rician channels, we have the pdf given by

$$f_r\left(x_k\right) = \frac{x_k}{\sigma_k^2}\exp\left(-\frac{x_k^2+u_k^2}{2\sigma_k^2}\right)I_0\left(\frac{x_k u_k}{\sigma_k^2}\right), x_k \geq 0 \tag{2.11}$$

where $I_0\left(.\right)$ is the modified Bessel function of the first kind with order zero. A Rician fading channel can be described by two parameters: the ratio between the power in the direct path and the power in the other, scattered, paths (i.e., K) and the total power from both paths (i.e., Ω). Where ($\Omega = u_k^2 + 2\sigma_k^2$), and acts as a scaling factor to the distribution. The received signal amplitude (not the received signal power) is then Rice distributed with parameters $u_k^2 = \left(K/(K+1)\right)\Omega$ and $\sigma_k^2 = \left(\Omega/(2\left(1+K\right))\right)$. When $u_k = 0$, the distribution reduces to a Rayleigh distribution [66]. Assuming Rician distributed channels

and averaging the resulting expression (2.10) with respect to $\left|\beta_{p_1}^{sd}\right|$, we have

$$P_s\left(\mathbf{S}\to\hat{\mathbf{S}}\middle|\,\mathbf{h}_{srd}\right)\leq\Lambda_{sd}\exp\left(-\hat{K}^2\mathbf{h}_{srd}\chi_2\mathbf{h}_{srd}^{\mathrm{H}}\frac{\gamma}{4}\right) \tag{2.12}$$

where

$$\Lambda_{sd}=\prod_{p_1=0}^{r_1-1}\int_0^{\infty}2\left|\beta_{p_1}^{sd}\right|e^{\left(-\left|\beta_{p_1}^{sd}\right|^2\left(1-\frac{\lambda_{p_1}}{4}\gamma\right)-u_{sd}^2\right)}I_0\left(\left|\beta_{p_1}^{sd}\right|+u_{sd}\right)d\left|\beta_{p_1}^{sd}\right| \tag{2.13}$$

We now need to average (2.13) over $\mathbf{h}_{srd}$. From the definition of $\mathbf{h}_{srd}$ we have

$$\begin{aligned}&\mathbf{h}_{srd}\\&=\left[h_{rd}\left(0\right)h_{sr}\left(0\right),\left(h_{rd}\left(1\right)h_{sr}\left(0\right)+h_{rd}\left(0\right)h_{sr}\left(1\right)\right),\ldots,\sum_{p_2=0}^{N_t-1}h_{rd}\left(N_t-1-p_2\right)h_{sr}\left(p_2\right)\right]^{\mathrm{T}}\end{aligned} \tag{2.14}$$

where $h_{rd}\left(.\right)$ and $h_{sr}\left(.\right)$ are the corresponding channels entries for the R→D channel matrix $\mathbf{H}_{rd,q_3}^{(0)}$ and the S→R channel vector $\mathbf{h}_{sr,q_2}$, respectively. The channel autocorrelation matrix is given by $\mathbf{C}_{h,srd}:=\mathbb{E}[\mathbf{h}_{srd}^{\mathrm{H}}\mathbf{h}_{srd}]$ and the channel rank is $r_b:=\mathrm{rank}\left(\mathbf{C}_{h,srd}\right)\leq\left(Q_{sr}+1\right)\left(L_{sr}+1\right)$. Following similar steps above, we have

$$\mathbf{D}_{h2}:=\mathrm{diag}\ \left[\sigma_{rd,0}^2\sigma_{sr,0}^2,\quad\ldots\quad,\sum_{p_2=0}^{r_b-1}\sigma_{rd,N_t-1-p_2}^2\sigma_{sr,p_2}^2\right]$$

Define $\bar{\mathbf{h}}_{srd}$ with its p_2^{th} element $\hat{\beta}=\left|\sum_{g=0}^{p_2}\beta_{p_2-g}^{rd}\beta_g^{sr}\right|^2$. Since $\beta_{p_2-g}^{rd}$ and β_g^{sr} are linearly independent, we can apply Cauchy-Schwarz inequality to $\hat{\beta}$. After some mathematical manipulations, we have

$$\bar{\mathbf{h}}_{srd}^{\mathrm{H}}\mathbf{A}_{e2}\bar{\mathbf{h}}_{srd}=\sum_{p_2=0}^{r_2-1}\left|\beta_{p_2}^{rd}\right|^2\left(\sum_{j=p_2}^{r_2-1}\kappa_j\sum_{i=o}^{p_2}\left|\beta_i^{sr}\right|^2\right) \tag{2.15}$$

where κ_j's are the eigenvalues of $\mathbf{A}_{e2}$. Substituting (2.15) in (2.13), we have

$$P_s\left(\mathbf{S}\to\hat{\mathbf{S}}\middle|\,\mathbf{h}_{srd}\right)\leq\Lambda_{sd}\exp\left(-\hat{K}^2\frac{\gamma}{4}\sum_{p_2=0}^{r_2-1}\left|\beta_{p_2}^{rd}\right|^2\left(\sum_{j=p_2}^{r_2-1}\kappa_j\sum_{i=o}^{p_2}|\beta_i^{sr}|^2\right)\right) \tag{2.16}$$

Averaging (2.16) over $\left|\beta_{p_2}^{rd}\right|$ and $|\beta_i^{sr}|$, and defining

$$\begin{aligned}\Lambda_{srd}=&\\ &\prod_{p_2=0}^{r_2-1}\prod_{j=p_2}^{r_2-1}\prod_{i=0}^{p_2}\int_0^\infty\int_0^\infty 4\left|\beta_i^{sr}\right|\left|\beta_{p_1}^{sd}\right|e^{\left(-\hat{K}^2\frac{\gamma}{4}\kappa_j\left|\beta_{p_2}^{rd}\right|^2\left|\beta_i^{sr}\right|^2-\left|\beta_{p_2}^{rd}\right|^2-\left|\beta_i^{sr}\right|^2-u_{sr}-u_{rd}\right)}\\ &\qquad\times I_0\left(\left|\beta_i^{sr}\right|+u_{sr}\right)I_0\left(\left|\beta_{p_2}^{rd}\right|+u_{sd}\right)d\beta_i^{sr}d\beta_{p_2}^{rd}\end{aligned} \tag{2.17}$$

yields

$$P_r\left(\mathbf{S}\to\hat{\mathbf{S}}\right)\leq\Lambda_{sd}\Lambda_{srd} \tag{2.18}$$

We have $P_r\left(\mathbf{S}\to\hat{\mathbf{S}}\right)$ as the unconditional PEP expression, while Λ_{sd} and Λ_{srd} can be found by numerically computing the integral expressions of (2.13) and (2.17) through the random generation of the proper statistics via Monte-Carlo techniques.

The relatively low-heights of the antennas on the communicating vehicles implies that the LOS communication can easily be blocked by an obstruction, either static (immovable objects, such as buildings or terrain features, like crests, hills and foliage) or mobile (such as (parked/non-parked) vehicles on the road). However, it is reasonable to expect that a significant portion of the V2V communication will be bound to the road surface, especially in highway environments, thus making the LOS between two communicating nodes susceptible to interruptions by other vehicles. Even in urban areas, it is likely that other vehicles, especially large public transportation and commercial vehicles such as buses and trucks, will often obstruct the LOS i.e., [29, 67–71] and the references therein. In the following,

we will study the case where the LOS is obstructed. This leads to Rayleigh channel model which is in fact a special case of the Rician channel.

Starting from (2.10) and averaging the resulting expression with respect to $\left|\beta_{p_1}^{sd}\right|$ which is assumed to be Rayleigh distributed, we obtain

$$P_s\left(\mathbf{S}\to\hat{\mathbf{S}}\middle|\,\mathbf{h}_{srd}\right)\leq\exp\left(-K^2\mathbf{h}_{srd}^{\mathrm{H}}\boldsymbol{\chi}_2\mathbf{h}_{srd}\frac{\gamma}{4}\right)\prod_{p_1=0}^{r_1-1}\left(\frac{4}{4+\lambda_{p_1}\gamma}\right) \tag{2.19}$$

We now need to average (2.19) over $\mathbf{h}_{srd}$. Following similar steps above and defining $\bar{\mathbf{h}}_{srd}$ with its p_2^{th} element $\hat{\beta}=\left|\sum_{g=0}^{p_2}\beta_{p_2-g}^{rd}\beta_g^{sr}\right|^2$. Since $\beta_{p_2-g}^{rd}$ and β_g^{sr} are linearly independent, we can apply Cauchy-Schwarz inequality to $\hat{\beta}$. After some mathematical manipulations, we have

$$\bar{\mathbf{h}}_{srd}^{\mathrm{H}}\mathbf{A}_{e2}\bar{\mathbf{h}}_{srd}=\sum_{p_2=0}^{r_2-1}\left|\beta_{p_2}^{rd}\right|^2\left(\sum_{j=p_2}^{r_2-1}\kappa_j\sum_{i=o}^{p_2}\left|\beta_i^{sr}\right|^2\right) \tag{2.20}$$

where κ_j's are the eigenvalues of $\mathbf{A}_{e2}$. Substituting $z_{p_2}=\sum_{j=p_2}^{r_2-1}\kappa_j\sum_{i=o}^{p_2}\left|\beta_i^{sr}\right|^2$ and (2.20) in (2.19), we have

$$P_s\left(\mathbf{S}\to\hat{\mathbf{S}}\middle|\,\underset{p_2=0,..,r_2-1}{\beta_{p_2}^{rd}},\underset{p_2=0,..,r_2-1}{\beta_{p_2}^{sr}}\right)\leq\exp\left(-K^2\sum_{p_2=0}^{r_2-1}\left|\beta_{p_2}^{rd}\right|^2z_{p_2}\frac{\gamma}{4}\right)\prod_{p_1=0}^{r_2-1}\left(\frac{4}{4+\lambda_{p_1}\gamma}\right) \tag{2.21}$$

Averaging (2.21) over $\left|\beta_{p_2}^{rd}\right|$ yields

$$P_s\left(\mathbf{S}\to\hat{\mathbf{S}}\right)\leq\prod_{p_2=0}^{r_2-1}\underset{z_{p_2}}{\mathbb{E}}\left(\frac{4}{4+K^2z_{p_2}\gamma}\right)\prod_{p_1=0}^{r_1-1}\left(\frac{4}{4+\lambda_{p_1}\gamma}\right) \tag{2.22}$$

Note that $z_{p_2}>0$ is the sum of different exponential random variables resulting in the 'hypoexponential distribution' also known as the 'generalized Erlang distribution' [72, 73].

Its pdf is given by

$$p\left(z_{p_2}\right)=\left(\prod_{i=0}^{r_2-1-p_2}\kappa_i\right)\sum_{j=0}^{r_2-1-p_2}\frac{\exp\left(-\kappa_j z_{p_2}\right)}{\prod\limits_{\substack{k\neq j\\k=0}}^{r_2-1-p_2}\left(\kappa_k-\kappa_j\right)} \tag{2.23}$$

Using (2.23), we can evaluate the expectation term in (2.22) and have the unconditional PEP as

$$P_s\left(\mathbf{S}\rightarrow\hat{\mathbf{S}}\right)\leq\left(\prod_{p_1=0}^{r_1-1}\frac{4}{4+\lambda_{p_1}\gamma}\right)\left(\prod_{p_2=0}^{r_2-1}\frac{4}{K^2\gamma}\right)\left(\prod_{p_3=0}^{r_2-1}\left(\prod_{i=0}^{r_2-1-p_3}\kappa_i\sum_{j=0}^{r_2-1-p_3}\left(\delta_j\Gamma\left(0,\frac{4\kappa_j}{K^2\gamma}\right)\right)\right)\right) \tag{2.24}$$

where $\delta_j=\exp\left(-4\kappa_j/(K^2\gamma)\right)\Big/\prod_{k\neq j,k=0}^{r_2-1-p_2}\left(\kappa_k-\kappa_j\right)$ and $\Gamma\left(0,x\right)$ is the incomplete gamma function. From (2.24), we observe that the first and second terms have the SNR raised to the order of r_1+r_2 . From (2.14), define $L_{srd}=\min\left(L_{sr},L_{rd}\right)$ and $Q_{srd}=\min\left(Q_{sr},Q_{rd}\right)$. This will result in a diversity gain of

$$r_1+r_2=\left(L_{sd}+1\right)\left(Q_{sd}+1\right)+\left(L_{srd}+1\right)\left(Q_{srd}+1\right) \tag{2.25}$$

Note that the third term in (2.24) involves an exponential function and incomplete Gamma function. This results in slower asymptotic convergence towards the maximum diversity order.

In the highway/suburban areas scenario, source and relaying vehicles are assumed to be traveling in same direction with similar speeds. This results in a relative velocity nearly equal to zero, hence leading to a time-flat and frequency-flat fading in S→R link. On the other hand, S→D and R→D links are still modeled as doubly-selective fading. Under this assumption, we replace $\sum\mathbf{D}\left(w_q\right)\mathbf{H}_{sr,q}^{(0)}\left(n\right)$ with $h_{sr}\left(n\right)$, $\mathbf{\Phi}_{srd}\left(n\right)$ with $\mathbf{\Phi}\left(n\right)$ and

$\mathbf{h}_{srd}(n)$ with $h_{sr}(n)\,\mathbf{h}_{rd}(n)$ in (2.2). Furthermore, the channel vector in (2.14) will have the form $\mathbf{h}_{srd} = [h_{sr}h_{rd}(0) \quad h_{sr}h_{rd}(1) \quad \ldots \quad h_{sr}h_{rd}(N_t-1)]^{\mathrm{T}}$ with $r_2 := \mathrm{rank}\,(\mathbf{C}_{h,srd}) = 1$. Consequently, the PEP expression in (2.24) reduces to a form of

$$P_h\left(\mathbf{S}\to\hat{\mathbf{S}}\right) \le \frac{4}{K^2\gamma}\left(\prod_{p_1=0}^{r_1-1}\frac{4}{4+\lambda_{p_1}\gamma}\right)\left(\prod_{i=0}^{r_2-1}\kappa_i\sum_{j=0}^{r_2-1}\left(\delta_j\Gamma\left(0,\frac{4\kappa_j}{K^2\gamma}\right)\right)\right) \tag{2.26}$$

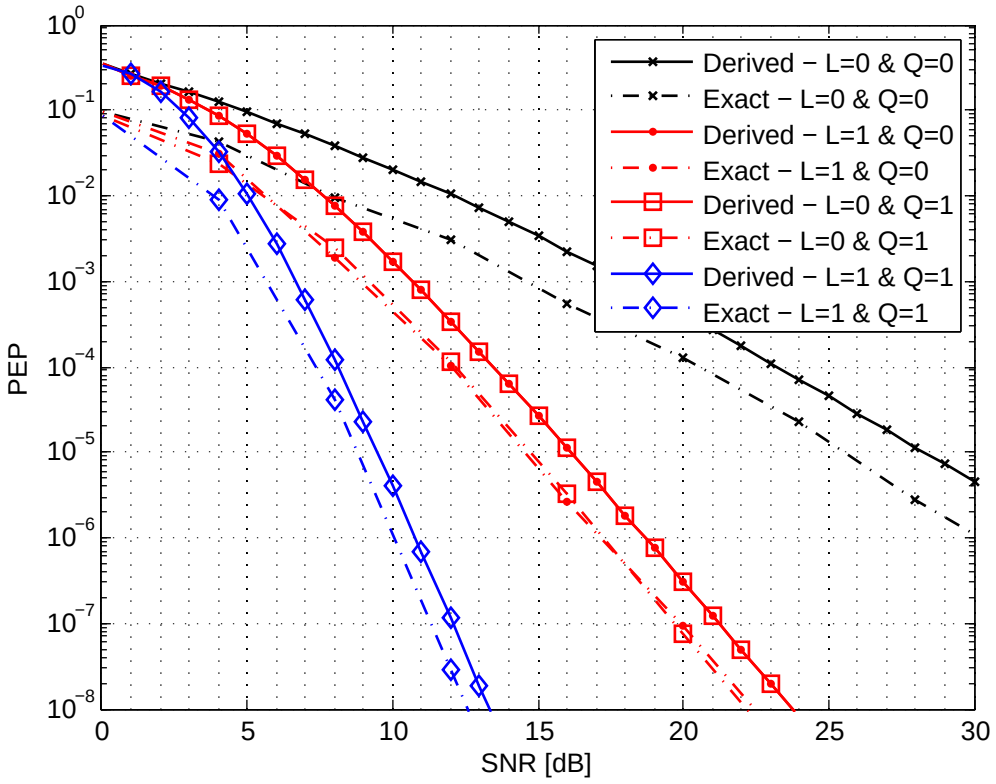

Figure 2.5: Comparison of derived PEP in (2.24) and exact PEP in (2.7) for SISO scheme.

From (2.26), we observe that the first and second terms have the SNR raised to the order of r_1+1 yielding a diversity gain $(L_{sd}+1)\,(Q_{sd}+1)+1$. This is obviously less than what is gained from (2.24) as a result of the lacking time- and multipath- diversity in the S→R link. This observation is consistent with the results of [74] which states that the

diversity gain from the S→R→D link is restricted to the minimum of the S→R and R→D diversity gains.

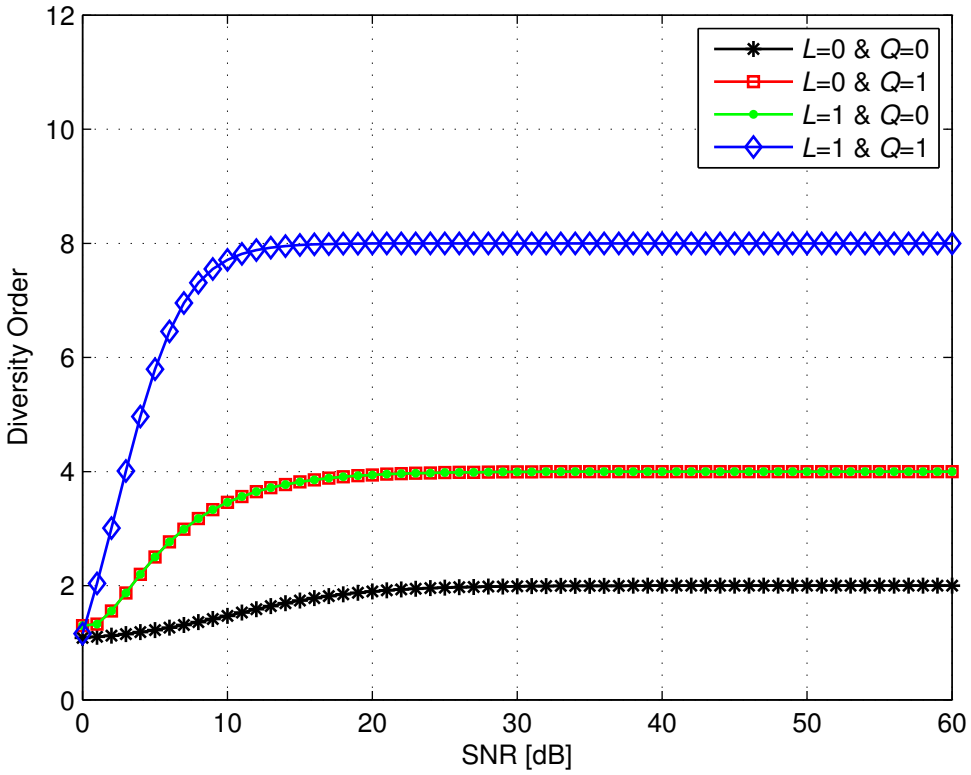

Figure 2.6: Diversity order of the V2V-SISO cooperative scheme.

Finally, we verify the accuracy of the derived PEPs comparing them with the exact PEP. Exact PEP can be found by numerically computing the conditional PEP of (2.7) through the random generation of $\mathbf{h}$ with proper statistics via Monte-Carlo techniques. As an example, we assume precoder parameters $P = 2$ and $Z = 2$. In Figure 2.5, we compare the derived PEP given by (2.24) with the exact one. We observe that they are in good agreement and the derived expression lies within ≈ 2 dB of the exact PEP. We further plot $-\log P\left(\mathbf{S} \to \hat{\mathbf{S}}\right) \Big/ \log(\gamma)$ in Figure 2.6, to precisely observe the slope of the PEPs. It

is clearly seen from Figure 2.6 that diversity gains of 2, 4, and 8 are obtained as expected from (2.25).

2.2.2 MIMO Cooperation

After dropping the block indices $n-1$ and n in (2.6) for convenience of the presentation, the exact PEP is given by (2.7) and the $\mathbf{S}$ matrix that holds the transmitted data information is now represented in terms of $\mathbf{S}_1$ and $\mathbf{S}_2$ earlier defined. The Euclidean distance conditioned on the fading channel coefficients is $d^2\left(\mathbf{S}\to\hat{\mathbf{S}}\middle|\,\mathbf{h}\right)=\mathbf{h}_1^{\mathrm{H}}\boldsymbol{\Delta}_1\mathbf{h}_1+\mathbf{h}_2^{\mathrm{H}}\boldsymbol{\Delta}_2\mathbf{h}_2+\mathbf{h}_1^{\mathrm{H}}\boldsymbol{\Delta}_3\mathbf{h}_2+\mathbf{h}_2^{\mathrm{H}}\boldsymbol{\Delta}_4\mathbf{h}_1$ where $\boldsymbol{\Delta}_1=\left(\mathbf{S}_1-\hat{\mathbf{S}}_1\right)^{\mathrm{H}}\left(\mathbf{S}_1-\hat{\mathbf{S}}_1\right)$, $\boldsymbol{\Delta}_2=\left(\mathbf{S}_2-\hat{\mathbf{S}}_2\right)^{\mathrm{H}}\left(\mathbf{S}_2-\hat{\mathbf{S}}_2\right)$, $\boldsymbol{\Delta}_3=\left(\mathbf{S}_1-\hat{\mathbf{S}}_1\right)^{\mathrm{H}}\left(\mathbf{S}_2-\hat{\mathbf{S}}_2\right)$ and $\boldsymbol{\Delta}_4=\left(\mathbf{S}_2-\hat{\mathbf{S}}_2\right)^{\mathrm{H}}\left(\mathbf{S}_1-\hat{\mathbf{S}}_1\right)$. Defining $\boldsymbol{\chi}_{a,b}(\mathcal{J})=([\hat{\mathbf{S}}_a^{\mathrm{H}}]_{\mathcal{J},\mathcal{J}}-[\hat{\mathbf{S}}_b^{\mathrm{H}}]_{\mathcal{J},\mathcal{J}})([\hat{\mathbf{S}}_a]_{\mathcal{J},\mathcal{J}}-[\hat{\mathbf{S}}_b]_{\mathcal{J},\mathcal{J}})$, where $\mathcal{J}\in\{1,2,\ldots,N_t\}$ and $a,b\in\{1,2\}$, we can rewrite (2.8) as

$$P_m\left(\mathbf{S}\to\hat{\mathbf{S}}\middle|\,\mathbf{h}_1,\mathbf{h}_2\right)\leq\exp\left(-\left(\sum_{a=1}^{2}\sum_{b=1}^{2}\mathbf{h}_a^{\mathrm{H}}\boldsymbol{\chi}_{a,b}\mathbf{h}_b\right)\frac{\gamma}{4}\right) \tag{2.27}$$

We need to average (2.27) over $\mathbf{h}_1$ and $\mathbf{h}_2$. Using the eigenvectors decomposition for the channel vectors $\mathbf{h}_{sd}^{(a,b)}(n-1)$ and $\mathbf{h}_{sd}^{(a,b)}(n)$, we have

$$\begin{aligned}&P_m\left(\mathbf{S}\to\hat{\mathbf{S}}\middle|\,\underset{c\in\{5,6,7,8\}}{[\mathbf{h}_1]_{c,1},[\mathbf{h}_2]_{c,1}}\right)\\&\quad\leqslant\exp\left(-\left(\sum_{a=1}^{2}\sum_{b=1}^{2}\mathbf{h}_a^{\mathrm{H}}\boldsymbol{\chi}_{a,b}\mathbf{h}_b\right)\frac{\gamma}{4}\right)\left(\sum_{l=1}^{2}\prod_{\mathfrak{e}(l)=1}^{4}\prod_{p_{\mathfrak{e}(l)}=0}^{r_{\mathfrak{e}(l)}-1}\left(\frac{4}{4+\sqrt{G_{sd}/2}\lambda_{p_{\mathfrak{e}(l)}}\gamma}\right)\right)\end{aligned} \tag{2.28}$$

where the indices $\mathfrak{e}(l)\in\{1,2,3,4\}$ are associated sequentially for autocorrelation matrices $\mathbf{C}_{h,sd}^{(a,b)}:=\mathbb{E}[(\mathbf{h}_{sd}^{(a,b)})^{\mathrm{H}}\mathbf{h}_{sd}^{(a,b)}]$ with ranks $r_{\mathfrak{e}(l)}$. The eigenvector entries for the associated

links are given by $\lambda_{p_{\mathfrak{e}(l)}}$. We now need to average (2.28) over $\mathbf{H}_{rd}^{(1,b)}(n-1)\,\mathbf{h}_{sr}^{(a,1)}(n-1)$ and $\mathbf{H}_{rd}^{(1,b)}(n)\,(\mathbf{h}_{sr}^{(a,1)}(n))^*$. Following similar steps as in Section 2.2, we obtain the unconditional PEP as

$$P_m\left(\mathbf{S}\to\hat{\mathbf{S}}\right)\leqslant\left(\sum_{l=1}^{2}\prod_{\mathfrak{e}(l)=1}^{4}\prod_{p_{\mathfrak{e}(l)}=0}^{r_{\mathfrak{e}(l)}-1}\left(\frac{4}{4+\sqrt{G_{sd}/2}\lambda_{p_{\mathfrak{e}(l)}}\gamma}\right)\right)$$
$$\times\left(\sum_{k=1}^{2}\prod_{\mathfrak{g}(k)=5}^{8}\left(\prod_{p_2=0}^{r_{\mathfrak{g}(k)}-1}\frac{4}{K_k^2\gamma}\left(\prod_{p_3=0}^{r_{\mathfrak{g}(k)}-1}\left(\prod_{i_{\mathfrak{g}(k)}=0}^{r_{\mathfrak{g}(k)}-1-p_3}\kappa_{i_{\mathfrak{g}(k)}}\sum_{j_{\mathfrak{g}(k)}=0}^{r_{\mathfrak{g}(k)}-1-p_3}\left(\delta_{j_{\mathfrak{g}(k)}}\Gamma\left(0,\frac{4\kappa_{j_{\mathfrak{g}(k)}}}{K_k^2\gamma}\right)\right)\right)\right)\right)\right)\right) \tag{2.29}$$

where

$$\mathbf{R}_{h,srd}^{(a,b)}(n-1):=\mathbb{E}[(\mathbf{H}_{rd}^{(1,b)}(n-1)\mathbf{h}_{sr}^{(a,1)}(n-1))^{\mathrm{H}}(\mathbf{H}_{rd}^{(1,b)}(n-1)\mathbf{h}_{sr}^{(a,1)}(n-1))]$$

and

$$\mathbf{R}_{h,srd}^{(a,b)}(n):=\mathbb{E}[(\mathbf{H}_{rd}^{(1,b)}(n)(\mathbf{h}_{sr}^{(a,1)}(n))^*)^{\mathrm{H}}(\mathbf{H}_{rd}^{(1,b)}(n)(\mathbf{h}_{sr}^{(a,1)}(n))^*)]$$

with rank $r_{\mathfrak{g}(k)}$.

The eigenvector entries for the associated links are given by $\kappa_{i_{\mathfrak{g}(k)}}$. From (2.29), we observe that an asymptotical diversity gain of

$$\begin{aligned}\min_{l\in\{1,2\}}\left(4r_{\mathfrak{e}(l)}\right)+\min_{k\in\{1,2\}}\left(4r_{\mathfrak{g}(k)}\right)&\\ =\sum_{a=1}^{2}\sum_{b=1}^{2}\left(\left(L_{sd}^{a,b}+1\right)\left(Q_{sd}^{a,b}+1\right)\right)&\\ +\sum_{a=1}^{2}\sum_{b=1}^{2}\left(\left(\min\left(L_{sr}^{a,1},L_{rd}^{1,b}\right)+1\right)\left(\min\left(Q_{sr}^{a,1},Q_{rd}^{1,b}\right)+1\right)\right)&\end{aligned} \tag{2.30}$$

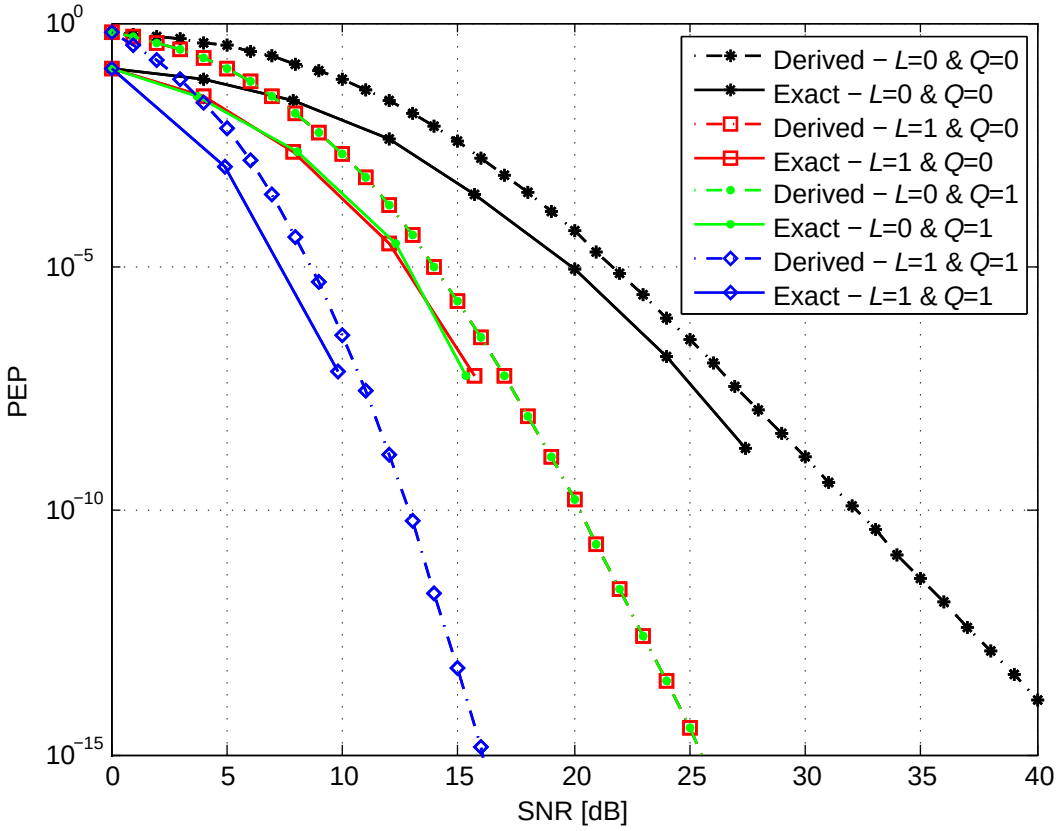

Figure 2.7: Comparison of the derived PEP in (2.29) and the exact PEP in (2.7) for the MIMO scheme.

is available. In the highway/suburban areas scenario, the diversity order reduces to

$$\min_{l\in\{1,2\}}\left(4r_{\mathfrak{e}(l)}\right)+\min_{k\in\{1,2\}}\left(4r_{\mathfrak{g}(k)}\right)=\sum_{a=1}^{2}\sum_{b=1}^{2}\left(\left(L_{sd}^{a,b}+1\right)\left(Q_{sd}^{a,b}+1\right)\right)+4 \tag{2.31}$$

In Figure 2.7, to verify the accuracy of the derived PEPs, we compare the derived PEP given by (2.29) with the exact one based on (2.7). The system and channel parameters of Figure 2.5 are used here as well. From Figure 2.7, we observe that the derived expression provides a good match with the exact PEP lying within ≈ 2 dB apart. It can be verified from asymptotical PEP evaluation that diversity gains of 5, 10 and 20 are obtained as

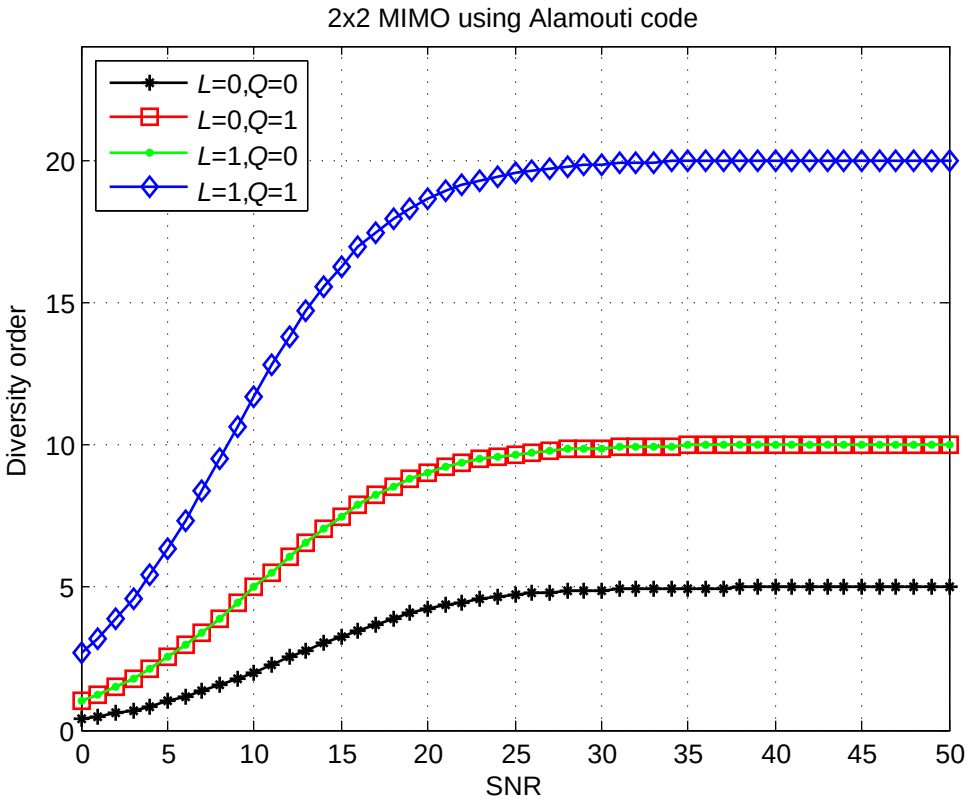

Figure 2.8: Diversity order of the V2V-MIMO cooperative scheme.

expected from (2.30) as illustrated in Figure 2.8.

2.3 Channel Estimation

In the PEP derivation, we have assumed perfect-CSI at the receiver side. We now discuss how the channel can be estimated and discuss the effect of imperfect-CSI on the PEP.

2.3.1 Pilot Symbol Assisted Channel Estimation

In the cooperative scheme under consideration, we need to estimate the direct S→D channel and indirect S→R→D channel. For the estimation of indirect channel, based on whether the relay terminal is equipped with a channel estimator or not, we can consider two strategies which are named in [75] as *cascaded channel estimation* (C-CE) and *disintegrated channel estimation* (D-CE). In D-CE method, the relaying path is disintegrated into S→R and R→D channels that are, respectively, estimated at the relay and destination terminals. This requires the relay terminal be equipped with a channel estimator and feed-forward a quantized version of the source-to-relay channel estimate to the destination terminal. In this work, we will consider C-CE method. In this method, the cascaded channel is estimated at the destination terminal avoiding the need for channel estimation at the relay terminal.

We adopt pilot assisted channel estimation (PACE) technique [58] that relies on the insertion of known pilot symbols in information-bearing data. The known symbols are inserted periodically into the data sequence. Assume that the received pilot symbols are denoted by a vector $\mathbf{v}$ with length m_p. Following the well-known minimum mean square estimation (MMSE) technique, a Wiener filter is used to minimize the variance of the estimation error. The estimated channel vector is given by

$$\hat{\mathbf{h}}\,(n) = \mathbf{x}_f \mathbf{v} \tag{2.32}$$

where $\hat{\mathbf{h}}\,(n)$ is the augmented estimated channel vector, defined for the SISO case in (2.5) as $\hat{\mathbf{h}}(n) = [\ \hat{\mathbf{h}}_{sd}(n) \quad \hat{\mathbf{h}}_{srd}(n)\ ]^{\mathrm{T}}$, is the corresponding set of the filter coefficients optimized

for minimizing the estimation error variance and is given by

$$\mathbf{x}_f = \mathbf{C}^{-1}\mathbf{w}_c \tag{2.33}$$

Here, $\mathbf{w}_c$ is the optimum interpolation coefficient matrix of the estimator, and $\mathbf{C}$ is the received pilots' vector $\mathbf{v}$ autocorrelation matrix. Let $q_p = (E_P/((N_t-1)E_s)))$ be the ratio of the pilot power E_p to the data power E_s. Define n_s as the number of bits per symbol and $c = q_p n_s\left(N_t-1\right)/\left(1+q_p\right)$, therefore, we have $\sigma_{\mathbf{h}}^2 = \gamma c/|E_p|^2$, and $\mathbf{C} = \gamma c\tilde{\mathbf{C}} + \mathbf{I}$ with $\tilde{\mathbf{C}}$ as the normalized channel autocorrelation matrix. The normalized double Doppler channels' autocorrelation matrix has entries of $\tilde{\mathbf{C}}\left(\tau\right) = J_0\left(2\pi v_1\tau/\lambda\right)J_0\left(2\pi v_2\tau/\lambda\right)$, and the optimum interpolation matrix is given by

$$\mathbf{w}_c = \gamma c\tilde{R}\Big/E_p^* \tag{2.34}$$

In Appendix A, we investigate the effect of imperfect-CSI through an asymptotical PEP analysis where we prove that imperfect-CSI on time-varying channels severely degrades performance and error floors occurs. In MIMO case, channel estimation can be performed in a similar manner by first shutting off one transmit antenna and estimating the other individual channel, then repeating the same for the second antenna.

2.4 Simulation Results

In this section, we present simulation results for the error rate performance of the cooperative vehicular schemes under consideration. In our Monte-Carlo simulations, we assume path loss coefficient $\alpha = 2$, $\theta = \pi$, $G_{sr}/G_{rd} = -30$ dB and 4-QAM modulation. Maximum velocities for source, relay and destination vehicles are assumed to be equal to 60km/h. In

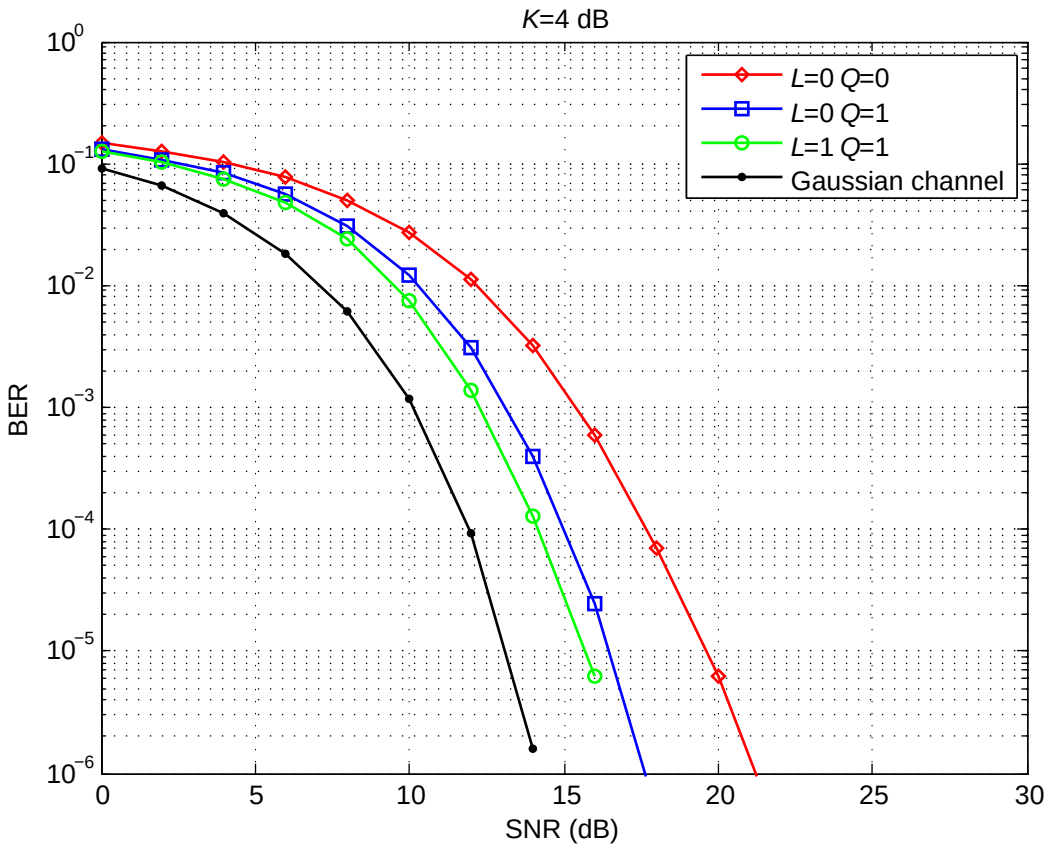

Figure 2.9: BER performance of the cooperative SISO scheme for the urban scenario and Rician fading channels.

line with the IEEE 802.11p standards, we choose an operating frequency of $f_c = 5.9$GHz. For the traffic densities under consideration, the maximum delay spreads are $\tau_d = 1.113$ μs and 1.773 μs [44]. Assuming symbols duration of $T_{\rm s} = 48\mu s$ [76], we have the number of multipaths $L \in (0, 1)$ calculated through $L = \lceil \tau_d / T_s \rceil$. For $P = 2$ and $Z = 2$, we have the number of Doppler shifts $Q \in (0, 1)$, therefore we consider the possible L and Q combinations as $(L, Q) \in \{(0, 0), (0, 1), (1, 0), (1, 1)\}$.

In Figure 2.9, we consider the city/urban scenario and perfect-CSI at the receiver side. We assume Rician fading channel and Rician K-factor = 4dB [69]. Figure 2.9 present

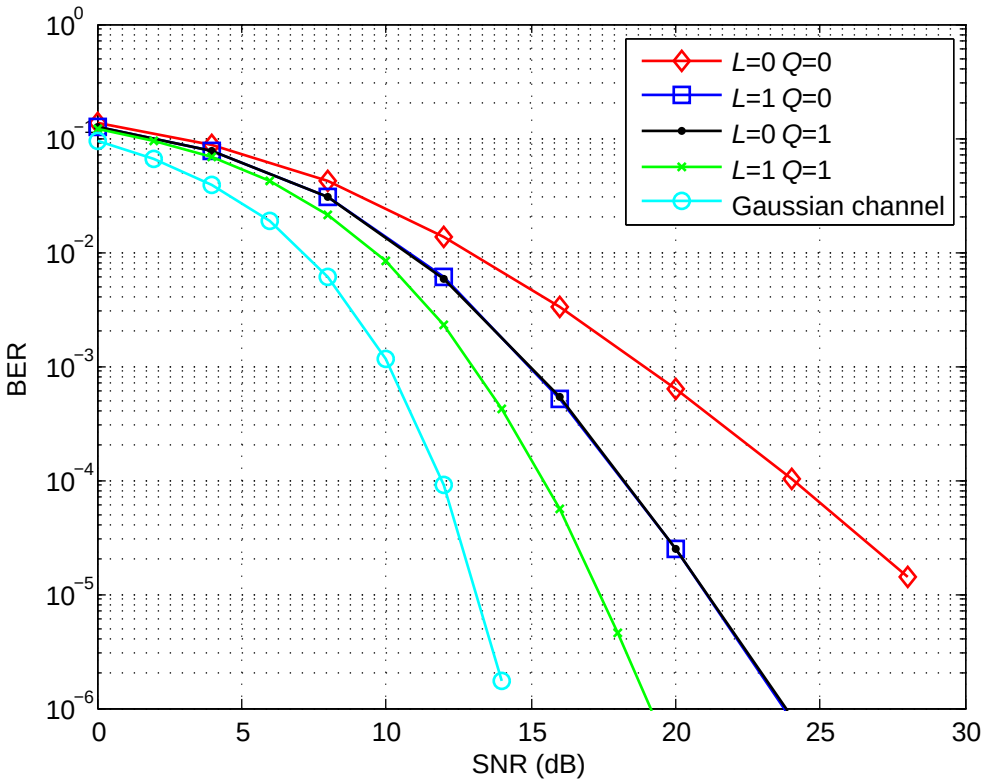

Figure 2.10: BER performance of the cooperative SISO scheme for the urban scenario and Rayleigh fading channels.

the bit error rate (BER) performance of SISO cooperative transmission over doubly-selective channels using Monte-Carlo simulations. We include the performance of cooperative scheme over frequency- and time-flat channel (i.e., $L = 0$ and $Q = 0$) as a benchmark, as well as the AWGN channel. We observe that as the number of the resolvable multipath components (L) and/or the number of Doppler shifts (Q) increase, significant improvements are observed through precoding that takes advantages of diversity gains. For example at a target BER of 10^{-4}, the precoded system over a channel with $L = 0$ and $Q = 1$ is 2.5 dB superior to the benchmark curve. This performance improvement climbs up to 3.5 dB for $L = 1$ and $Q = 1$. Our results demonstrate that, if properly exploited,

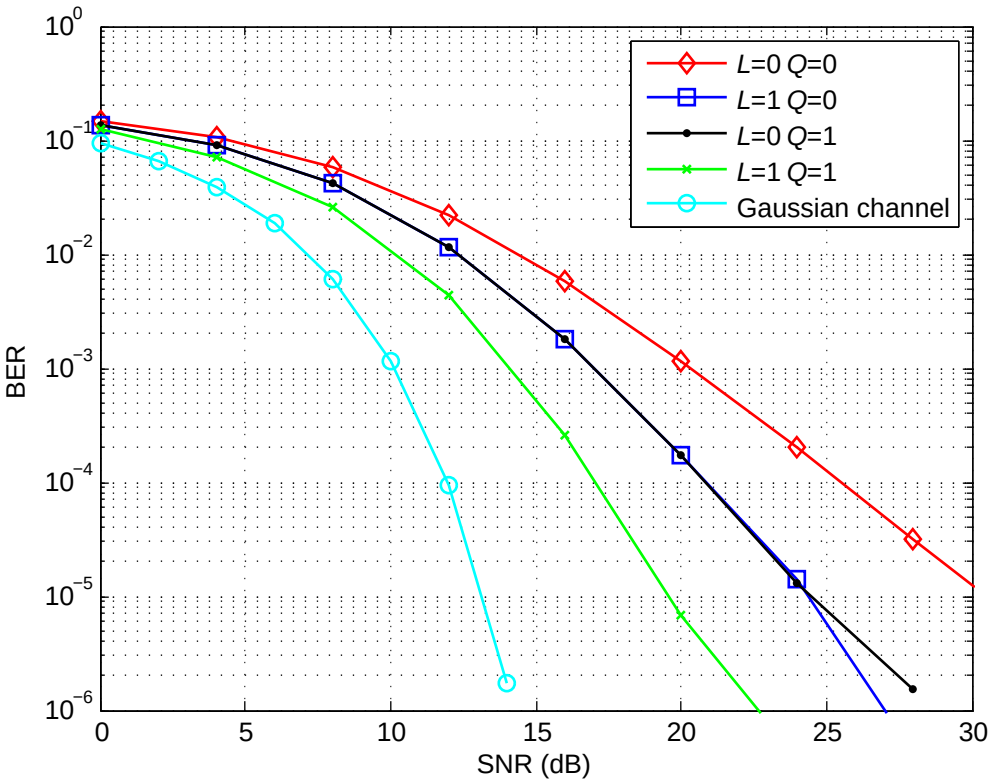

Figure 2.11: BER performance of the cooperative SISO scheme for the highway scenario and Rayleigh fading channels.

the performance can be improved for channels with higher time and spectral variations.

In Figure 2.10, again we consider the city/urban scenario, assume perfect-CSI at the receiver side, and present the bit error rate (BER) performance of SISO cooperative transmission over doubly-selective channels using Monte-Carlo simulations for a Rayleigh fading channel. We observe that as the number of the resolvable multipath components (L) and/or the number of Doppler shifts (Q) increase, significant improvements are observed through precoding that takes advantages of diversity gains. For example at a target BER of 10^{-4}, the precoded system over a channel with $L = 0$ and $Q = 1$ is 6 dB superior to the benchmark curve. This performance improvement climbs up to 9 dB for $L = 1$ and $Q = 1$.

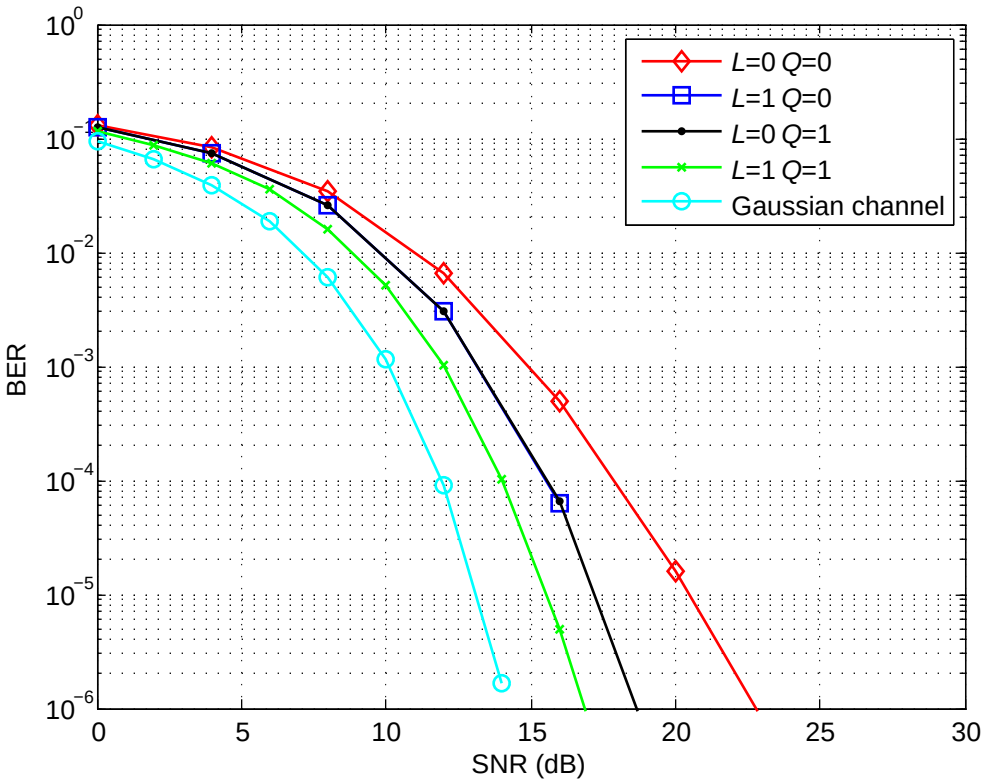

Figure 2.12: BER performance of the cooperative MIMO scheme using Alamouti STBC and Rayleigh fading channels.

Our results demonstrate that, if properly exploited, the performance can be improved for channels with higher time and spectral variations. However, when compared to the Rician fading channel case in Figure 2.9, we find that higher SNR is required to attain the same BER due to the absence of LOS component.

In Figure 2.11, we consider the highway/urban scenario and a Rayleigh fading channel. In comparison to previous city/urban scenario, for ($L = 0$, $Q = 1$) and ($L = 1$, $Q = 1$), the improvements in the BER curves reduce to 4 dB and 7 dB, respectively. This is as a result of the fact that the diversity order achieved in the S→R→D link is restricted by the frequency-flat and time-flat characteristics of the S→R link.

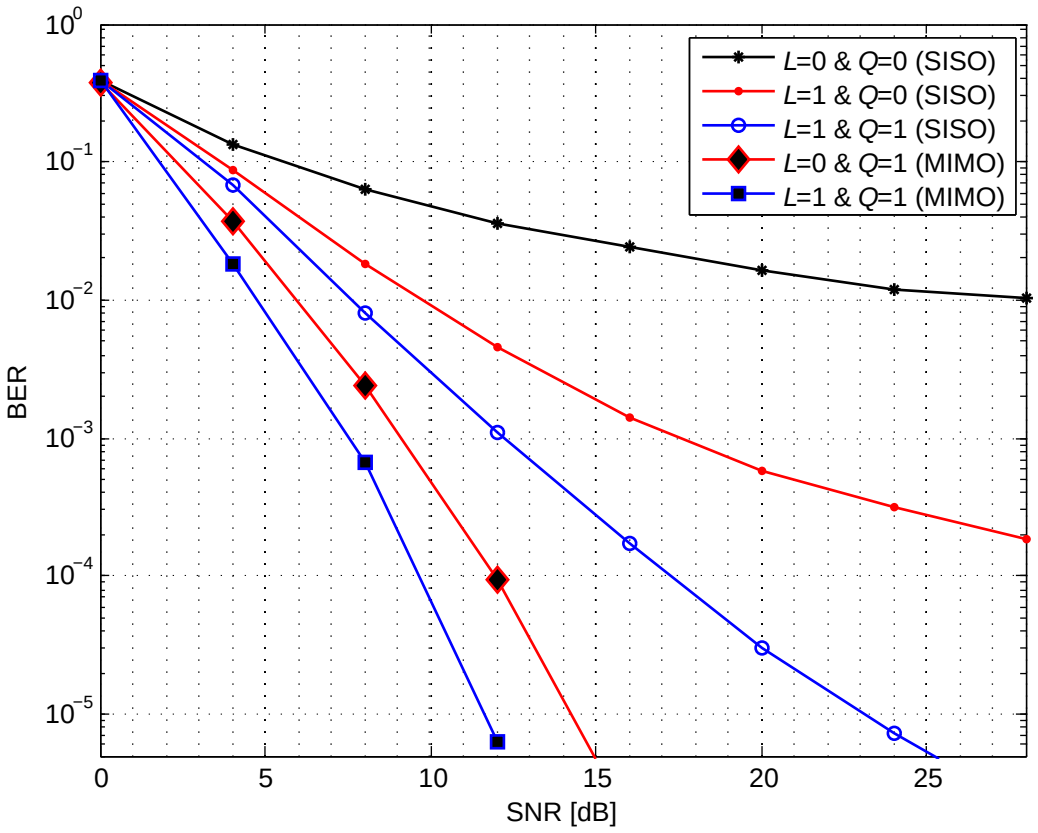

Figure 2.13: The effect of imperfect channel estimation on the error rate performance and Rayleigh fading channels.

In Figure 2.12, we consider the city/urban scenario, assuming perfect-CSI at the receiver side, for a Rayleigh fading channel, and present the performance of MIMO cooperative transmission over doubly-selective channels. Similar to the SISO case, we observe that the scheme benefits from the increase in the number of the resolvable multipath components and/or the number of Doppler shifts. Furthermore, compared to the single antenna setting, we notice a reduction in the required transmit power due to the use of STBC. For example, at a target BER of 10^{-4}, we need only SNR=13.5 dB. This is 2 dB less than we observed in Figure 2.10 for the SISO scheme.

In Figure 2.13, we assume for a Rayleigh fading channel and investigate the effect of imperfect channel estimation on the BER of SISO and MIMO schemes through simulation. A single known pilot symbol is inserted periodically in each input block $\mathbf{s}(n)$. A sliding window covering a total of 11 pilots from preceding and following blocks is used for the channel estimation of a fading coefficient in a particular data slot. In this figure, we assume $L \in (0, 1)$ and $Q \in (0, 1)$. As observed from Figure 2.13 and proved in Appendix A, imperfect-CSI on time-varying channel severely degrades performance and error floors occurs for small values of L and Q. It is observed that imperfect channel estimate severely degrades the performance for SISO transmission and results in error floors. This observation confirms the error floor effect observed through the mathematical analysis presented in Section 2.3. On the other hand, due to extra spatial diversity, the MIMO cooperative transmission is able to suppress the error floor in the simulated SNR ranges.

2.5 Conclusions

In this chapter, we have investigated the performance of V2V communications assuming doubly-selective fading channels and double-ring channel second-order statistics for SISO and MIMO cooperation scenarios. To extract the underlying rich multipath-Doppler-spatial diversity over the doubly-selective relaying channel, we have employed precoded cooperative transmission. Through the derivation of PEP, we have analyzed the achievable diversity gains. We have presented Monte-Carlo simulation results for the error rate performance to confirm the analytical derivations and further discussed the effect of imperfect channel estimation.

Chapter 3

Road-to-Vehicle Cooperative Communications

In this chapter, we consider road-to-vehicle (R2V) cooperative communications in which roadside access points use vehicles as relaying terminals. This can be particularly useful in suburban or remote areas where the frequent deployment of roadside access points is not either possible or cost-effective. For the doubly-selective vehicular channel under consideration, we employ a precoded cooperative transmission technique to extract the underlying rich multipath-Doppler-spatial diversity. Under the assumption of DF relaying, we derive a PEP expression and demonstrate the achievable diversity gains. Furthermore, we investigate relay selection schemes to take advantage of the potentially large number of relaying vehicles.

The rest of the chapter is organized as follows: In Section 3.1, we describe the proposed two phases dual-hop cooperative R2V systems, extending our work into a best relay-selection from M available relays willing to be involved in the transmission session.

In Section 3.2, we derive the PEP expression and demonstrate the achievable diversity gains. In Section 3.3, we present numerical results to confirm the analytical derivations and provide insight into the system performance. Finally, we conclude in Section 3.4.

3.1 System Model

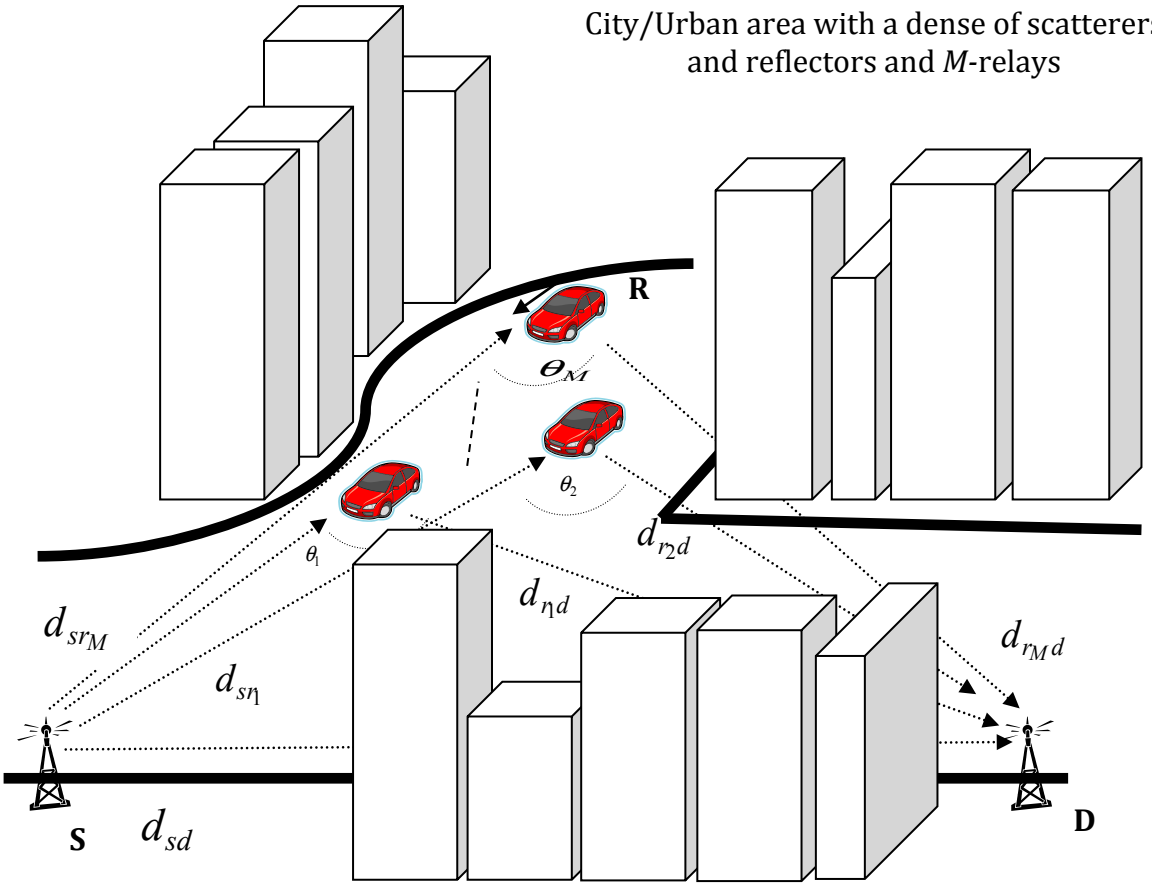

Figure 3.1: Road-to-vehicle cooperative communication, M-relays deployment.

We consider a cooperative scenario (See Figure 3.1 in which a roadside access point (source) communicates with another roadside access point (destination) through a vehicle

that serves as a relaying terminal. Source (S), relay (R) and destination (D) are assumed to be equipped with single transmit and receive antennas, and operate in half-duplex mode. We assume orthogonal cooperation protocol of [17] with DF relaying. In the broadcasting phase, the source transmits its precoded signal to the relaying vehicle and the destination. In the relaying phase, the relay is engaged in forwarding the received signal only if it has decoded correctly, otherwise the relay is silent. The relay decodes and then forwards a fresh decoded copy of the precoded signal to the destination. The destination makes its decision based on the two received signals over broadcasting and relaying phases.

Our aggregate channel model takes into account both small-scale fading and path-loss. Path loss is proportional to d^{α} where α is the path loss coefficient and d is the propagation distance. Let d_{sr_i} and d_{r_id} denotes the distances (S $\rightarrow$ R$_i$) and (R$_i$ $\rightarrow$ D), respectively, $i = 1, 2, \ldots, M$. θ_i is the angle between lines S $\rightarrow$ R$_i$ and R$_i$ $\rightarrow$ D. The relative geometrical gains are now defined as $G_{sr_i} = (d_{sd}/d_{sr_i})^{\alpha}$ and $G_{r_id} = (d_{sd}/d_{r_id})^{\alpha}$. Further defined using the law of cosines as $G_{sr_i}^{-2/\alpha} + G_{r_id}^{-2/\alpha} - 2G_{sr_i}^{-2/\alpha}G_{r_id}^{-2/\alpha}\cos\theta_i = 1$.

As for short-term fading, it should be noted that relay and destination vehicles have low elevation antennas and are located within a highly scattering urban area. This requires considering the local scattering around both transmitter and receivers. The time correlation function will be given by (1.11). For the V2R scenario under consideration, we have a stationary road-side antenna (i.e., $v_2 = 0$). Assuming single Rayleigh distribution with a single Doppler, the power spectrum and time correlation mathematical functions reduce back to have the autocorrelation function and the power spectrum of the complex envelope given by (1.6) and (1.7), respectively, with v_r as the relaying vehicles maximum velocity. The channel satisfies the condition $2f_d\tau_d < 1$. A discrete-time baseband equivalent channel for the doubly-selective channel is given by (2.1).

Similar to Section 2.1.2, the input data blocks (generated from an M-QAM constellation) of length N_t are divided into shorter sub-blocks of length N_s ($N_s \leq N_t$). Let each of these sub-blocks be denoted by $\mathbf{s}(n)$ which will be the input to the linear precoder $\mathbf{\Theta}$ of size $N_s \times N_t$. We have $N_s = PZ$, $N_t = (P+Q)(Z+L)$. The number of the resolvable multipath components is given by $L = \lceil \tau_d / T_s \rceil$ and the number of Doppler shifts experienced over the data block is given by $Q = \lceil N_t T_s f_d \rceil$. For the cooperative scheme under consideration, define $\mathbf{H}_{sd,q}^{(0)}$, $\mathbf{H}_{sr,q}^{(0)}$ and $\mathbf{H}_{rd,q}^{(0)}$ as the lower triangular Toeplitz channel matrices with entries given by (2.1). Let L_{sd}, L_{sr} and L_{rd} denote the channel multipath lengths for the S→D, S→R and R→D links, respectively. Further, let Q_{sd}, Q_{sr} and Q_{rd} denotes the number of resolvable Doppler components for corresponding links.

In the broadcasting phase, the received signals at the relay can be expressed in a matrix form as

$$\mathbf{y}_{sr}(n) = \sqrt{G_{sr} E_s} \sum_{q=0}^{Q} \mathbf{D}(w_q) \mathbf{H}_{sr,q}^{(0)}(n)\, \mathbf{u}(n) + \mathbf{n}_{sr}(n) \tag{3.1}$$

where $\mathbf{u}(n) = \mathbf{\Theta}\mathbf{s}(n)$ is the transmitted data block, $Q = \max(Q_{sd}, Q_{sr}, Q_{rd})$ and E_s is the modulated symbol energy. We have $\mathbf{D}(w_q) := \mathrm{diag}[1, \ldots, \exp(j w_q (N_t - 1))]$ and $\mathbf{n}_{sr}(n)$ the S→R additive white Gaussian noise (AWGN) vector with entries of zero mean and $N_0/2$ variance. Using the commutativity of products of Toeplitz matrices with vectors, we can replace $\mathbf{H}_{sr,q}^{(0)}(n)\mathbf{u}(n)$ with $\mathbf{U}(n)\mathbf{h}_{sr,q}(n)$, and rewrite (3.1) as

$$\mathbf{y}_{sr}(n) = \sqrt{G_{sr} E_s} \sum_{q=0}^{Q} \mathbf{D}(w_q) \mathbf{U}(n)\, \mathbf{h}_{sr,q}(n) + \mathbf{n}_{sr}(n) \tag{3.2}$$

Defining the augmented matrices $\mathbf{h}_{sr}(n) = [\ \mathbf{h}_{sr,0}^{\mathrm{T}}(n) \ \cdots \ \mathbf{h}_{sr,Q}^{\mathrm{T}}(n)\ ]^{\mathrm{T}}$ and $\mathbf{\Phi}(n) =$

$[\ \mathbf{D}(w_0)\mathbf{U}(n) \quad \cdots \quad \mathbf{D}(w_Q)\mathbf{U}(n)]$, we have

$$\mathbf{y}_{sr}(n) = \sqrt{G_{sr}E_s}\mathbf{\Phi}(n)\,\mathbf{h}_{sr}(n) + \mathbf{n}_{sr}(n) \tag{3.3}$$

Similarly, the received signal at the destination during the broadcasting phase is given by

$$\mathbf{y}_{sd}(n) = \sqrt{E_s}\mathbf{\Phi}(n)\,\mathbf{h}_{sd}(n) + \mathbf{n}_{sd}(n) \tag{3.4}$$

where $\mathbf{n}_{sd}(n)$ is the associated S→D AWGN vector with entries of zero mean and $N_0/2$ variance. During the relaying phase, the relay-received signals are fed to the ML detector given by

$$\arg\min_{\bar{\mathbf{s}}} \left\{ \left\| \mathbf{y}_{sr}(n) - \sqrt{G_{sr}E_s} \sum_{q=0}^{Q} \mathbf{D}(w_q)\mathbf{H}_{sr,q}^{(0)}(n)\,\mathbf{\Theta}\bar{\mathbf{s}} \right\|^2 \right\} \tag{3.5}$$

with $\bar{\mathbf{s}}$ as all the possible signal block combination. We implement ideal DF at the relay [77], the relay then forwards a fresh decoded copy of the received precoded signal, i.e., $\dot{\mathbf{u}}(n)$. We have the received signal during the relaying phase at destination

$$\mathbf{y}_{rd}(n) = \sqrt{G_{rd}E_s}\dot{\mathbf{\Phi}}(n)\,\mathbf{h}_{rd}(n) + \mathbf{n}_{rd}(n) \tag{3.6}$$

where $\mathbf{n}_{rd}(n)$ is the associated R→D AWGN vector with entries of zero mean and $N_0/2$ variance. $\dot{\mathbf{\Phi}}(n) = [\ \mathbf{D}(w_0)\dot{\mathbf{U}}(n) \quad \cdots \quad \mathbf{D}(w_Q)\dot{\mathbf{U}}(n)\ ]$. Finally, arranging (3.4) and (3.6) in matrix form, we have

$$\underbrace{\begin{bmatrix} \mathbf{y}_{sd}(n) \\ \mathbf{y}_{rd}(n) \end{bmatrix}}_{\mathbf{Y}(n)} = \underbrace{\sqrt{E_s}\begin{bmatrix} \mathbf{\Phi}(n) & 0 \\ 0 & \sqrt{G_{rd}}\dot{\mathbf{\Phi}}(n) \end{bmatrix}}_{\mathbf{S}(n)} \underbrace{\begin{bmatrix} \mathbf{h}_{sd}(n) \\ \mathbf{h}_{rd}(n) \end{bmatrix}}_{\mathbf{h}(n)} + \underbrace{\begin{bmatrix} \mathbf{n}_{sd}(n) \\ \mathbf{n}_{rd}(n) \end{bmatrix}}_{\mathbf{n}(n)} \tag{3.7}$$

ML detection is then performed at the destination with the metric

$$\arg\min_{\bar{\mathbf{s}}} \left\{ \left\| \mathbf{y}_{sd}(n) - \sqrt{E_s} \sum_{q=0}^{Q} \mathbf{D}(w_q) \mathbf{H}_{sd,q}^{(0)}(n) \boldsymbol{\Theta} \bar{\mathbf{s}} \right\|^2 + \left\| \mathbf{y}_{rd}(n) - \sqrt{G_{rd} E_s} \sum_{q=0}^{Q} \mathbf{D}(w_q) \mathbf{H}_{rd,q}^{(0)}(n) \bar{\dot{\mathbf{u}}} \right\|^2 \right\} \tag{3.8}$$

with $\bar{\dot{\mathbf{u}}}$ as all the possible block combination for the relayed signal.

The above signal model developed for single relay can be easily extended for a multi-relay scenario with relay selection. Let $\dot{\gamma}_{sd}(n)$, $\dot{\gamma}_{sr_i}(n)$ and $\dot{\gamma}_{r_i d}(n)$ denotes the average end-to-end SNRs per block for the S $\rightarrow$ D, S $\rightarrow$ R$_i$ and R$_i$ $\rightarrow$ D links, respectively. The best relay will be chosen based on

$$r_{sel} = \arg\max_{r_i} \left\{ \min\left(\dot{\gamma}_{sr_i}, \dot{\gamma}_{r_i d} \right) \right\} \tag{3.9}$$

with r_{sel} as the selected relaying vehicle. The received signal matrix has the a similar form as (3.7) and given by

$$\underbrace{\begin{bmatrix} \mathbf{y}_{sd}(n) \\ \mathbf{y}_{r_{sel}d}(n) \end{bmatrix}}_{\mathbf{Y}(n)} = \underbrace{\sqrt{E_s} \begin{bmatrix} \boldsymbol{\Phi}(n) & 0 \\ 0 & \sqrt{G_{r_{sel}d}} \dot{\boldsymbol{\Phi}}_{sel}(n) \end{bmatrix}}_{\mathbf{S}(n)} \underbrace{\begin{bmatrix} \mathbf{h}_{sd}(n) \\ \mathbf{h}_{r_{sel}d}(n) \end{bmatrix}}_{\mathbf{h}(n)} + \underbrace{\begin{bmatrix} \mathbf{n}_{sd}(n) \\ \mathbf{n}_{r_{sel}d}(n) \end{bmatrix}}_{\mathbf{n}(n)} \tag{3.10}$$

3.2 PEP Derivation and Diversity Gain Analysis

In this section, we will investigate the achievable diversity gain order for the precoded infrastructure-to-vehicle cooperative communication. We assume perfect-CSI at the relay and destination.

3.2.1 PEP for Single-Relay Case

For the orthogonal cooperative protocol with DF relaying, after removing the block index n for mathematical convenience, the PEP at the destination node is given by [77]

$$P\left(\mathbf{S}\to\hat{\mathbf{S}}\right)\leq\left(1-P_{sr}\left(\mathbf{S}\to\hat{\mathbf{S}}\right)\right)P_{Coop}\left(\mathbf{S}\to\hat{\mathbf{S}}\right)+P_{sr}\left(\mathbf{S}\to\hat{\mathbf{S}}\right)P_{sd}\left(\mathbf{S}\to\hat{\mathbf{S}}\right) \quad (3.11)$$

with $\hat{\mathbf{S}}$ representing the erroneously decoded data matrix instead of the originally transmitted $\mathbf{S}$. $P\left(\mathbf{S}\to\hat{\mathbf{S}}\right)$ is the end-to-end PEP, $P_{sr}\left(\mathbf{S}\to\hat{\mathbf{S}}\right)$ is the PEP results from the S→R link, $P_{sd}\left(\mathbf{S}\to\hat{\mathbf{S}}\right)$ is the PEP results from the S→D link and $P_{Coop}\left(\mathbf{S}\to\hat{\mathbf{S}}\right)$ is the PEP results from the cooperative link (i.e., S→R and R→D, in the case that the relay detects the signal correctly but the signal resulting from the cooperative link is detected wrong). The PEP in (3.11) can be further upper bounded as in [77]

$$P\left(\mathbf{S}\to\hat{\mathbf{S}}\right)\leq P_{Coop}\left(\mathbf{S}\to\hat{\mathbf{S}}\right)+P_{sr}\left(\mathbf{S}\to\hat{\mathbf{S}}\right)P_{sd}\left(\mathbf{S}\to\hat{\mathbf{S}}\right) \quad (3.12)$$

The Chernoff bound [78] on the conditional PEP for the cooperative link is given by (2.8), where the Euclidean distance conditioned on the fading channel coefficients is $d^2\left(\mathbf{S}\to\hat{\mathbf{S}}\middle|\,\mathbf{h}\right)=\mathbf{h}^{\mathrm{H}}\left(\mathbf{S}-\hat{\mathbf{S}}\right)^{\mathrm{H}}\left(\mathbf{S}-\hat{\mathbf{S}}\right)\mathbf{h}$. This can be rewritten as

$$P_{Coop}\left(\mathbf{S}\to\hat{\mathbf{S}}\middle|\,\mathbf{h}\right)\leq\exp\left(-\frac{\mathbf{h}_{sd}^{\mathrm{H}}\boldsymbol{\chi}\mathbf{h}_{sd}+G_{rd}\mathbf{h}_{rd}^{\mathrm{H}}\boldsymbol{\chi}\mathbf{h}_{rd}}{4}\gamma\right) \quad (3.13)$$

where $\boldsymbol{\chi}=\left(\boldsymbol{\Phi}-\hat{\boldsymbol{\Phi}}\right)^{\mathrm{H}}\left(\boldsymbol{\Phi}-\hat{\boldsymbol{\Phi}}\right)$. Note that the channel autocorrelation matrix is given by $\mathbf{C}_{h,sd}:=\mathbb{E}[\mathbf{h}_{sd}\mathbf{h}_{sd}^{\mathrm{H}}]$, and the channel rank is $r_a:=\mathrm{rank}\left(\mathbf{C}_{h,sd}\right)\leq\left(Q_{sd}+1\right)\left(L_{sd}+1\right)$. For the S→D link, we have $Q_{sd}=0$ and $r_a\leq\left(L_{sd}+1\right)$. Using the eigenvalues de-

composition of the autocorrelation matrix, we have $\mathbf{C}_{h,sd} = \mathbf{V}_{sd}\mathbf{D}_{sd}\mathbf{V}_{sd}^{\mathrm{H}}$ where $\mathbf{D}_{sd} := \mathrm{diag}[\sigma_0^2, \sigma_1^2, \ldots, \sigma_{r_a-1}^2]$ and $\mathbf{V}_{sd}\mathbf{V}_{sd}^{\mathrm{H}} = \mathbf{I}_{r_{sd}}$. Let the normalized channel vector be denoted as $\bar{\mathbf{h}}_{sd}$ of size $r_a \times 1$ whose entries are independent and identically distributed (i.i.d.) Gaussian random variables with zero mean and unit variance. We can replace $\mathbf{h}_{sd}$ with $\mathbf{V}_{sd}\mathbf{D}_{sd}^{1/2}\bar{\mathbf{h}}_{sd}$ since both will have identical distribution, so the PEP will remain statistically invariant. Further define $\mathbf{A}_{sd} := \left(\mathbf{V}_{sd}\mathbf{D}_{sd}^{1/2}\right)^{\mathrm{H}}\boldsymbol{\chi}\mathbf{V}_{sd}\mathbf{D}_{sd}^{1/2}$, where $\mathbf{A}_{sd}$ is Hermitian (i.e. $\mathbf{A}_{sd} = \mathbf{A}_{sd}^{\mathrm{H}}$), so there exists a unitary matrix $\bar{\mathbf{V}}_{sd}$ and a real non-negative definite matrix $\bar{\mathbf{D}}_{sd}$ such that $\bar{\mathbf{V}}_{sd}^{\mathrm{H}}\mathbf{A}_{sd}\bar{\mathbf{V}}_{sd} := \bar{\mathbf{D}}_{sd}$. The eigenvector of $\mathbf{A}_{sd}$ is $\bar{\mathbf{D}}_{sd} := \mathrm{diag}[\lambda_0, \lambda_1, \ldots, \lambda_{r_a-1}]$. Since $\bar{\mathbf{V}}_{sd}$ is unitary, the vector $\tilde{\mathbf{h}}_{sd} = \bar{\mathbf{V}}_{sd}\bar{\mathbf{h}}_{sd}$ will have correlation matrix identical to $\bar{\mathbf{h}}_{sd}$, namely we have $\tilde{\mathbf{C}} := \mathbb{E}[\tilde{\mathbf{h}}_{sd}\tilde{\mathbf{h}}_{sd}^{\mathrm{H}}] = \mathbb{E}[\bar{\mathbf{V}}_{sd}\bar{\mathbf{h}}_{sd}\bar{\mathbf{h}}_{sd}^{\mathrm{H}}\bar{\mathbf{V}}_{sd}^{\mathrm{H}}]$. From (3.13), we have

$$P_{Coop}\left(\mathbf{S} \to \hat{\mathbf{S}}\middle|\, \mathbf{h}\right) \leq \exp\left(-\frac{G_{rd}\mathbf{h}_{rd}^{\mathrm{H}}\boldsymbol{\chi}\mathbf{h}_{rd}}{4}\gamma\right)\exp\left(-\frac{\tilde{\mathbf{h}}_{sd}^{\mathrm{H}}\mathbf{A}_{sd}\tilde{\mathbf{h}}_{sd}}{4}\gamma\right) \tag{3.14}$$

Defining β_p^{sd} as the p^{th} element of $\tilde{\mathbf{h}}_{sd}$ we have $\tilde{\mathbf{h}}_{sd}^{\mathrm{H}}\mathbf{A}_{sd}\tilde{\mathbf{h}}_{sd} = \sum_{p=0}^{r_{sd}-1}\lambda_p|\beta_p^{sd}|^2$, with $r_{sd} := \mathrm{rank}(\mathbf{A}_{sd})$. Inserting this into (3.14) and averaging the resulting expression with respect to $\left|\beta_p^{sd}\right|$ which is Rayleigh distributed. We obtain

$$P_{Coop}\left(\mathbf{S} \to \hat{\mathbf{S}}\middle|\, \mathbf{h}_{rd}\right) \leq \exp\left(-\frac{G_{rd}\mathbf{h}_{rd}^{\mathrm{H}}\boldsymbol{\chi}\mathbf{h}_{rd}}{4}\gamma\right)\prod_{p=0}^{r_{sd}-1}\left(1+\frac{\lambda_p}{4}\gamma\right)^{-1} \tag{3.15}$$

following the previous approach used for $\mathbf{h}_{sd}$, we now need to average (3.14) over $\mathbf{h}_{rd}$. The normalized eigenvector of R→D channel is $\bar{\mathbf{D}}_{rd} := \mathrm{diag}[\kappa_0, \kappa_1, \ldots, \kappa_{r_b-1}]$ with rank r_{rd}. Using this, we can evaluate the averaging in (3.15) and have the unconditional PEP as

$$P_{Coop}\left(\mathbf{S} \to \hat{\mathbf{S}}\right) \leq \prod_{j=0}^{r_{rd}-1}\left(\frac{4+G_{rd}\kappa_j\gamma}{4}\right)^{-1}\prod_{p=0}^{r_{sd}-1}\left(\frac{4+\lambda_p\gamma}{4}\right)^{-1} \tag{3.16}$$

Similarly, we obtain

$$P_{sd}\left(\mathbf{S}\to\hat{\mathbf{S}}\right)\leq\prod_{p=0}^{r_{sd}-1}\left(1+\left(\lambda_p/4\right)\gamma\right)^{-1}$$

and

$$P_{sr}\left(\mathbf{S}\to\hat{\mathbf{S}}\right)\leq\prod_{k=0}^{r_{sr}-1}\left(1+G_{sr}\left(\alpha_k/4\right)\gamma\right)^{-1}$$

where the eigenvector of $\bar{\mathbf{h}}_{sr}$ is $\bar{\mathbf{D}}_{sr}:=\mathrm{diag}[\alpha_0,\alpha_1,\ldots,\alpha_{r_{sr}-1}]$ and r_{sr} is the channel rank of $\mathbf{h}_{sr}$. Substituting $P_{Coop}\left(\mathbf{S}\to\hat{\mathbf{S}}\right)$, $P_{sd}\left(\mathbf{S}\to\hat{\mathbf{S}}\right)$ and $P_{sr}\left(\mathbf{S}\to\hat{\mathbf{S}}\right)$ in (3.12), we have the end-to-end PEP expression as

$$P\left(\mathbf{S}\to\hat{\mathbf{S}}\right)\leq\prod_{p=0}^{r_{sd}-1}\left(1+\frac{\lambda_p}{4}\gamma\right)^{-1}\left(\prod_{j=0}^{r_{rd}-1}\left(1+G_{rd}\frac{\kappa_j}{4}\gamma\right)^{-1}+\prod_{k=0}^{r_{sr}-1}\left(1+G_{sr}\frac{\alpha_k}{4}\gamma\right)^{-1}\right)\tag{3.17}$$

From (3.17), due to the fact that the relative speeds between the relay and each of the stationary road-side terminals are the same, we will have $Q_{Coop}=Q_{sr}=Q_{rd}$ and $L_{Coop}=L_{sr}=L_{rd}$. Also it can be easily shown that the performance is directly proportional to d_{rd}, so as the relay is getting closer to the destination the performance improves. In Figure 3.2, we compare the derived PEP expressions given by (3.17) with the exact PEP expressions. Exact PEP can be found by taking the expectation numerically for (2.7) through random generation of $\mathbf{h}$ using proper statistics via numerical techniques. From Figure 3.2, we observe that the derived PEP provides a good upper bound on the exact one. There is about 2dB difference between the exact PEP and the derived PEP as a result of the upper bound in (3.12) and the Chernoff bound (2.8).

At relatively high SNR, we observe from (3.17) that an asymptotical diversity gain of $D_{gain}=r_{sd}+\min(r_{sr},r_{rd})$ is available where $r_{sd}=(L_{sd}+1)(Q_{sd}+1)$ and $\min(r_{sr},r_{rd})=$

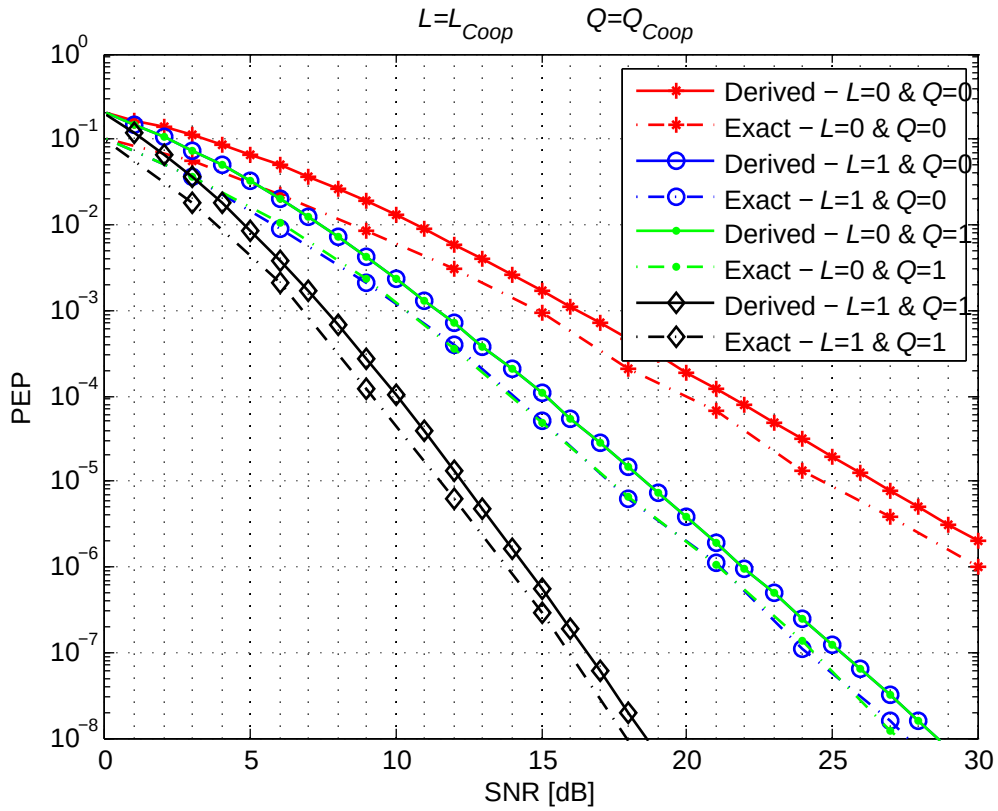

Figure 3.2: Comparison of derived PEP (3.17) and exact PEP expressions for single relay deployment.

$(L_{Coop}+1)(Q_{Coop}+1)$. In Figure 3.3, we plot the slope of the PEPs, i.e. $-\log P(\mathbf{S} \to \hat{\mathbf{S}}) \Big/ \log(\gamma)$. As clearly illustrated, diversity gains of 2, 3, and 5 are obtained as expected from the derived diversity gain.

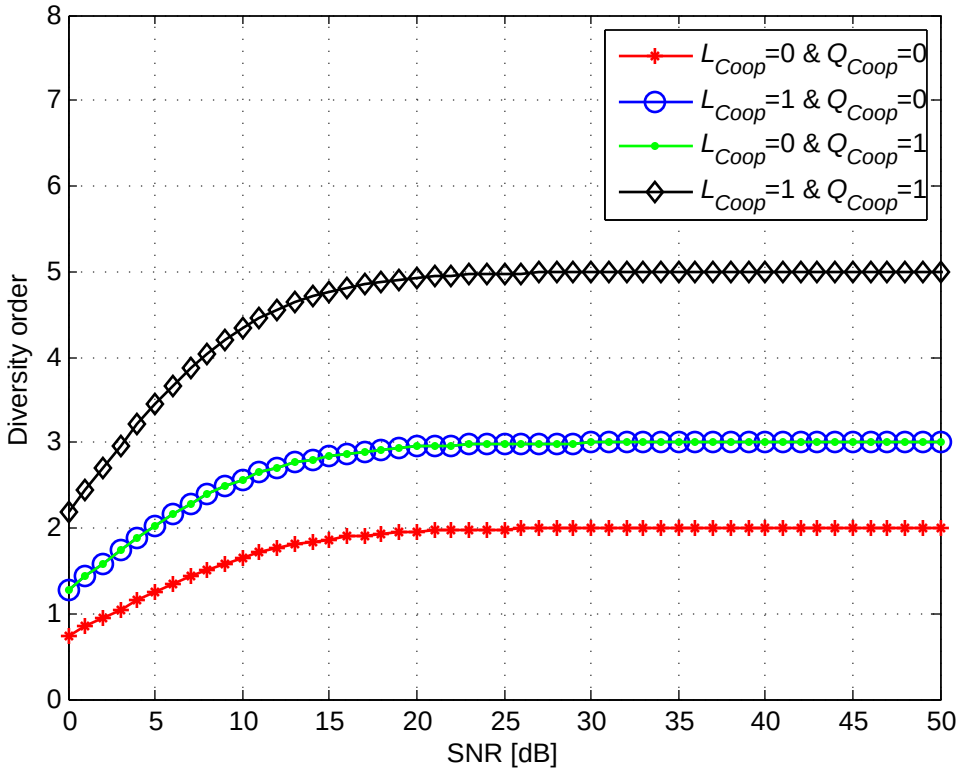

Figure 3.3: Diversity order gains for single relay deployment.

3.2.2 PEP for Multi-Relay Case with Relay Selection

In this section, we investigate the PEP for R2V system with relay selection. The conditional PEP expression has the same form of (3.12) and is given by

$$\begin{aligned} &P_{R_{sel}}\left(\mathbf{S}\to\hat{\mathbf{S}}\middle|\,\mathbf{h}_{sd},\mathbf{h}_{sr_i},\mathbf{h}_{r_id}\right) \\ &\qquad\le P_{Coop_i}\left(\mathbf{S}\to\hat{\mathbf{S}}\middle|\,\mathbf{h}_{sd},\mathbf{h}_{r_id}\right)+P_{sr_i}\left(\mathbf{S}\to\hat{\mathbf{S}}\middle|\,\mathbf{h}_{sr_i}\right)P_{sd}\left(\mathbf{S}\to\hat{\mathbf{S}}\middle|\,\mathbf{h}_{sd}\right) \end{aligned} \tag{3.18}$$

where $P_{Coop_i}(n)$ is the PEP for the selected relay cooperative transmission and $P_{sr_i}(n)$ is the PEP for the $\mathrm{S} \rightarrow \mathrm{R}_i$ link. Following similar steps in Section 3.2.1, we have

$$P_{R_{sel}}\left(\mathbf{S} \rightarrow \hat{\mathbf{S}} \middle| \mathbf{h}_{sd}, \mathbf{h}_{sr_i}, \mathbf{h}_{r_id}\right) \leq \exp\left(-\frac{\gamma_{sd}}{4}\gamma\right)\left(\exp\left(-\frac{\gamma_{sr_i}}{4}\gamma\right) + \exp\left(-\frac{\gamma_{r_id}}{4}\gamma\right)\right) \quad (3.19)$$

where $\gamma_{sd} = \mathbf{h}_{sd}^{\mathrm{H}}\boldsymbol{\chi}\mathbf{h}_{sd} = \sum_{p=0}^{r_{sd}-1}\lambda_p|\beta_p^{sd}|^2$, $\gamma_{sr_i} = G_{sr_i}\mathbf{h}_{sr_i}^{\mathrm{H}}\boldsymbol{\chi}\mathbf{h}_{sr_i} = G_{sr_i}\sum_{k=0}^{r_{sr_i}-1}\alpha_k|\beta_k^{sr_i}|^2$ and $\gamma_{r_id} = G_{r_id}\mathbf{h}_{r_id}^{\mathrm{H}}\boldsymbol{\chi}\mathbf{h}_{r_id} = G_{r_id}\sum_{j=0}^{r_{r_id}-1}\kappa_j|\beta_j^{r_id}|^2$. Define $\gamma_i = \min_i(\gamma_{sr_i}, \gamma_{r_id})$ and $\gamma_i^{'} = \max_i(\gamma_{sr_i}, \gamma_{r_id})$. Note that $-\infty \leq (\gamma_i - \gamma_i^{'}) \leq 0$. Based on the analysis of (3.17) we assume that the relay is very close to the destination, hence $G_{sr_i} \ll G_{r_id}$ and $\gamma_i \ll \gamma_i^{'}$. We can rewrite (3.19) as

$$P_{R_{sel}}\left(\mathbf{S} \rightarrow \hat{\mathbf{S}} \middle| \dot{\gamma}_{sd}, \dot{\gamma}_b\right) \leq \exp\left(-\frac{\dot{\gamma}_{sd} + \dot{\gamma}_b}{4}\right) \quad (3.20)$$

where $\dot{\gamma}_{sd} = \gamma\gamma_{sd}$ is the SNR results from the $\mathrm{S} \rightarrow \mathrm{D}$ link. $\dot{\gamma}_b = \arg\max_{r_i}(\dot{\gamma}_i)$, i.e. $\dot{\gamma}_i = \gamma^{d_i}\gamma_i$, is the SNR results from the relaying link $\mathrm{S} \rightarrow \mathrm{R}_i \rightarrow \mathrm{D}$, where $d_i = \min(r_{sr}, r_{rd})$. Define $\dot{\gamma} = \dot{\gamma}_{sd} + \dot{\gamma}_b$ as the total end-to-end SNR. The CDF of $\dot{\gamma}_i$ is given by [79]

$$F_{\dot{\gamma}_i}(x) = 1 - P_{sr_i}\left(\mathbf{S} \rightarrow \hat{\mathbf{S}} \middle| \gamma_{sr_i} > x\right) P_{r_id}\left(\mathbf{S} \rightarrow \hat{\mathbf{S}} \middle| \gamma_{r_id} > x\right) \quad (3.21)$$

$\dot{\gamma}_{sr_i}$ and $\dot{\gamma}_{r_id}$ are a summation of weighted independent exponential distributed random variables and follow the "hypoexponential distribution" known as the "generalized Erlang distribution" [72, 73]. The pdfs are given by

$$f(\gamma_{sr_i}) = \sum_{j=0}^{r_{sr_i}-1}\left(\alpha_{i,j}e^{-(\alpha_{i,j}\gamma_{sr_i})}\prod_{\substack{k\neq j\\k=0}}^{r_{sr_i}-1}\frac{\alpha_{i,k}}{(\alpha_{i,k}-\alpha_{i,j})}\right) \quad (3.22)$$

and

$$f\left(\gamma_{r_i d}\right) = \sum_{j=0}^{r_{r_i d}-1} \left(\kappa_{i,j} e^{-\left(\kappa_{i,j}\gamma_{r_i d}\right)} \prod_{\substack{k\neq j \\ k=0}}^{r_{r_i d}-1} \frac{\kappa_{i,k}}{\left(\kappa_{i,k}-\kappa_{i,j}\right)} \right) \tag{3.23}$$

$P_{sr_i}\left(\mathbf{S}\to\hat{\mathbf{S}}\middle|\,\gamma_{sr_i}>x\right)$ and $P_{r_i d}\left(\mathbf{S}\to\hat{\mathbf{S}}\middle|\,\gamma_{r_i d}>x\right)$ can be easily obtained using (3.22) and (3.23). Substituting them in (3.21), we have

$$\begin{aligned} &F_{\gamma_i}(x) \\ &= 1 - \sum_{j_1=0}^{r_{sr_i}-1} \sum_{j_2=0}^{r_{r_i d}-1} \left(\left(\prod_{\substack{k\neq j_1 \\ k=0}}^{r_{sr_i}-1} \frac{\alpha_{i,k}}{\left(\alpha_{i,k}-\alpha_{i,j_1}\right)} \right) \left(\prod_{\substack{k\neq j_2 \\ k=0}}^{r_{r_i d}-1} \frac{\kappa_{i,k}}{\left(\kappa_{i,k}-\kappa_{i,j_2}\right)} \right) e^{-\left(\alpha_{i,j_1}+\kappa_{i,j_2}\right)x} \right) \end{aligned} \tag{3.24}$$

The pdf can be calculated differentiating (3.24) which yields

$$f_{\gamma_i}(x) = \sum_{j_1=0}^{r_{sr_i}-1} \sum_{j_2=0}^{r_{r_i d}-1} \left(c_{i,j_1,j_2} \left(\alpha_{i,j_1}+\kappa_{i,j_2}\right) e^{-\left(\alpha_{i,j_1}+\kappa_{i,j_2}\right)x} \right) \tag{3.25}$$

where

$$c_{i,j_1,j_2} = \left(\prod_{\substack{k\neq j_1 \\ k=0}}^{r_{sr_i}-1} \frac{\alpha_{i,k}}{\left(\alpha_{i,k}-\alpha_{i,j_1}\right)} \right) \left(\prod_{\substack{k\neq j_2 \\ k=0}}^{r_{r_i d}-1} \frac{\kappa_{i,k}}{\left(\kappa_{i,k}-\kappa_{i,j_2}\right)} \right) \tag{3.26}$$

The average SNR for the relaying link $\mathrm{S}\to\mathrm{R}_i\to\mathrm{D}$ is given by $\bar{\gamma}_i = \mathbb{E}\left[\dot{\gamma}_i\right]$

$$\bar{\gamma}_i = \int_0^\infty \dot{\gamma}_i f_{\gamma_i}\left(\gamma_i\right) d\gamma_i = \gamma^{d_i} \sum_{j_1=0}^{r_{sr_i}-1} \sum_{j_2=0}^{r_{r_i d}-1} \frac{c_{i,j_1,j_2}}{\left(\alpha_{i,j_1}+\kappa_{i,j_2}\right)} \tag{3.27}$$

Recalling the definition of $\dot{\gamma}_b = \max_i\left(\dot{\gamma}_i\right)$, we have

$$F_{\dot{\gamma}_b}(x) = P\left(\max_{i\in R}\left(\dot{\gamma}_i\right) < x\right) = \prod_{i=1}^{M} P\left(\dot{\gamma}_i < x\right) \tag{3.28}$$

where

$$P\left(\dot{\gamma}_i < x\right) = \int_0^x f_{\dot{\gamma}_i}\left(z\right) dz = \frac{1}{\bar{\gamma}_i} \sum_{j_1=0}^{r_{sr_i}-1} \sum_{j_2=0}^{r_{r_i d}-1} \left(c_{i,j_1,j_2} - c_{i,j_1,j_2} e^{-\left(\alpha_{i,j_1}+\kappa_{i,j_2}\right)x} \right) \tag{3.29}$$

From (3.28) and (3.29), we obtain

$$F_{\dot{\gamma}_b}\left(x\right) = \prod_{i=1}^{M} \left(\frac{1}{\bar{\gamma}_i} - \frac{1}{\bar{\gamma}_i} \sum_{j_1=0}^{r_{sr_i}-1} \sum_{j_2=0}^{r_{r_i d}-1} \left(c_{i,j_1,j_2} e^{-\left(\alpha_{i,j_1}+\kappa_{i,j_2}\right)x} \right) \right) \tag{3.30}$$

noting $\sum \sum c_{i,j_1,j_2} = 1$ [72].

In the following, we consider two cases: a) independent identical distributed (i.i.d.) S $\rightarrow$ R$_i$ $\rightarrow$ D channels b) independent non-identical distributed (i.n.i.d.) channels. For i.i.d. channel case, (3.30) assumes the form of

$$F_{\dot{\gamma}_b}\left(x\right) = \left(\frac{1}{\bar{\gamma}_i} - \frac{1}{\bar{\gamma}_i} \sum_{j_1=0}^{r_{sr}-1} \sum_{j_2=0}^{r_{rd}-1} \left(c_{j_1,j_2} e^{-\left(\alpha_{j_1}+\kappa_{j_2}\right)x} \right) \right)^M \tag{3.31}$$

where we have removed the relay index i for the sake of presentation. The pdf of $\dot{\gamma}_b$ is given by

$$\begin{aligned} & f_{\dot{\gamma}_b}\left(x\right) \\ & \quad = \tfrac{M}{\left(\bar{\gamma}_i\right)^M} \left(1 - \sum_{j_1=0}^{r_{sr}-1} \sum_{j_2=0}^{r_{rd}-1} c_{j_1,j_2} e^{-\left(\alpha_{j_1}+\kappa_{j_2}\right)x} \right)^{M-1} \\ & \qquad \times \left(\sum_{j_1=0}^{r_{sr}-1} \sum_{j_2=0}^{r_{rd}-1} c_{j_1,j_2} \left(\alpha_{j_1}+\kappa_{j_2}\right) e^{-\left(\alpha_{j_1}+\kappa_{j_2}\right)x} \right) \end{aligned} \tag{3.32}$$

Using the binomial theorem [80] along with some mathematical manipulations, we can

rewrite (3.32) in a compact form as

$$f_{\dot{\gamma}_b}(x) = A \sum_{j_3=0}^{M-1} B_{j_3} \mathcal{K}_{j_3} \tag{3.33}$$

where

$$A = \frac{M}{(\bar{\gamma}_i)^M} \sum_{j_1=0}^{r_{sr}-1} \sum_{j_2=0}^{r_{rd}-1} (\alpha_{j_1} + \kappa_{j_2}), \tag{3.34}$$

$$B_{j_3} = \begin{pmatrix} M-1 \\ j_3 \end{pmatrix} (-1)^{j_3} \left(\prod_{p_3=0}^{r_{sr}-1} \prod_{p_4=0}^{r_{rd}-1} c_{p_3,p_4}^{j_3} \right), \tag{3.35}$$

$$\mathcal{K}_{j_3} = \sum_{p_5=0}^{r_{sr}-1} \sum_{p_6=0}^{r_{rd}-1} \left(c_{p_5,p_6} e^{-\left(\left(\alpha_{p_5}+\kappa_{p_6}\right) + j_3 \sum_{p_1=0}^{r_{sr}-1} \sum_{p_2=0}^{r_{rd}-1} \left(\alpha_{p_1}+\kappa_{p_2}\right) \right) x} \right) \tag{3.36}$$

Further, the pdf for S $\rightarrow$ D link is given by

$$f(\gamma_{sd}) = \sum_{j=0}^{r_{r_i d}-1} \left(\lambda_{i,j} e^{-\left(\lambda_{i,j}\gamma_{r_i d}\right)} \prod_{\substack{k=0 \\ k\neq j}}^{r_{r_i d}-1} \frac{\lambda_{i,k}}{(\lambda_{i,k} - \lambda_{i,j})} \right) \tag{3.37}$$

The pdf for the end-to-end SNR is

$$f_{\dot{\gamma}}(x) = f_{\dot{\gamma}_{sd}}(x) * f_{\dot{\gamma}_b}(x) \tag{3.38}$$

Substituting (3.33) and (3.37) in (3.38), we get

$$f_{\dot{\gamma}}(x) = A \sum_{p_7=0}^{r_{sd}-1} \sum_{j_3=0}^{M-1} \left(B_{j_3} \sum_{p_5=0}^{r_{sr}-1} \sum_{p_6=0}^{r_{rd}-1} \left(D_{j_3,p_5,p_6,p_7} \left(e^{-\left(\left(\alpha_{p_5}+\kappa_{p_6}\right) + j_3 \sum_{p_1=0}^{r_{sr}-1} \sum_{p_2=0}^{r_{rd}-1} \left(\alpha_{p_1}+\kappa_{p_2}\right) \right) x} - e^{-\frac{\lambda_{p_7} x}{\gamma}} \right) \right) \right) \tag{3.39}$$

where

$$D_{j_3,p_5,p_6,p_7} = \frac{1}{\left(1+\gamma\left(\alpha_{p_5}+\kappa_{p_6}\right)-\gamma j_3 \sum\limits_{p_1=0}^{r_{sr}-1}\sum\limits_{p_2=0}^{r_{rd}-1}\left(\alpha_{p_1}+\kappa_{p_2}\right)\right)} \prod_{\substack{k=0 \\ k\neq p_7}}^{r_{r_i d}-1} \frac{\lambda_k}{\left(\lambda_k-\lambda_{p_7}\right)}$$

Substituting $\dot{\gamma}=\dot{\gamma}_{sd}+\dot{\gamma}_b$ in the conditional pairwise error probability expression (3.20), we have $P_{R_{sel}}\left(\mathbf{S}\to\hat{\mathbf{S}}\middle|\,\dot{\gamma}\right)\leq\exp\left(-0.25\dot{\gamma}\right)$. By averaging (3.20), we obtain

$$P_{R_{sel}}\left(\mathbf{S}\to\hat{\mathbf{S}}\right) \leq A\sum_{p_7=0}^{r_{sd}-1}\sum_{j_3=0}^{M-1}\left(B_{j_3}\sum_{p_5=0}^{r_{sr}-1}\sum_{p_6=0}^{r_{rd}-1}\mathcal{G}_1\right) \tag{3.40}$$

with

$$\mathcal{G}_1 = D_{j_3,p_5,p_6,p_7}\left(\frac{4}{1+4\left(\alpha_{p_5}+\kappa_{p_6}\right)+4j_3\sum\limits_{p_1=0}^{r_{sr}-1}\sum\limits_{p_2=0}^{r_{rd}-1}\left(\alpha_{p_1}+\kappa_{p_2}\right)}-\frac{4\gamma}{4+\lambda_{p_7}\gamma}\right)$$

For i.n.i.d. channels, starting from (3.30) and using the generalized binomial expansion property [81] we have

$$F_{\dot{\gamma}_b}(x) = 1+\sum_{k=1}^{M}\sum_{p_1=1}^{M-k+1}\sum_{p_2=p_1+1}^{M-k+2}\cdots\sum_{p_k=p_{k-1}+1}^{M}(-1)^k\prod_{i=1}^{k}\left(\frac{1}{\bar{\gamma}_i}\sum_{j_1=0}^{r_{sr_{p_i}}-1}\sum_{j_2=0}^{r_{r_{p_i}d}-1}c_{i,j_1,j_2}e^{-\left(\alpha_{p_i,j_1}+\kappa_{p_i,j_2}\right)x}\right) \tag{3.41}$$

The pdf for the relaying link SNR $\dot{\gamma}$

$$f_{\dot{\gamma}_b}(x) = \sum_{k=1}^{M}\sum_{p_1=1}^{M-k+1}\sum_{p_2=p_1+1}^{M-k+2}\cdots\sum_{p_k=p_{k-1}+1}^{M}(-1)^{k+1}\prod_{i=1}^{k}\mathcal{G}_2 \tag{3.42}$$

with

$$\mathcal{G}_2 = \frac{1}{\bar{\gamma}_i} \sum_{j_1=0}^{r_{sr_{p_i}}-1} \sum_{j_2=0}^{r_{r_{p_i}d}-1} \left(\alpha_{p_i,j_1} + \kappa_{p_i,j_2}\right) c_{i,j_1,j_2} e^{-\left(\alpha_{p_i,j_1}+\kappa_{p_i,j_2}\right)x}$$

Using similar steps to the i.i.d. case, the pdf for the i.n.i.d end-to-end SNR $\dot{\gamma}$ can be obtained as

$$f_{\dot{\gamma}}(x) = \sum_{j_3=0}^{r_{sd}-1} \sum_{k=1}^{M} \sum_{p_1=1}^{M-k+1} \cdots \sum_{p_k=p_{k-1}+1}^{M} \frac{(-1)^{k+1}}{\gamma} \prod_{i=1}^{k} \mathcal{G}_3 \tag{3.43}$$

with

$$\mathcal{G}_3 = \frac{1}{\bar{\gamma}_i} \sum_{j_1=0}^{r_{sr_{p_i}}-1} \sum_{j_2=0}^{r_{r_{p_i}d}-1} \frac{\gamma\left(\alpha_{p_i,j_1} + \kappa_{p_i,j_2}\right) c_{i,j_1,j_2}}{\gamma\left(\alpha_{p_i,j_1} + \kappa_{p_i,j_2}\right) - 1} \left(e^{-\frac{\lambda_{j_3}}{\gamma}x} - e^{-\left(\alpha_{p_i,j_1}+\kappa_{p_i,j_2}\right)x}\right)$$

The unconditional PEP can be evaluated by averaging (3.20) and using the pdf for the i.n.i.d. links given by (3.43). This yield

$$\begin{aligned} &P_{R_{sel}}\left(\mathbf{S} \to \hat{\mathbf{S}}\right) \\ &\quad \leq \sum_{j_3=0}^{r_{sd}-1} \sum_{k=1}^{M} \sum_{p_1=1}^{M-k+1} \sum_{p_2=p_1+1}^{M-k+2} \cdots \sum_{p_k=p_{k-1}+1}^{M} \frac{(-1)^{k+1}}{\lambda_{j_3}\gamma} \prod_{i=1}^{k} \left(\frac{1}{\bar{\gamma}_i} \sum_{j_1=0}^{r_{sr_{p_i}}-1} \sum_{j_2=0}^{r_{r_{p_i}d}-1} A_{i,j_1,j_2} T_{i,j_1,j_2}\right) \end{aligned} \tag{3.44}$$

where

$$A_{i,j_1,j_2,j_3} = \left(\frac{4\gamma}{4 + \lambda_{j_3}\gamma} - \frac{4}{1 + 4\left(\alpha_{p_i,j_1} + \kappa_{p_i,j_2}\right)}\right)$$

and

$$T_{p_i,j_1,j_2} = \frac{\gamma\left(\alpha_{p_i,j_1} + \kappa_{p_i,j_2}\right) c_{i,j_1,j_2}}{\gamma\left(\alpha_{p_i,j_1} + \kappa_{p_i,j_2}\right) - 1}$$

From (3.40) and (3.44), assuming sufficiently high SNR, we find that the asymptotic diversity gain $D_{gain,M}$ is given by

$$D_{gain,M} = r_{sd} + M\left(\min\left(r_{sr}, r_{rd}\right)\right) \tag{3.45}$$

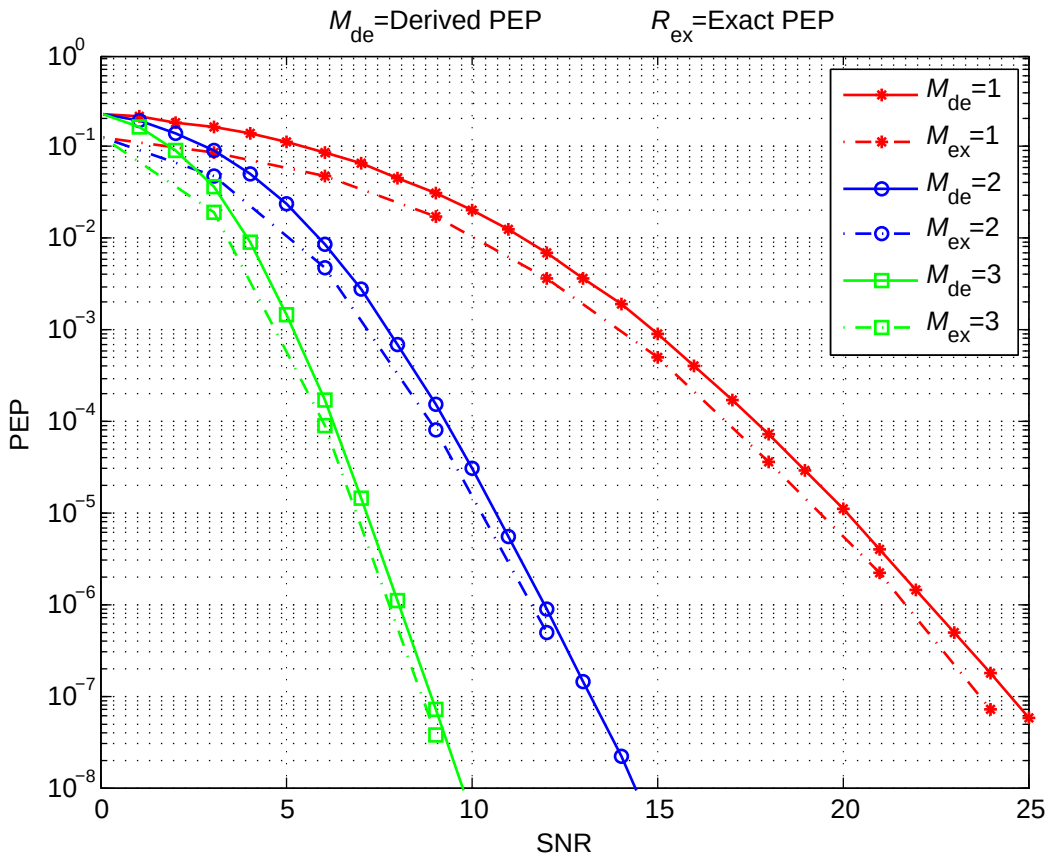

Figure 3.4: Comparison of derived PEP in (3.43) and exact PEP expressions for R2V case with relay selection.

In Figure 3.4, we illustrate the PEP expression (3.44) derived for relay selection case under i.n.i.d channels. We assume $M = 1$, 2 and 3 available relaying vehicles with $[L_{Coop}, Q_{Coop}] = [1, 1]$. We observe that the derived PEP provides a good upper bound on the exact one with about $\simeq$ 3dB difference.

In Figure 3.5, we plot the slope of the best-relay selection case PEPs to precisely observe the gain we achieved from our proposed scheme, the achieved asymptotic diversity orders are consistent with $D_{gain,M} = r_{sd} + M\left(\min\left(r_{sr}, r_{rd}\right)\right)$.

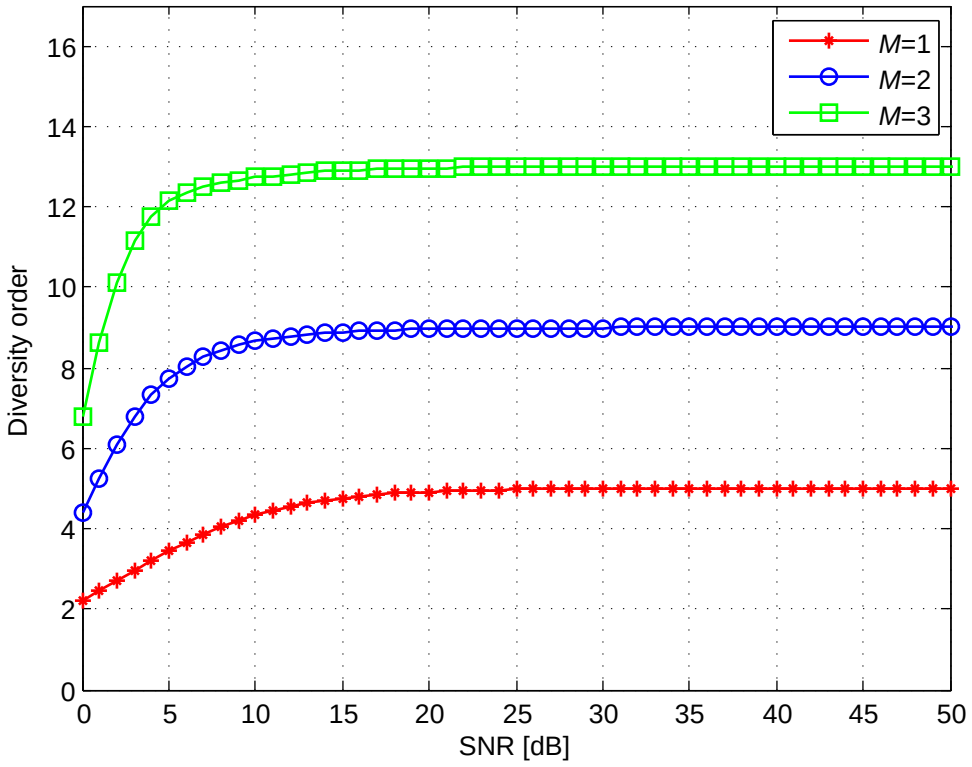

Figure 3.5: Diversity order gains for R2V case with relay selection.

3.3 Simulation Results

In this section, we present Monte-Carlo simulation results to demonstrate the error rate performance. Unless otherwise stated in our numerical results, we consider 4-QAM modulation and assume $f_c = 5.9$GHz, $T_\mathrm{s} = 48\mu s$, $v_r = 60$km/h, $\alpha = 2$, $\theta = \pi$, $G_{sr}/G_{rd} = -30$dB and $\tau_d = 1.328$ μs. Perfect channel state information is available at the receiving terminals. We use the precoder Θ with parameters $P = 2$ and $Z = 2$. This results in $[L_{Coop}, Q_{Coop}] \in ([0,0],[0,1],[1,0],[1,1])$ for S→R and R→D links. A frequency-time flat channel is used for S→D link, i.e. $[L_{sd}, Q_{sd}] = [0,0]$.

Figure 3.6 illustrates the performance R2V cooperative system with relay selection and

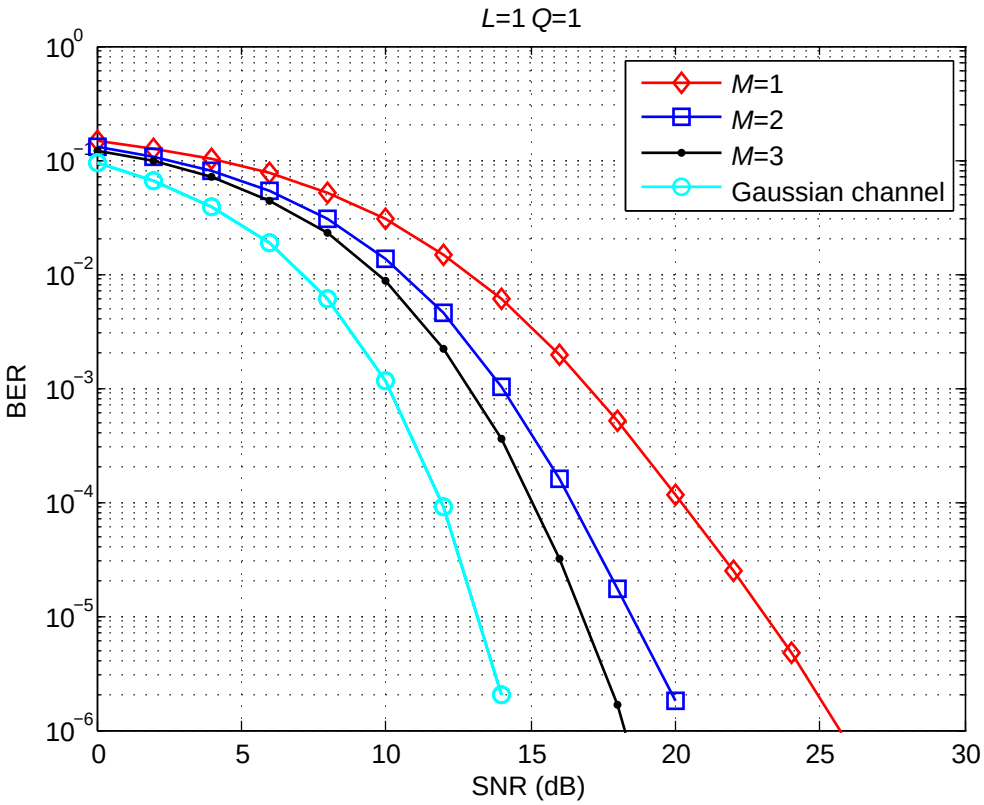

Figure 3.6: Bit error rate performance for R2V multi-relay deployment.

$E_s/2$ associated for each relay. One can note the slope changes in the performance curve indicating the diversity gain in consistent with the previous PEP analysis in Section 3.2.1.

In Figure 3.7, instead of the perfect-CSI assumption used in the PEP derivation, we assume that the channel is estimated through pilot symbols. A single pilot symbol is inserted in each transmitted block, where a total of 11 pilots from preceding and following blocks are used for channel estimation of a fading coefficient in a particular slot of the block. As observed from Figure 3.7 and proved in Appendix A, imperfect-CSI on time-varying channel severely degrades performance and error floors occur for small values of L_{Coop} and Q_{Coop}. However, for higher values of L_{Coop} and Q_{Coop}, the precoded scheme

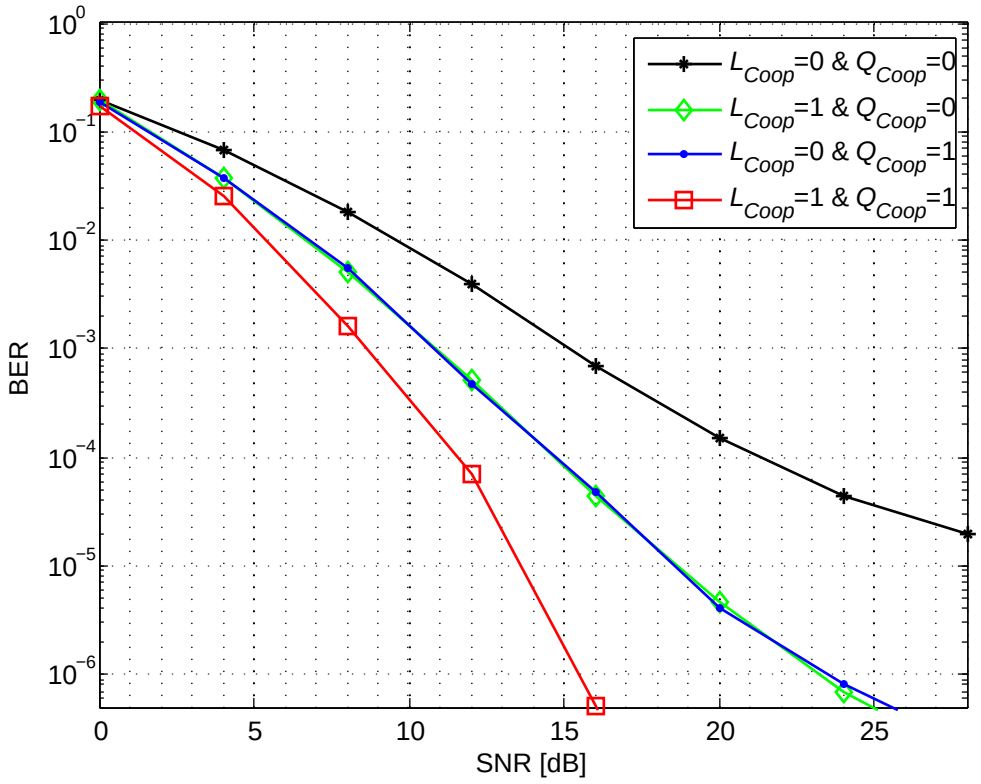

Figure 3.7: Effect of imperfect channel estimation on the bit error rate performance for R2V single relay deployment.

is able to exploit the underlying rich multipath-Doppler diversity and suppress the error floors in the desired SNR range.

3.4 Conclusion

In this chapter, we have investigated the performance of a R2V cooperative communication system in which roadside access points use cooperating vehicles as relaying terminals. For the doubly-selective vehicular channel under consideration, we have employed a precoded cooperative transmission technique to extract the underlying rich multipath-

Doppler-spatial diversity. We have derived closed form expressions for the error performance and diversity analysis. Through the derivation of PEP as well as the numerical simulation results, we have demonstrated significant performance gains through cooperation and proper precoding.

Chapter 4

Multi-hop V2V Cooperative Communications

In the previous chapters, we have assumed the presence of direct transmission between source and destination along with the relayed signal. In this chapter, we assume that no direct link exists and the communication between the source and destination takes place through a number of hops via relaying vehicles. We derive closed form expressions of the error performance for the case of single relay per hop, and for best-relay selection per hop.

The rest of the chapter is organized as follows: In Section 4.1, we present the channel and system models. In Section 4.2, we derive the PEP expression and demonstrate the achievable diversity gains. In Section 4.3, we present numerical results to confirm the analytical derivations. Finally, we conclude in Section 4.4.

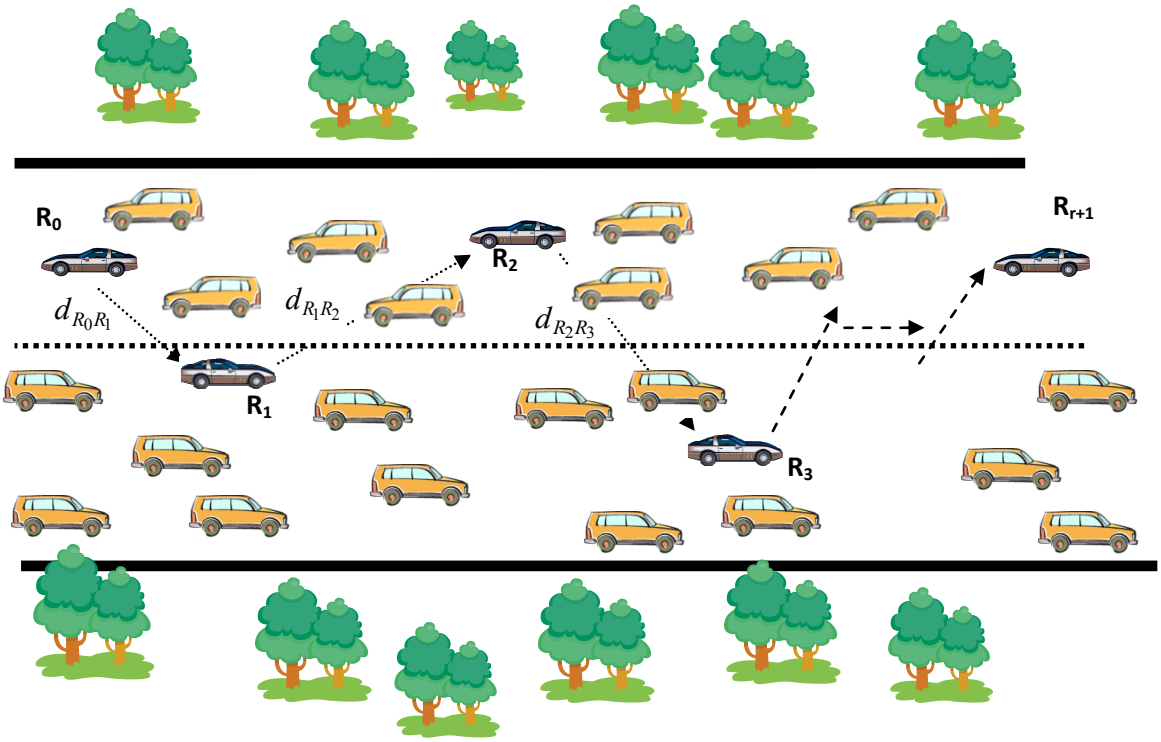

Figure 4.1: Multi-hop vehicular network.

4.1 System Model

We consider a multi-hop transmission scheme (see Figure 4.1) in which the transmitted signal propagates through $(r+1)$-sequential vehicle hops to arrive to the destination vehicle. Each vehicle is equipped with single transmit and receive antennas, and relays operate in half-duplex mode. Similar to the previous chapters, we consider an aggregate channel model which takes into account both path-loss and small-scale fading. Path loss is proportional to $d^{\alpha}_{R_jR_i}$ where $d_{R_jR_i}$ is the propagation distance between the j^{th} transmitting relay and the i^{th} receiving relay. The geometrical gains for source-to-relay, relay-to-relay, and relay-to-destination links can be therefore defined as $G_{R_0R_1} = (1/d_{R_0R_1})^{\alpha}$,

$G_{R_jR_i} = \left(1/d_{R_jR_i}\right)^{\alpha}$ and $G_{R_rR_{r+1}} = \left(1/d_{R_rR_{r+1}}\right)^{\alpha}$ [29] where R_0 and R_{r+1} are respectively used to denote source and destination terminals.

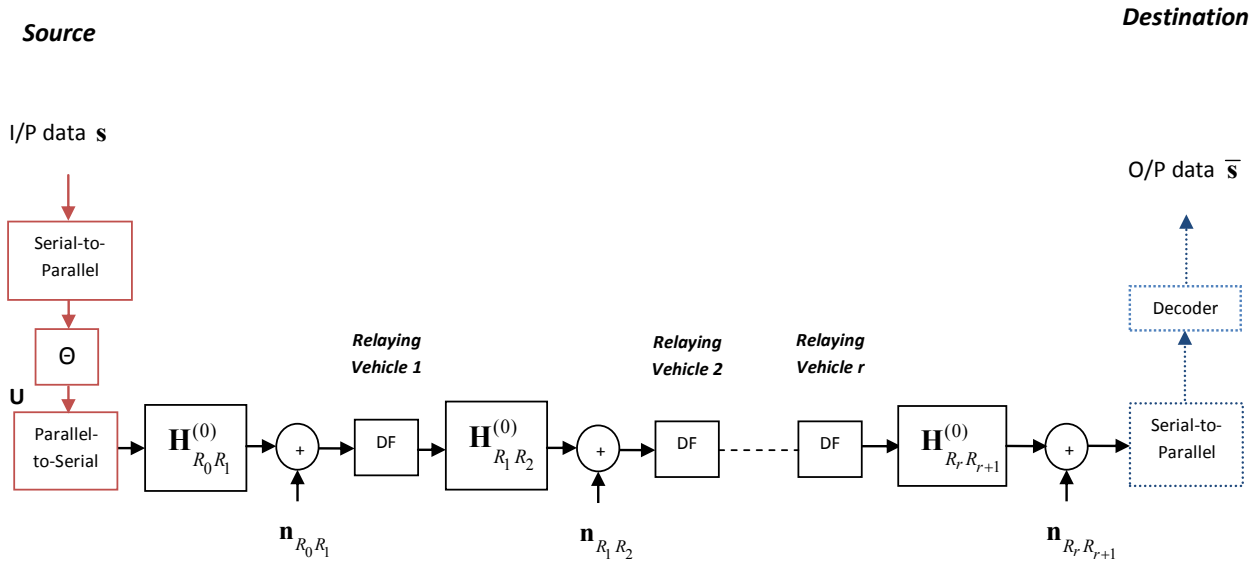

Figure 4.2: Multi-hop transmission model.

As for the short-term fading model, we adopt the single Rayleigh - double Doppler channel model, which is given by the channel autocorrelation function

$$C(\tau) = \sigma_{ji}^2 J_0\left(\frac{2\pi}{\lambda} v_{R_j}\tau\right) J_0\left(\frac{2\pi}{\lambda} v_{R_i}\tau\right) \tag{4.1}$$

where σ_{ji}^2 is the channel variance of the link between j^{th} and i^{th} vehicles, and v_{R_j} and v_{R_i} are the vehicles' maximum velocities. Corresponding power spectral density is expressed as (1.12). The maximum Doppler shift is given by $f_{D_m} = (v_{R_j}\cos(\vartheta_j) + v_{R_i}\cos(\vartheta_i))/\lambda$ with ϑ_j and ϑ_i representing the angle of incidence of the signal on j^{th} and i^{th} vehicles, respectively. The channel satisfies the condition $2f_d\tau_d < 1$, and classified as underspread doubly-selective channel. A block diagram of the system under consideration is given in

Figure 4.2.

The most common frame format for the IEEE 802.11p will have 32-bytes for preamble, signaling field and MAC headers, beside a maximum of 2304-bytes of data frame-body [7, 82, 83]. The full 802.11p input frames (generated from an M-QAM constellation) of length N_t are further divided into shorter sub-blocks of length N_s ($N_s \leq N_t$) using the serial-to-parallel converter. Let each of these sub-blocks be denoted by $\mathbf{s}(n)$ which will be the input to the linear precoder $\mathbf{\Theta}$ of size $N_s \times N_t$. We use the precoder proposed in [51] which ensures the maximum diversity over doubly-selective channels and eliminates the inter-block interference (IBI) term. It is given by $\mathbf{\Theta} = \mathbf{F}_{P+Q}^{\mathrm{H}} \mathbf{T_1} \otimes \mathbf{T_2}$ where $\mathbf{F}_{P+Q}^{\mathrm{H}}$ is a $(P+Q)$-point IFFT matrix, $\mathbf{T}_1 := [\mathbf{I}_P,\ \mathbf{0}_{P\times Q}]^{\mathrm{T}}$ and $\mathbf{T}_2 := [\mathbf{I}_Z,\ \mathbf{0}_{Z\times L}]^{\mathrm{T}}$. Here, $P \geq 1$ and $Z \geq 1$ are the precoder design parameters such that $N_s = PZ$, $N_t = (P+Q)(Z+L)$. We have $L = \lceil \tau_d / T_s \rceil$ as the number of the resolvable multipath components and the number of Doppler shifts experienced over the transmitted sub-blocks is given by $Q = \lceil N_t T_s f_{D_m} \rceil$.

The input data blocks $\mathbf{s}(n)$ are of length $N_s \times 1$ and the output of the precoder $\mathbf{u}(n)$ are of length $N_t \times 1$. Hence, the precoder output rate is equal to

$$\frac{N_s}{N_t} = \frac{PZ}{(P+Q)(Z+L)} \tag{4.2}$$

from (4.2) we find that increasing the precoder output rate can be achieved by increasing P and Z. This will be a trade-off when compared to the system complexity (mainly the detection complexity), by increasing the transmitted/received block length. Furthermore, the diversity order is a function of the channel order $(Q+1)(L+1)$. From the definition

Table 4.1: The number of Doppler shifts Q for a given block length and P - Z parameters.

$[P, Z]$	Q	Transmitted block length N_t	ML search possibilities. $^*M_m$ is the number of bits per symbol
$[1, 1]$	1	4	$(M_m)^4$
$[13, 13]$	2	210	$(M_m)^{210}$
$[18, 18]$	3	399	$(M_m)^{399}$
$[22, 22]$	4	598	$(M_m)^{598}$
$[25, 25]$	5	780	$(M_m)^{780}$
$[18, 18]$	6	986	$(M_m)^{986}$
$[31, 31]$	7	1216	$(M_m)^{1216}$

of L and Q, we have

$$Q\left(1-(Z+L)\,T_s f_d\right)-1 < P(Z+L)T_s f_d \leq Q\left(1-(Z+L)\,T_s f_d\right) \tag{4.3}$$

from (4.3) we can choose P and Z to target a certain specified Q (i.e. as illustrated in Table 4.1). However, in many communication problems, ML detection reduces to solving an integer least-squares problem, i.e., a search for the closest integer lattice point to the given vector and the N_t-dimensional vectors will have to span the N_t-dimensional lattice. In applications with huge search possibilities, ML detection is rarely performed, on the grounds that it requires exponential complexity and is, therefore, computationally intractable. For higher vehicles speeds or larger values of P and Z resulting in $Q > 1$, sphere decoders techniques can be used [64].

Based on the BEM, a discrete-time baseband equivalent channel for the doubly-selective channel is given by (2.1). The source transmits the signal to the next relaying vehicle, and then each relay retransmits the signal to the next relay until the signal reaches to the destination. At each relay, we implement ideal DF [77] where the relay is capable of error detection and will be engaged in forwarding only if it has decoded correctly. The destination

makes its decision based on maximum likelihood (ML) detection. Let $\mathbf{H}^{(0)}_{R_0R_1,q}$, $\mathbf{H}^{(0)}_{R_{i-1}R_i,q}$ and $\mathbf{H}^{(0)}_{R_rR_{r+1},q}$ denote the lower triangular Toeplitz channel matrices for $\mathrm{R}_0 \to \mathrm{R}_1$, $\mathrm{R}_{i-1} \to \mathrm{R}_i$ and $\mathrm{R}_r \to \mathrm{R}_{r+1}$ links, respectively, with entries given by (2.1). Let $L_{R_0R_1}$, $L_{R_{i-1}R_i}$ and $L_{R_rR_{r+1}}$ denote the channel multipath lengths for the associated links. Furthermore, define $Q_{R_0R_1}$, $Q_{R_{i-1}R_i}$ and $Q_{R_rR_{r+1}}$ as the number of resolvable Doppler components for corresponding links. The received signals at the first relay can be expressed in a matrix form as

$$\mathbf{y}_{R_0R_1}(n) = \sqrt{G_{R_0R_1}E_s}\sum_{q=0}^{Q}\mathbf{D}(w_q)\mathbf{H}^{(0)}_{R_0R_1,q}(n)\,\mathbf{u}_1(n) + \mathbf{n}_1(n) \tag{4.4}$$

in (4.4) we have $Q = \max\left(Q_{R_0R_1}, Q_{R_1R_2}, \ldots, Q_{R_{r-1}R_r}, Q_{R_rR_{r+1}}\right)$ and $\mathbf{u}_1(n) = \mathbf{\Theta}\mathbf{s}(n)$ as the transmitted data block. $\mathbf{D}(w_q) := \mathrm{diag}[1, \ldots, \exp(jw_q(N_t-1))]$ and $\mathbf{n}_1(n)$ is the AWGN vector for the $\mathrm{R}_0 \to \mathrm{R}_1$ link with entries of zero mean and $N_0/2$ variance. Using the commutative of products of Toeplitz matrices with vectors, we can replace $\mathbf{H}^{(0)}_{R_0R_1,q}(n)\mathbf{u}_1(n)$ with $\mathbf{U}_1(n)\mathbf{h}_{R_0R_1,q}(n)$.

Furthermore, defining the augmented matrix $\mathbf{h}_1(n) = \left[\ \mathbf{h}^{\mathrm{T}}_{R_0R_1,0}(n) \quad \ldots \quad \mathbf{h}^{\mathrm{T}}_{R_0R_1,Q}(n)\ \right]^{\mathrm{T}}$ and $\mathbf{\Phi}_1(n) = \left[\mathbf{D}(w_0)\mathbf{U}_1(n) \quad \cdots \quad \mathbf{D}(w_Q)\mathbf{U}_1(n)\right]$, we can rewrite (4.4) as

$$\mathbf{y}_{R_0R_1}(n) = \sqrt{G_{R_0R_1}E_s}\mathbf{\Phi}_1(n)\,\mathbf{h}_1(n) + \mathbf{n}_1(n) \tag{4.5}$$

Similarly lets define $i \in \{1, 2, ..., r+1\}$ as the relay index. The relays decode and forward a fresh copy of the received signal, i.e., $\mathbf{u}_i(n)$. Then we have the received signal at the i^{th} relaying vehicle expressed as

$$\mathbf{y}_{R_{i-1}R_i}(n) = \sqrt{G_{R_{i-1}R_i}E_s}\mathbf{\Phi}_i(n)\,\mathbf{h}_i(n) + \mathbf{n}_i(n) \tag{4.6}$$

4.2 PEP Derivation and Diversity Gain Analysis

In this section, we will investigate the performance of multi-hop cooperative scheme under consideration through the PEP derivation for two scenarios. In the first scenario we assume a single relay per each relaying hop, while in the second scenario we assume that relay selection is performed among M_i relays per each relaying hop. We assume perfect-CSI at the receiver side and intermediate relays.

4.2.1 PEP for Single-Relay Case

For the multi-hop system under consideration, after dropping the block index n for mathematical convenience the PEP is given by [84]

$$P_e\left(\mathbf{S}\rightarrow\hat{\mathbf{S}}\Big|_{i=1,\ldots,r+1}^{\mathbf{h}_i}\right)=1-\prod_{i=1}^{r+1}\left(1-P_{e,i}\left(\mathbf{S}\rightarrow\hat{\mathbf{S}}\Big|\,\mathbf{h}_i\right)\right) \tag{4.7}$$

which can be expanded as

$$P_e\left(\mathbf{S}\rightarrow\hat{\mathbf{S}}\Big|_{i=1,\ldots,r+1}^{\mathbf{h}_i}\right)=\sum_{k=1}^{r+1}\left(\begin{array}{l}(-1)^{k-1}\sum\limits_{i_1=1}^{r+1}\sum\limits_{\substack{i_2=1\\ i_2\neq i_1}}^{r+1}\cdots\sum\limits_{\substack{i_k=1\\ i_k\neq i_1\\ i_k\neq i_2\\ \vdots\\ i_k\neq i_{k-1}}}^{r+1}\prod\limits_{p_2=1}^{i_k}P_{e,i_{p_2}}\left(\mathbf{S}\rightarrow\hat{\mathbf{S}}\Big|\,\mathbf{h}_{p_2}\right)\end{array}\right) \tag{4.8}$$

In (4.8), $P_e(.)$ is the end-to-end PEP and $P_{e,i}(.)$ is the PEP at the i^{th} relay. The conditional PEP on the fading channels is defined by (2.7), and upper bounded by the Chernoff bound (2.8). The Euclidean distance conditioned on the fading channel coeffi-

cients is $d^2\left(\mathbf{S},\hat{\mathbf{S}}\middle|\,\mathbf{h}_{i_k}\right)=\mathbf{h}_{i_k}^{\mathrm{H}}\boldsymbol{\Delta}\mathbf{h}_{i_k}$. Defining $\boldsymbol{\Delta}=\left(\mathbf{S}-\hat{\mathbf{S}}\right)^{\mathrm{H}}\left(\mathbf{S}-\hat{\mathbf{S}}\right)$, we can rewrite (2.8) as

$$P_{e,i_k}\left(\mathbf{S}\to\hat{\mathbf{S}}\middle|\,\mathbf{h}_{i_k}\right)\leqslant\exp\left(-\frac{G_{R_{i_k-1}R_{i_k}}\mathbf{h}_{i_k}^{\mathrm{H}}\boldsymbol{\chi}\mathbf{h}_{i_k}}{4}\gamma\right) \tag{4.9}$$

where $\boldsymbol{\chi}=\left(\boldsymbol{\Phi}-\hat{\boldsymbol{\Phi}}\right)^{\mathrm{H}}\left(\boldsymbol{\Phi}-\hat{\boldsymbol{\Phi}}\right)$. We need to average (4.9) over $\mathbf{h}_{R_{i_k}}$. Note that the channel autocorrelation matrix is given by $\mathbf{C}_{h,i_k}:=\mathbb{E}[\mathbf{h}_{i_k}\mathbf{h}_{i_k}^{\mathrm{H}}]$ and the channel rank is $\bar{\Upsilon}_{i_k}:=\mathrm{rank}(\mathbf{C}_{h,i_k})\leqslant(Q_{i_k}+1)(L_{i_k}+1)$, where Q_{i_k} and L_{i_k} is the associated number of Doppler shifts and multipath for the i_k-hop relaying vehicle. Using the eigenvalues decomposition of the autocorrelation matrix, we have $\mathbf{C}_{h,i_k}=\mathbf{V}_{i_k}\mathbf{D}_{i_k}\mathbf{V}_{i_k}^{\mathrm{H}}$ where $\mathbf{D}_{i_k}:=\mathrm{diag}[\sigma_0^2,\sigma_1^2,\ldots,\sigma_{\bar{\Upsilon}_{i_k}-1}^2]$ and $\mathbf{V}_{i_k}^{\mathrm{H}}\mathbf{V}_{i_k}=\mathbf{I}_{\bar{\Upsilon}_{i_k}}$. Let the normalized channel vector be denoted as $\bar{\mathbf{h}}_{i_k}$ of size $\bar{\Upsilon}_{i_k}\times 1$ whose entries are independent and identically distributed (i.i.d.) Gaussian random variables with zero mean and unit variance. We can replace $\mathbf{h}_{i_k}$ with $\mathbf{V}_{i_k}\mathbf{D}_{i_k}^{1/2}\bar{\mathbf{h}}_{i_k}$ since both will have identical distribution, so the PEP will remain statistically invariant. Further define $\mathbf{A}_{i_k}:=\mathbf{V}_{i_k}\mathbf{D}_{i_k}^{1/2}\boldsymbol{\chi}\left(\mathbf{V}_{i_k}\mathbf{D}_{i_k}^{1/2}\right)^{\mathrm{H}}$, where $\mathbf{A}_{i_k}$ is Hermitian (i.e. $\mathbf{A}_{i_k}=\mathbf{A}_{i_k}^{\mathrm{H}}$), so there exists a unitary matrix $\bar{\mathbf{V}}_{i_k}$ and a real non-negative definite matrix $\bar{\mathbf{D}}_{i_k}$ such that $\bar{\mathbf{V}}_{i_k}^{\mathrm{H}}\mathbf{A}_{i_k}\bar{\mathbf{V}}_{i_k}:=\bar{\mathbf{D}}_{i_k}$. The eigenvector of $\mathbf{A}_{i_k}$ is $\bar{\mathbf{D}}_{i_k}:=\mathrm{diag}[\lambda_0,\lambda_1,\ldots,\lambda_{\bar{\Upsilon}_{i_k}-1}]$. Since $\bar{\mathbf{V}}_{i_k}$ is unitary, the vector $\tilde{\mathbf{h}}_{i_k}=\bar{\mathbf{V}}_{i_k}\bar{\mathbf{h}}_{i_k}$ will have correlation matrix identical to $\bar{\mathbf{h}}_{i_k}$, namely we have $\bar{\mathbf{C}}:=\mathbb{E}[\tilde{\mathbf{h}}_{i_k}\tilde{\mathbf{h}}_{i_k}^{\mathrm{H}}]=\mathbb{E}[\bar{\mathbf{V}}_{i_k}\bar{\mathbf{h}}_{i_k}\bar{\mathbf{h}}_{i_k}^{\mathrm{H}}\bar{\mathbf{V}}_{i_k}^{\mathrm{H}}]$. From (4.9), we have

$$P_{e,i_k}\left(\mathbf{S}\to\hat{\mathbf{S}}\middle|\,\mathbf{h}_{i_k}\right)\leqslant\exp\left(-\frac{G_{R_{i_k-1}R_{i_k}}\tilde{\mathbf{h}}_{i_k}^{\mathrm{H}}\mathbf{A}_{i_k}\tilde{\mathbf{h}}_{i_k}}{4}\gamma\right) \tag{4.10}$$

Defining $\beta_p^{i_k}$ as the p^{th} element of $\tilde{\mathbf{h}}_{i_k}$, we have $\tilde{\mathbf{h}}_{i_k}\mathbf{A}_{i_k}\tilde{\mathbf{h}}_{i_k}^{\mathrm{H}}=\sum_{p=0}^{\bar{\Upsilon}_{i_k}-1}\lambda_p|\beta_p^{i_k}|^2$ where $\Upsilon_{i_k}:=\mathrm{rank}(\mathbf{A}_{i_k})$. Assuming normalized Rician distributed fading channels, and averaging

the resulting expression with respect to $\left|\beta_{p_1}^{sd}\right|$, we obtain

$$P_{e,i_k}\left(\mathbf{S}\to\hat{\mathbf{S}}\right)\leq\prod_{p=0}^{\bar{\Upsilon}_{i_k}-1}\int_0^{\infty}2\left|\beta_p^{i_k}\right|e^{\left(-\left|\beta_p^{i_k}\right|^2\left(1-\frac{\lambda_p}{4}\gamma\right)-u^2\right)}I_0\left(\left|\beta_p^{i_k}\right|+u\right)d\left|\beta_p^{i_k}\right| \tag{4.11}$$

define

$$\Lambda_{i_k}=\prod_{p=0}^{\bar{\Upsilon}_{i_k}-1}\int_0^{\infty}2\left|\beta_p^{i_k}\right|e^{\left(-\left|\beta_p^{i_k}\right|^2\left(1-\frac{\lambda_p}{4}\gamma\right)-u^2\right)}I_0\left(\left|\beta_p^{i_k}\right|+u\right)d\left|\beta_p^{i_k}\right| \tag{4.12}$$

Substituting (4.11) and (4.12) in (4.8) and after averaging the conditional PEP over all the i.i.d. links, we obtain

$$P\left(\mathbf{S}\to\hat{\mathbf{S}}\right)\leq\sum_{k=1}^{r+1}\left(\begin{array}{l}(-1)^{k-1}\displaystyle\sum_{i_1=1}^{r+1}\sum_{\substack{i_2=1\\i_2\neq i_1}}^{r+1}\cdots\sum_{\substack{i_k=1\\i_k\neq i_1\\i_k\neq i_2\\\vdots\\i_k\neq i_k-1}}^{r+1}\prod_{p_2=1}^{i_k}\Lambda_{i_k}\end{array}\right) \tag{4.13}$$

We have $P_r\left(\mathbf{S}\to\hat{\mathbf{S}}\right)$ as the unconditional PEP expression, while Λ_{i_k} can be found by numerically computing the integral expressions of (4.13) through the random generation of proper statistics via Monte-Carlo techniques. The relatively low-heights of the antennas on the communicating vehicles implies that the LOS communication can easily be blocked by an obstruction, either static (immovable objects, such as buildings or terrain features, like crests, hills and foliage) or mobile (such as (parked/non-parked) vehicles on the road). However, it is reasonable to expect that a significant portion of the V2V communication will be bound to the road surface, especially in highway environments, thus making the LOS between two communicating nodes susceptible to interruptions by other vehicles. Even

in urban areas, it is likely that other vehicles, especially large public transportation and commercial vehicles such as buses and trucks, will often obstruct the LOS, i.e., [29, 67–71] and the references therein. In the following, we will study the case where the LOS is obstructed. This leads to Rayleigh channel model which is in fact a special case of the Rician channel.

Starting from (4.10) and averaging the resulting expression with respect to $\left|\beta_p^{i_k}\right|$ which is assumed now to Rayleigh distributed, we obtain

$$P_{e,i_k}\left(\mathbf{S}\to\hat{\mathbf{S}}\middle|\,\mathbf{h}_{i_k}\right)\leq\prod_{p=0}^{\Upsilon_{i_k}-1}\left(1+G_{R_{i_k-1}R_{i_k}}\frac{\lambda_{p,i_k}}{4}\gamma\right)^{-1}\tag{4.14}$$

Substituting (4.14) in (4.8) and after averaging the conditional PEP over all the i.i.d. links, we obtain

$$\begin{aligned}&P\left(\mathbf{S}\to\hat{\mathbf{S}}\right)\\&\leq\sum_{k=1}^{r+1}\left(\begin{array}{l}(-1)^{k-1}\sum\limits_{i_1=1}^{r+1}\sum\limits_{\substack{i_2=1\\i_2\neq i_1}}^{r+1}\cdots\sum\limits_{\substack{i_k=1\\i_k\neq i_1\\i_k\neq i_2\\\vdots\\i_k\neq i_k-1}}^{r+1}\prod\limits_{p_2=1}^{i_k}\left(\prod\limits_{p_1=0}^{\Upsilon_{i_{p_2}}-1}\left(1+G_{R_{p_2-1}R_{p_2}}\frac{\lambda_{p_1,i_{p_2}}}{4}\gamma\right)^{-1}\right)\end{array}\right)\end{aligned}\tag{4.15}$$

For high SNR values, (4.15) can be approximated as

$$P\left(\mathbf{S}\to\hat{\mathbf{S}}\right)\leq\sum_{i=1}^{r+1}\prod_{p=0}^{\Upsilon_i-1}\left(G_{R_{i-1}R_i}\frac{\lambda_{p,i}}{4}\gamma\right)^{-1}\tag{4.16}$$

From (4.15) and (4.16), a diversity order of $D_g=\min\limits_{1\leq i\leq r+1}(\Upsilon_i)$ is observed. In Figure

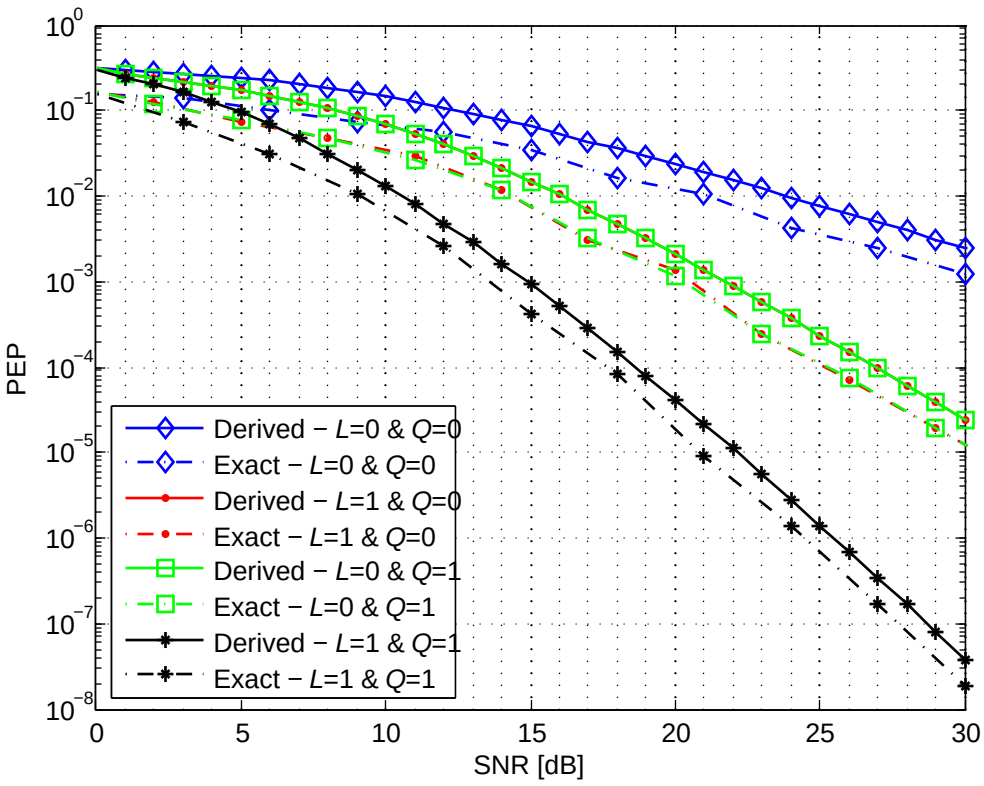

Figure 4.3: Derived PEP (4.15) and exact PEP for 5-hops relaying vehicles.

4.3, we verify the accuracy of the derived PEP where we compare the exact PEP in (2.7) with the derived PEP in (4.15). Exact PEP can be found by taking the expectation of (2.7) numerically. We observe that the derived PEP provides a good match to the exact one. There is approximately 4dB, 2dB and 1.5dB difference between the exact and derived PEP expressions for the cases of $[L, Q] = [0, 0]$, $[L, Q] = [0, 1]$ and $[L, Q] = [1, 1]$.

To double-check the diversity gains, in Figure 4.4 we further plot the slope of the PEPs (i.e., $-\log P\left(\mathbf{S} \to \hat{\mathbf{S}}\right) \Big/ \log(\gamma)$). As clearly observed, asymptotical diversity gains of $D_g = \{1, 2, 4\}$ are obtained as expected from (4.16).

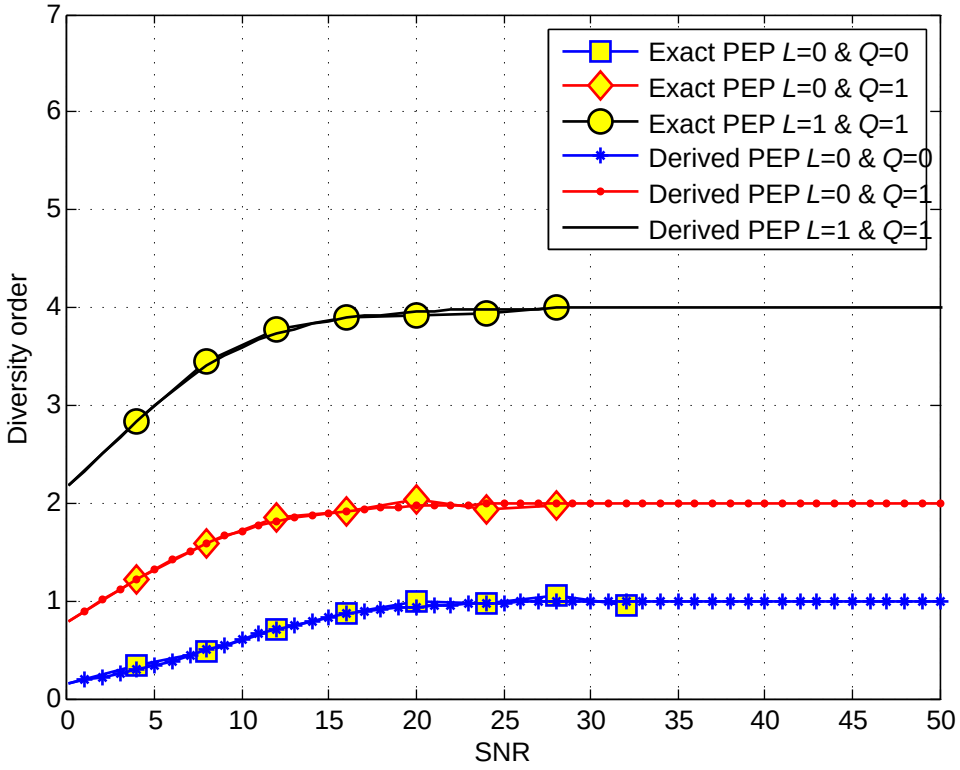

Figure 4.4: Diversity order assuming five hops and various values of L and Q.

4.2.2 PEP for Relay Selection

In this section we consider the case of a relay-selection at each relaying hop. With d_{m_i} denotes the distances between hop $i-1$ and hop i for the associated relaying vehicle m_i. Here $i = 1, \ldots, r+1$, $m_i = 1, 2, \ldots, M_i$ and M_i is the number of the available relaying vehicles at hop i. The relative geometrical gains are now defined as $G_{m_i} = (1/d_{m_i})^{\alpha}$. Let $\dot{\gamma}_{m_i}(n)$ and $\dot{\gamma}_{m_{i+1}}(n)$ denotes the average end-to-end SNRs per block for $\mathrm{R}_{m_{i-1}} \rightarrow \mathrm{R}_{m_i}$ and $\mathrm{R}_{m_i} \rightarrow \mathrm{R}_{m_{i+1}}$ links, respectively. For a dual-hop two-phase scenario, the i-hop relay will be first chosen following criterion

$$r_{sel} = \arg\max_{r_i} \left\{ \min\left(\dot{\gamma}_{sr_i}, \dot{\gamma}_{r_i d} \right) \right\} \tag{4.17}$$

For the multi-hop relaying scenario, the overall system SNR is dominated by that of the weakest hop regardless of modulation scheme employed [84, 85], hence, the best relays will be chosen based on the following criterion

$$R_{sel,i} = \arg\max_{m_i} \left\{ \min_{1 \le i \le r+1} \left(\dot{\gamma}_{m_i} \right) \right\} \tag{4.18}$$

with $R_{sel,i}$ as the selected i-hop relaying vehicle. From (4.4), the received signals at the i-hop relay will be

$$\mathbf{y}_{sel,i}(n) = \sqrt{G_{sel_i} E_s} \sum_{q=0}^{Q} \mathbf{D}(w_q) \mathbf{U}(n) \mathbf{h}_{sel,i,q}(n) + \mathbf{n}_{sel,i}(n) \tag{4.19}$$

defining $\mathbf{h}_{sel,i}(n) = [\ \mathbf{h}^{\mathrm{T}}_{sel,i,0}(n) \quad \ldots \quad \mathbf{h}^{\mathrm{T}}_{sel,i,Q}(n)\ ]^{\mathrm{H}}$, we have

$$\mathbf{y}_{sel,i}(n) = \sqrt{G_{sel_i} E_s} \mathbf{\Phi}(n) \mathbf{h}_{sel,i}(n) + \mathbf{n}_{sel,i}(n) \tag{4.20}$$

The selected relay is engaged in forwarding the received signal only if it has decoded correctly, otherwise the relay is silent. The relay decodes and then forwards a fresh decoded copy of the precoded signal to the next hop. We have the received signal during the (i)-relaying phase at $(i+1)$-hop

$$\mathbf{y}_{sel,i+1}(n) = \sqrt{G_{sel_{i+1}} E_s} \mathbf{\Phi}(n) \mathbf{h}_{sel,i+1}(n) + \mathbf{n}_{sel,i+1}(n) \tag{4.21}$$

The performance metric will follow the PEP expression in (4.8) and given by

$$P_{R_{sel}}\left(\mathbf{S}\to\hat{\mathbf{S}}\middle|\,\mathbf{h}_{m_1},\mathbf{h}_{m_2},\ldots,\mathbf{h}_{m_{r+1}}\right) \leq \sum_{k=1}^{r+1}\left(\begin{array}{l}(-1)^{k-1}\sum\limits_{i_1=1}^{r+1}\sum\limits_{\substack{i_2=1\\ i_2\neq i_1}}^{r+1}\cdots\sum\limits_{\substack{i_k=1\\ i_k\neq i_1\\ i_k\neq i_2\\ \vdots\\ i_k\neq i_{k-1}}}^{r+1}\prod\limits_{p_2=1}^{i_k}P_{e,p_2}\left(\mathbf{S}\to\hat{\mathbf{S}}\middle|\,\mathbf{h}_{m_{p_2}}\right)\end{array}\right) \tag{4.22}$$

The Chernoff bound on the conditional PEP for the end-to-end PEP is

$$P_{R_{sel}}\left(\mathbf{S}\to\hat{\mathbf{S}}\middle|\,\mathbf{h}_{m_1},\mathbf{h}_{m_2},\ldots,\mathbf{h}_{m_{r+1}}\right) \leq \sum_{k=1}^{r+1}\left(\begin{array}{l}(-1)^{k-1}\sum\limits_{i_1=1}^{r+1}\sum\limits_{\substack{i_2=1\\ i_2\neq i_1}}^{r+1}\cdots\sum\limits_{\substack{i_k=1\\ i_k\neq i_1\\ i_k\neq i_2\\ \vdots\\ i_k\neq i_{k-1}}}^{r+1}\prod\limits_{p_2=1}^{i_k}\exp\left(-\frac{G_{m_{p_2}}\mathbf{h}_{m_{p_2}}^{\mathrm{H}}\boldsymbol{\chi}\mathbf{h}_{m_{p_2}}}{4}\gamma\right)\end{array}\right) \tag{4.23}$$

where $\mathbf{h}_{m_{p_2}}$ is the associated channel vector for the $\mathrm{R}_{m_{p_2-1}}\to\mathrm{R}_{m_{p_2}}$ link. Following the analysis in Section 4.2.1 and defining the associated channel gain for each link as $\gamma_{m_{p_2}}=$

$G_{m_{p_2}}\mathbf{h}_{m_{p_2}}^{\mathrm{H}}\boldsymbol{\chi}\mathbf{h}_{m_{p_2}} = G_{m_{p_2}}\sum_{p=0}^{\mathfrak{r}_{p_2}-1}\lambda_p|\beta_p^{m_{p_2}}|^2$, we can rewrite (4.23) as

$$P_{Rsel}\left(\mathbf{S}\to\hat{\mathbf{S}}\middle|\,\mathbf{h}_{m_1},\mathbf{h}_{m_2},\ldots,\mathbf{h}_{m_{r+1}}\right)$$
$$\leqslant\sum_{k=1}^{r+1}\left(\begin{array}{c}(-1)^{k-1}\sum_{i_1=1}^{r+1}\sum_{\substack{i_2=1\\ i_2\neq i_1}}^{r+1}\cdots\sum_{\substack{i_k\neq i_1\\ i_k\neq i_2\\ \vdots\\ i_k\neq i_{k-1}}}^{r+1}\exp\left(-\frac{\gamma_{m_1}+\gamma_{m_2}+\ldots+\gamma_{m_{i_k}}}{4}\gamma\right)\end{array}\right) \tag{4.24}$$

Similar to (4.16), at high SNR we can approximate (4.24) to

$$P_{Rsel}\left(\mathbf{S}\to\hat{\mathbf{S}}\middle|\,\mathbf{h}_{m_1},\mathbf{h}_{m_2},\ldots,\mathbf{h}_{m_{r+1}}\right)\leqslant\sum_{k=1}^{r+1}\exp\left(-\frac{\gamma_{m_k}}{4}\gamma\right) \tag{4.25}$$

Since the overall system end-to-end SNR is dominated by that of the weakest hop we can take an upper bound to (4.25) as

$$P_{R_{sel}}\left(\mathbf{S}\to\hat{\mathbf{S}}\middle|\,\dot{\gamma}_{b,j}\right)\leqslant\exp\left(-\frac{\gamma}{4}\dot{\gamma}_{b,j}\right) \tag{4.26}$$

where $\dot{\gamma}_{b,j}=\max\limits_{1\leqslant m\leqslant M_j}\left(\min\limits_{1\leqslant j\leqslant r+1}\left(\dot{\gamma}_{m_j}\right)\right)$. Define $\gamma_i=\min\limits_{1\leqslant j\leqslant r+1}\left(\dot{\gamma}_{m_j}\right)$, and $\dot{\gamma}_i=\gamma^{d_i}\gamma_i$ is the end-to-end SNR for the j-hop relaying links, where $d_j=\min\limits_{1\leqslant j\leqslant r+1}\left(\mathfrak{r}_j\right)$. In the following, we need to find the probability distribution function (pdf) of $\dot{\gamma}_{b,j}$. The CDF of $\dot{\gamma}_i$ has the form of [79]

$$F_{\dot{\gamma}_i}(x)=1-\prod_{j=1}^{r+1}P_{e,j}\left(\mathbf{S}\to\hat{\mathbf{S}}\middle|\,\gamma_{m,j}>x\right) \tag{4.27}$$

We have γ_{m_j} as a summation of weighted independent exponential random variables

and will have the 'Hypoexponential distributions' [72, 73]

$$f\left(\gamma_{m,j}\right) = G_{m,j} \sum_{b=0}^{\mathfrak{r}_{m,j}-1} \left(\alpha_{m,j,b} e^{-\left(\alpha_{m,j,b}\gamma_{m,j}\right)} \prod_{\substack{t\neq b \\ t=0}}^{\mathfrak{r}_{m,j}-1} \frac{\alpha_{m,j,t}}{\left(\alpha_{m,j,t}-\alpha_{m,j,b}\right)} \right) \tag{4.28}$$

where $\text{diag}[\alpha_{m,j,0}, \alpha_{m,j,1}, \ldots, \alpha_{m,j,\mathfrak{r}_j-1}]$ is the associated eigenvector of for $\mathbf{h}_j$. Furthermore, we have

$$P_{e,j}\left(\mathbf{S} \to \hat{\mathbf{S}} \middle| \gamma_{m,j} > x\right) = \int_x^\infty f_{\dot{\gamma}_{m,j}}\left(z\right) dz = G_{m,j} \sum_{b=0}^{\mathfrak{r}_{m,j}-1} \left(e^{-\left(\alpha_{m,j,b}x\right)} \prod_{\substack{t\neq b \\ t=0}}^{\mathfrak{r}_{m,j}-1} \frac{\alpha_{m,j,t}}{\left(\alpha_{m,j,t}-\alpha_{m,j,b}\right)} \right) \tag{4.29}$$

Substituting (4.29) in (4.27), we have

$$F_{\dot{\gamma}_i}\left(x\right) = 1 - \prod_{j=1}^{r+1} \left(G_{m,j} \sum_{b=0}^{\mathfrak{r}_{m,j}-1} \left(e^{-\left(\alpha_{m,j,b}x\right)} \prod_{\substack{t\neq b \\ t=0}}^{\mathfrak{r}_{m,j}-1} \frac{\alpha_{m,j,t}}{\left(\alpha_{m,j,t}-\alpha_{m,j,b}\right)} \right) \right) \tag{4.30}$$

The pdf of γ_i can obtained from $f_{\dot{\gamma}_i}\left(x\right) = dF_{\dot{\gamma}_i}\left(x\right)/dx$ which yields

$$f_{\dot{\gamma}_i}\left(x\right) = \sum_{j_1=1}^{r+1} \sum_{b=0}^{\mathfrak{r}_{m,j_1}-1} \prod_{\substack{j_2=1 \\ j_2\neq j_1}}^{r+1} \left(\sum_{b_4=0}^{\mathfrak{r}_{m,j_2}-1} c_{m,b,j_1,j_2} e^{-\left(\frac{1}{r}\alpha_{m,j_1,b}+\alpha_{m,j_2,b_4}\right)x} \right) \tag{4.31}$$

where

$$\begin{aligned} & c_{m,b,j_1,j_2} \\ & = \left(G_{m,j} \prod_{\substack{t\neq b \\ t=0}}^{\mathfrak{r}_{m,j_1}-1} \frac{\left(\alpha_{m,j_1,b}\right)^{\left(\mathfrak{r}_{m,j_1}-1\right)} \alpha_{m,j_1,t}}{\left(\alpha_{m,j_1,t}-\alpha_{m,j_1,b}\right)} \right)^{\frac{1}{r}} \prod_{\substack{t\neq b_4 \\ t=0}}^{\mathfrak{r}_{m,j_2}-1} \frac{\alpha_{m,j_2,t}}{\left(\alpha_{m,j_2,t}-\alpha_{m,j_2,b}\right)} \end{aligned}$$

and the associated average SNR for $\bar{\gamma}_i = \mathbb{E}\left[\dot{\gamma}_i\right]$ is

$$\bar{\gamma}_i = \left(\gamma^{d_i} r \sum_{j_1=1}^{r+1} \sum_{b=0}^{\mathfrak{r}_{m,j_1}-1} \prod_{\substack{j_2=1 \\ j_2 \neq j_1}}^{r+1} c_{m,b,j_1,j_2} \frac{1}{\left(\frac{1}{r}\alpha_{m,j_1,b} + \sum\limits_{\substack{j_2=1 \\ j_2 \neq j_1}}^{r+1} \sum\limits_{b_4=0}^{\mathfrak{r}_{m,j_2}-1} \alpha_{m,j_2,b_4} \right)^2} \right) \tag{4.32}$$

From $\dot{\gamma}_{b,j} = \max\limits_{i}\left(\dot{\gamma}_i\right)$, we have

$$F_{\dot{\gamma}_{b,j}}\left(x\right) = P\left(\max_{i \in r}\left(\dot{\gamma}_i\right) < x \right) = \prod_{m=1}^{M_j} P\left(\dot{\gamma}_i < x\right) \tag{4.33}$$

therefore,

$$P\left(\dot{\gamma}_i < x\right) = \sum_{j_1=1}^{r+1} \sum_{b=0}^{\mathfrak{r}_{m,j_1}-1} \left(\bar{B}_{m,j_1,b} \left(1 - \frac{e^{-\bar{A}_{m,j_1,b}x}}{\bar{A}_{m,j_1,b}} \right) \right) \tag{4.34}$$

where

$$\bar{A}_{m,j_1,b} = \left(\frac{1}{r}\alpha_{m,j_1,b} + \sum_{\substack{j_2=1 \\ j_2 \neq j_1}}^{r+1} \sum_{b_4=0}^{\mathfrak{r}_{m,j_2}-1} \alpha_{m,j_2,b_4} \right),$$

$$\bar{B}_{m,j_1,b} = \left(\frac{r}{\bar{\gamma}_i} \prod_{\substack{j_2=1 \\ j_2 \neq j_1}}^{r+1} c_{m,b,j_1,j_2} \right)$$

Substituting (4.34) in (4.33), we have

$$F_{\dot{\gamma}_{b,j}}\left(x\right) = P\left(\max_{i \in r}\left(\dot{\gamma}_i\right) < x \right) = \prod_{m=1}^{M_j} \sum_{j_1=1}^{r+1} \sum_{b=0}^{\mathfrak{r}_{m,j_1}-1} \bar{B}_{m,j_1,b} \left(1 - \frac{e^{-\bar{A}_{m,j_1,b}x}}{\bar{A}_{m,j_1,b}} \right) \tag{4.35}$$

For i.i.d. channels, (4.35) has the form of

$$F_{\dot{\gamma}_{b_j}}(x) = \left(\sum_{j_1=1}^{r+1} \sum_{b=0}^{\mathfrak{r}_{j_1}-1} \bar{B}_{j_1,b} - \sum_{j_1=1}^{r+1} \sum_{b=0}^{\mathfrak{r}_{j_1}-1} \frac{\bar{B}_{j_1,b}}{\bar{A}_{j_1,b}} e^{-\bar{A}_{j_1,b}x} \right)^{M_j} \tag{4.36}$$

using the binomial theorem [80] and after some mathematical steps we can write the pdf of $\dot{\gamma}_b$ in a compact form as

$$f_{\dot{\gamma}_b}(x) = A \sum_{j_3=0}^{M_j-1} B_{j_3} T_{j_3} \tag{4.37}$$

where

$$A = M_j \left(\sum_{j_1=1}^{r+1} \sum_{b=0}^{\mathfrak{r}_{j_1}-1} \bar{B}_{j_1,b} \right)^{M_j} \tag{4.38}$$

$$B_{j_3} = \begin{pmatrix} M_j - 1 \\ j_3 \end{pmatrix} (-1)^{j_3} \left(\prod_{p_3=0}^{r+1} \prod_{p_4=0}^{\mathfrak{r}_{j_1}-1} \left(\frac{1}{\bar{A}_{p_3,p_4}} \right)^{j_3} \right) \tag{4.39}$$

$$T_{j_3} = \left(\sum_{p_5=1}^{r+1} \sum_{p_6=0}^{\mathfrak{r}_{j_1}-1} \frac{1}{\bar{A}_{p_5,p_6}} e^{-\left(\bar{A}_{p_5,p_6} + j_3 \sum_{j_1=1}^{r+1} \sum_{b=0}^{\mathfrak{r}_{j_1}-1} \bar{A}_{j_1,b} \right) x} \right) \tag{4.40}$$

Using the pdf (4.37), the unconditional PEP can be evaluated as

$$P_{R_{sel}}\left(\mathbf{S} \to \hat{\mathbf{S}} \right) \leqslant A \sum_{j_3=0}^{M_j-1} B_{j_3} \left(\sum_{p_5=1}^{r+1} \sum_{p_6=0}^{\mathfrak{r}_{j_1}-1} \frac{1}{A_{p_5,p_6} \left(\frac{1}{4} + A_{p_5,p_6} + j_3 \sum_{j_1=1}^{r+1} \sum_{b=0}^{\mathfrak{r}_{j_1}-1} A_{j_1,b} \right)} \right) \tag{4.41}$$

For i.n.i.d. channels, starting from (4.33) and using the property [81]

$$\prod_{m=1}^{M_j} (1 + x_m) = 1 + \sum_{m=1}^{M_j} \sum_{p_1=1}^{M_j-m+1} \sum_{p_2=p_1+1}^{M_j-m+2} \cdots \sum_{p_m=p_{m-1}+1}^{M_j} \prod_{n=1}^{m} x_{p_n} \tag{4.42}$$

we have the CDF for the relaying link SNR $\dot{\gamma}_{b,j}$

$$F_{\dot{\gamma}_{b,j}}(x) = \mathcal{G}_4 + \mathcal{G}_4 \sum_{k=1}^{M_j} \sum_{p_1=1}^{M_j-k+1} \sum_{p_2=p_1+1}^{M_j-k+2} \cdots \sum_{p_k=p_{k-1}+1}^{M_j} \prod_{n=1}^{k} \mathcal{G}_5 \tag{4.43}$$

with

$$\mathcal{G}_4 = \left(\sum_{j_1=1}^{r+1} \prod_{m=1}^{M_{j_1}} \sum_{b=0}^{\mathfrak{r}_{m,j_1}-1} \bar{B}_{m,j_1,b} \right),$$

$$\mathcal{G}_5 = \left(\frac{- \sum\limits_{j_1=1}^{r+1} \sum\limits_{b=0}^{\mathfrak{r}_{p_n,j_1}-1} \frac{\bar{B}_{p_n,j_1,b}}{\bar{A}_{p_n,j_1,b}} e^{-\bar{A}_{p_n,j_1,b}x}}{\sum\limits_{j_1=1}^{r+1} \sum\limits_{b=0}^{\mathfrak{r}_{p_n,j_1}-1} \bar{B}_{p_n,j_1,b}} \right)$$

The pdf for the relaying link SNR $\dot{\gamma}_{b,j}$ is

$$f_{\dot{\gamma}_{b,j}}(x) = \left(\sum_{j_1=1}^{r+1} \prod_{m=1}^{M_{j_1}} \sum_{b=0}^{\mathfrak{r}_{m,j_1}-1} \bar{B}_{m,j_1,b} \right) \sum_{k=1}^{M_j} \sum_{p_1=1}^{M_j-k+1} \cdots \sum_{p_k=p_{k-1}+1}^{M_j} \Psi \tag{4.44}$$

where

$$\Psi = \prod_{n=1}^{k} \left(- \sum_{j_1=1}^{r+1} \sum_{b=0}^{\mathfrak{r}_{p_n,j_1}-1} \frac{\bar{B}_{p_n,j_1,b}}{\bar{A}_{p_n,j_1,b}} e^{-\bar{A}_{p_n,j_1,b}x} \right) \times \sum_{i=1}^{k} \left(\frac{\sum\limits_{j_1=1}^{r+1} \sum\limits_{b=0}^{\mathfrak{r}_{p_i,j_1}-1} \bar{A}_{p_n,j_1,b}}{\left(\sum\limits_{j_1=1}^{r+1} \sum\limits_{b=0}^{\mathfrak{r}_{p_i,j_1}-1} \bar{B}_{p_n,j_1,b} \right) \prod\limits_{\substack{n=1 \\ n \neq i}}^{k} \left(\sum\limits_{j_1=1}^{r+1} \sum\limits_{b=0}^{\mathfrak{r}_{p_n,j_1}-1} \bar{B}_{p_n,j_1,b} \right)} \right)$$

The unconditional PEP for the i.n.i.d. links is now obtained as

$$P_{R_{sel}}\left(\mathbf{S}\to\hat{\mathbf{S}}\right)\leqslant \sum_{j=1}^{r+1}\left(\mathcal{D}_j\sum_{k=1}^{M_j}\sum_{p_1=1}^{M_j-k+1}\sum_{p_2=p_1+1}^{M_j-k+2}\cdots\sum_{p_k=p_{k-1}+1}^{M_j}\prod_{n=1}^{k}\left(\sum_{j_1=1}^{r+1}\sum_{b=0}^{\mathfrak{r}_{p_n,j_1}-1}\frac{\bar{B}_{p_n,j_1,b}}{\bar{A}_{p_n,j_1,b}\left(\frac{1}{4}+\bar{A}_{p_n,j_1,b}\right)}\right)\right) \tag{4.45}$$

where

$$\mathcal{D}_j=\left(\sum_{j_1=1}^{r+1}\prod_{m=1}^{M_{j_1}}\sum_{b=0}^{\mathfrak{r}_{m,j_1}-1}\bar{B}_{m,j_1,b}\right)\frac{(r+1)\sum_{j_1=1}^{r+1}\sum_{b=0}^{\mathfrak{r}_{p_i,j_1}-1}\bar{A}_{p_n,j_1,b}}{\left(\sum_{j_1=1}^{r+1}\sum_{b=0}^{\mathfrak{r}_{p_i,j_1}-1}\bar{B}_{p_n,j_1,b}\right)\prod_{\substack{n=1\\n\neq i}}^{k}\left(\sum_{j_1=1}^{r+1}\sum_{b=0}^{\mathfrak{r}_{p_n,j_1}-1}\bar{B}_{p_n,j_1,b}\right)}$$

For i.i.d multi-hop relay selection (4.41) and i.n.i.d multi-hop relay selection (4.45), we find that the asymptotical diversity gain is given by

$$D_g=\min_{1\leqslant j\leqslant r+1}\left(M_j\times\mathfrak{r}_j\right) \tag{4.46}$$

In Figure 4.5, we compare the PEP expression given by (4.45) and the exact PEP expression. We assume 5 hops (i.e. $r=4$ relaying vehicles). We observe that the derived PEP provides a good asymptotic upper bound on the exact one. There is about $\simeq 3$ dB, $\simeq 2$ dB and $\simeq 1$ dB difference between the exact PEP and the derived PEP for the $M_j=1$, $M_j=2$ and $M_j=3$, respectively. One can also note the slope changes in the performance curve indicating the diversity gain. In Figure 4.6, for $[L,Q]=[1,1]$ we observe the diversity advantage gained while using the relay selection technique at each hop. As clearly illustrated, the asymptotical diversity gains of $D_g=\{4,8,12\}$ are obtained as expected in (4.46).

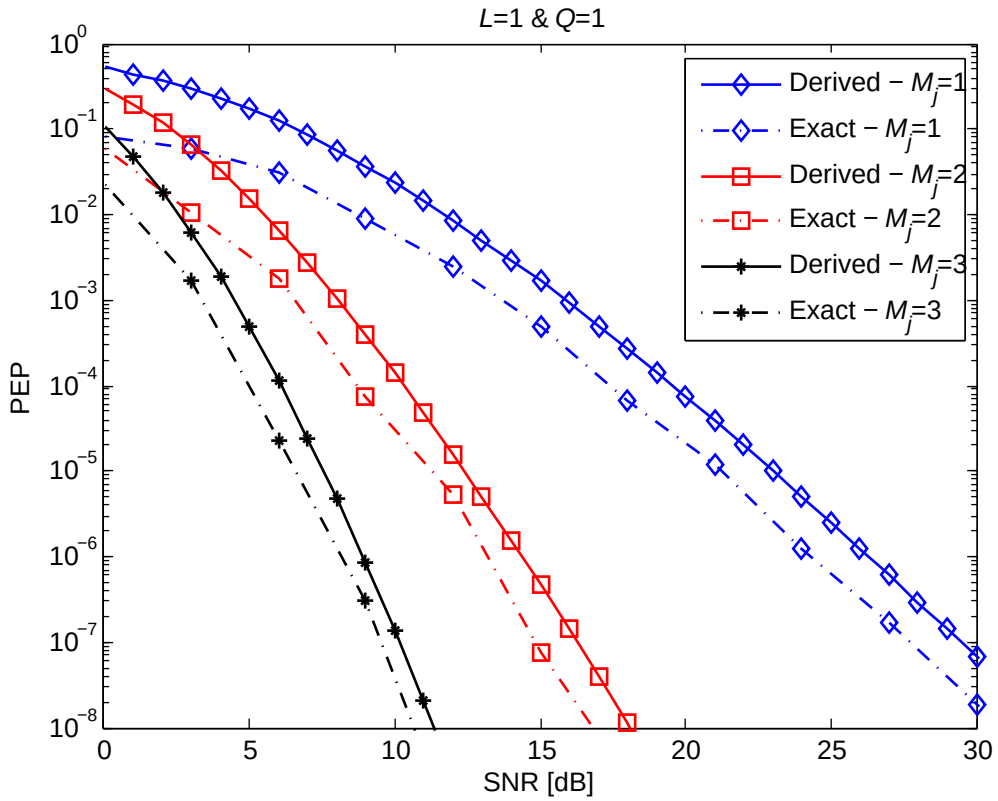

Figure 4.5: Derived vs. exact PEP expressions for multi-hop V2V system with relay selection.

4.3 Simulation Results

In this section, we present and investigate the error rate performance through Monte-Carlo simulations. We assume 4-QAM modulation, operating frequency $f_c = 5.9$ GHz, $T_s = 48\mu$s [76]. We consider a 5-hops (i.e., $r = 4$) system unless otherwise noted. The maximum relaying vehicle velocity is $v_r = 90$km/h, the path loss coefficient is $\alpha = 2$, and the distance between the relaying vehicles are equal to 1 kilometer [29]. Delay spreads are in the range of $\tau_d = 1.113\mu$s - 1.773μs (i.e., $L \in (0, 1)$) for different traffic densities [44]. We use the precoder $\mathbf{\Theta}$ with parameters $P = 2$ and $Z = 2$, i.e., $Q \in (0, 1)$. This therefore results

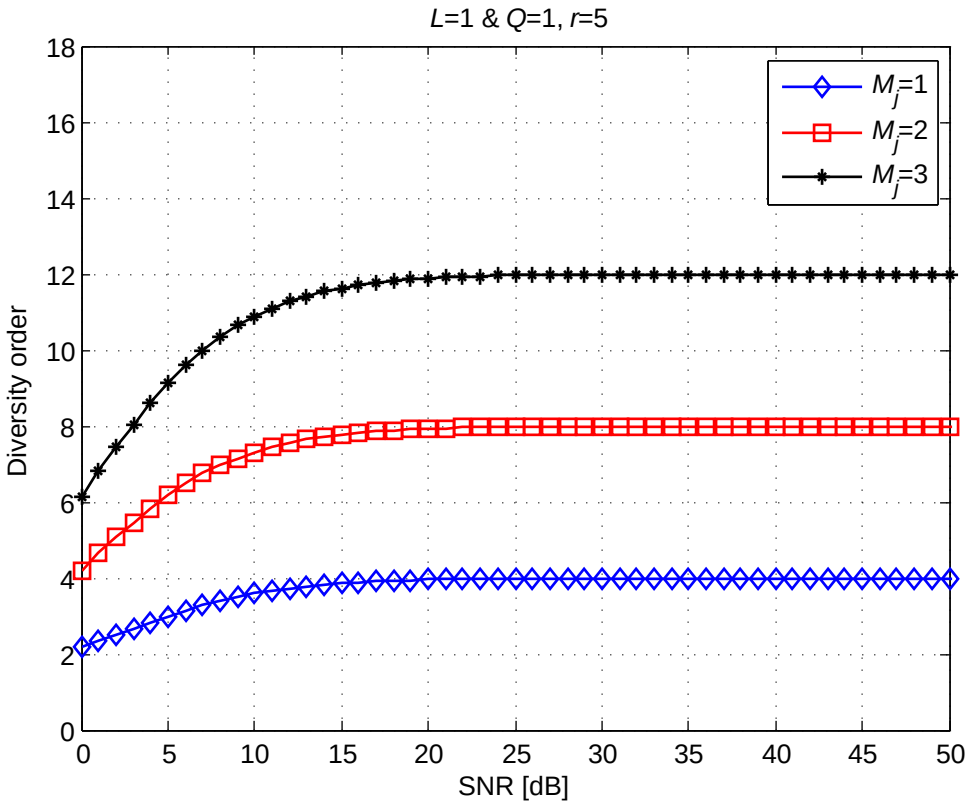

Figure 4.6: Diversity order for multi-hop V2V system with relay selection.

in $[L, Q] \in ([0, 0], [0, 1], [1, 0], [1, 1])$. Perfect-CSI is assumed at the receiving terminals.

In Figure 4.7, for $[L, Q] = [1, 1]$ and using (4.15) we investigate how increasing the number of hops affects the diversity order. It is observed that, with increasing the number of hops, the full diversity order is achieved at higher SNR regions.

In Figure 4.8, we present Monte-Carlo simulation results for BER performance assuming perfect-CSI and Rician fading channel with Rician K-factor = 1dB [69]. As a benchmark, we include the performance of cooperative scheme over frequency- and time-flat channel (i.e., $[L, Q] = [0, 0]$), as well as the AWGN channel. It is observed that as the number of the resolvable multipath components (L) and/or the number of Doppler shifts (Q) increase,

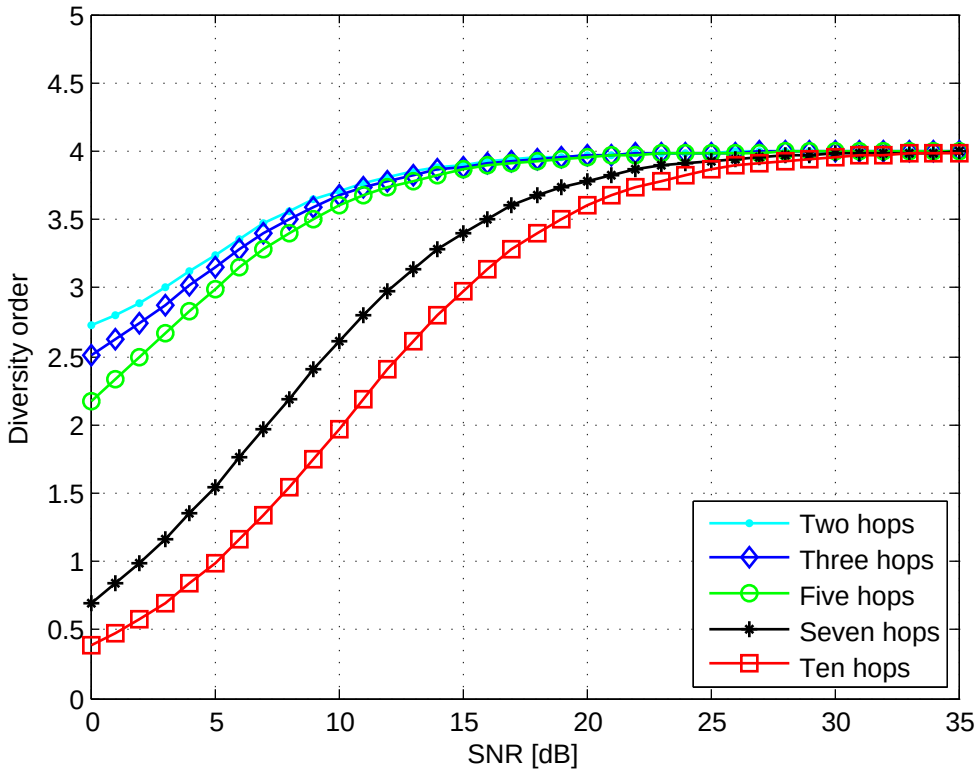

Figure 4.7: Effect of the number of hops on the diversity order.

significant improvements are obtained as a result of precoding that extracts the diversity in the underlying doubly-selective channels. For example at a target BER of 10^{-3}, the precoded system over a channel with $[L, Q] = [0, 1]$ is 8 dB superior to the benchmark curve. This performance improvement climbs up to 13 dB in a channel with $[L, Q] = [1, 1]$. Our results demonstrate that, if properly exploited, the performance can be improved for channels with higher time and spectral variations.

In Figure 4.9, we present Monte-Carlo simulation results for BER performance assuming perfect-CSI and Rayleigh fading channel. It is observed that as the number of the resolvable multipath components (L) and/or the number of Doppler shifts (Q) increase, significant

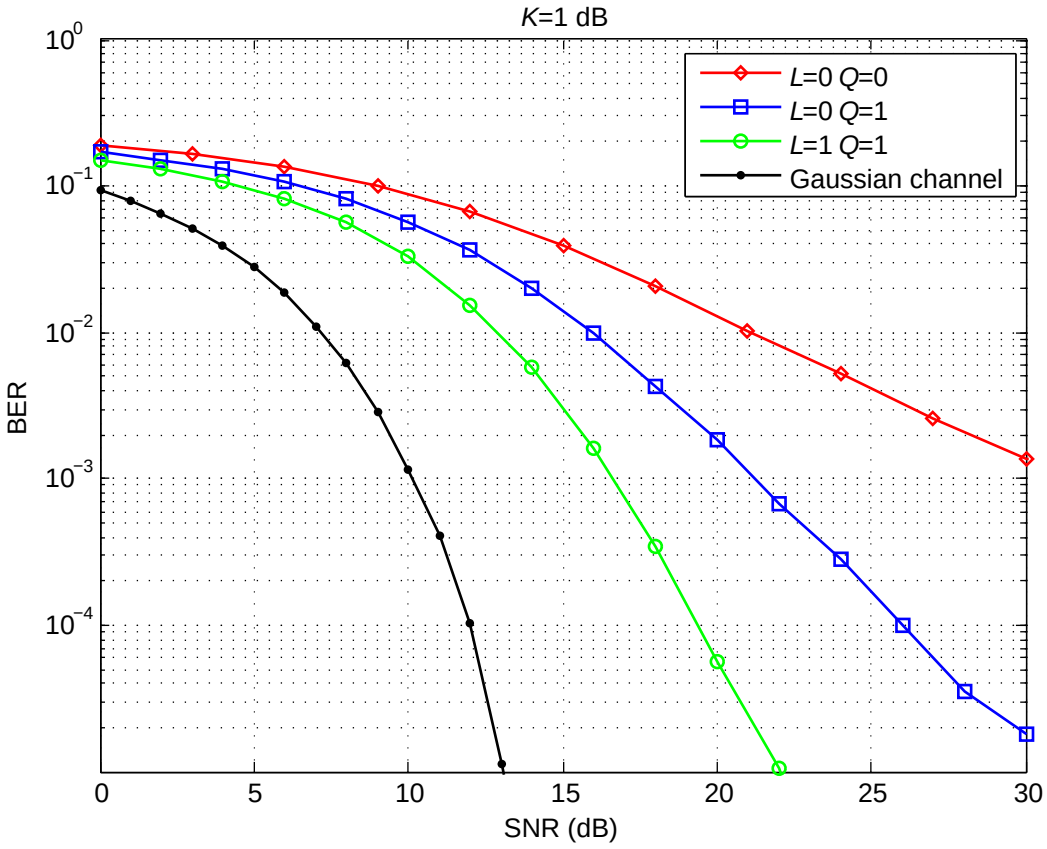

Figure 4.8: BER performance for 5-hops system with perfect-CSI and Rician fading channel.

improvements are obtained as a result of precoding that extracts the diversity in the underlying doubly-selective channels. For example at a target BER of 10^{-3}, the precoded system over a channel with $[L, Q] = [0, 1]$ is almost 9 dB superior to the benchmark curve. This performance improvement climbs up to 15 dB in a channel with $[L, Q] = [1, 1]$. Our results demonstrate that, if properly exploited, the performance can be improved for channels with higher time and spectral variations. However, when compared to the Rician fading channel case in Figure 2.9, we find that higher SNR is required to attain the same BER due to the absence of LOS component.

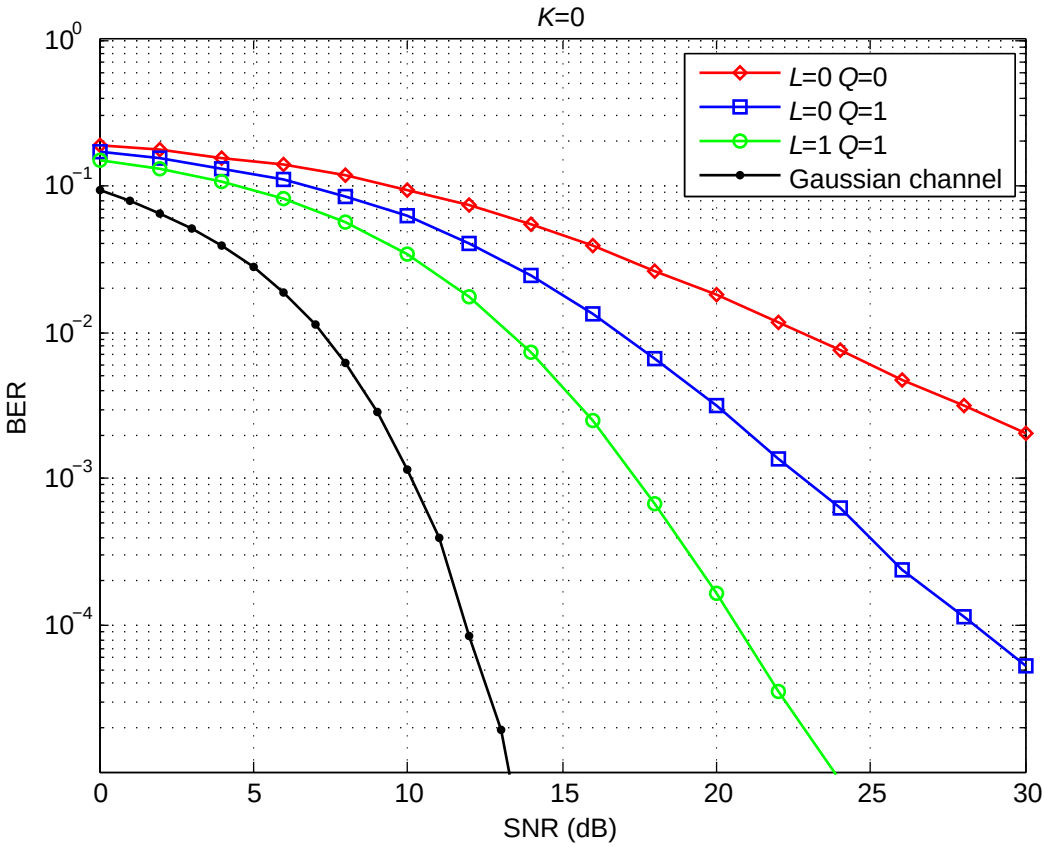

Figure 4.9: BER performance for 5-hops system with perfect-CSI and Rayleigh fading channel.

In Figure 4.10, we present Monte-Carlo simulation results for the BER performance assuming imperfect-CSI. We consider the deployment of pilot assisted channel estimation. In our simulations, a single pilot symbol is inserted in each transmitted block and a total of 11 pilots are used from preceding and following blocks for channel estimation of a fading coefficient in a particular slot of the block. As observed from Figure 4.10, imperfect channel estimation on time-varying channel severely degrades the performance, resulting in error floors and loss of diversity gains for small values of L and Q. However, for larger values, the precoded scheme is able to exploit the underlying rich multipath-Doppler diversity and

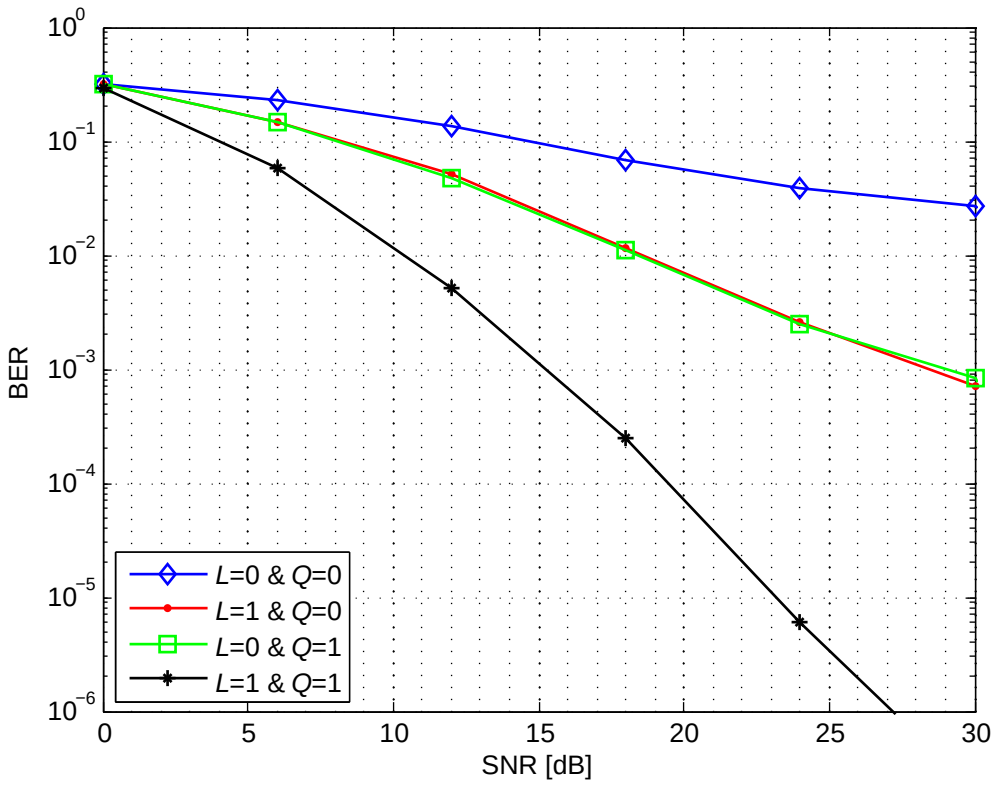

Figure 4.10: BER performance for 5-hops system with imperfect-CSI and Rayleigh fading channel.

suppress the error floors in the desired SNR range. In Figure 4.11, we have the BER plotted versus SNR for the relay selection scenario and one can notice the diversity improvement with the increase of M_j. As an example, to end up with a BER $= 10^{-3}$ using the relay selection technique we saved around $\simeq 10$ dB and $\simeq 11$ dB by using $M_j = 2$ and $M_j = 3$, respectively.

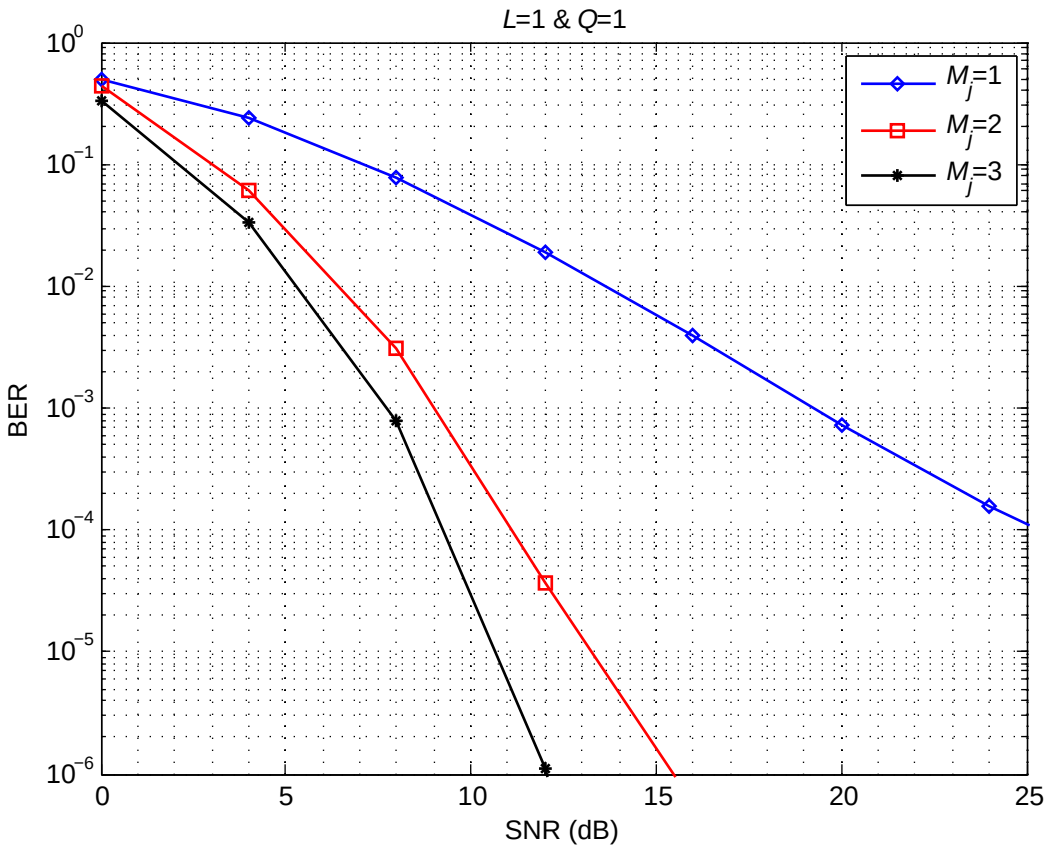

Figure 4.11: BER performance for 5-hops case with relay selection and Rayleigh fading channel.

4.4 Conclusion

In this chapter, we have investigated the performance of a multi-hop vehicular network over frequency-time and time-selective fading channels using DF relaying. For the error performance analysis, we have derived a closed form PEP expressions and shown that full temporal and multipath diversity can be obtained via precoding. Furthermore, we studied the ability to extract extra diversity gains by deploying a best-relay selection technique, where we choose the best relaying vehicle at each relaying hop based on the maximum SNR.

Chapter 5

Conclusions and Future Work

In this final chapter, we summarize the contributions presented in this dissertation and discuss some potential extensions to our work.

5.1 Research Contributions

In this dissertation, we have presented an error rate performance analysis of cooperative vehicular systems considering various traffic and deployment scenarios.

In Chapter 2, we have investigated the performance of V2V communications under the realistic assumption of doubly-selective fading channels and double-ring channel second-order statistics for the proposed SISO and MIMO cooperation scenarios. To extract the underlying rich multipath-Doppler-spatial diversity over the doubly-selective relaying channel, we have employed precoded cooperative transmission. Through the derivation of PEP, we have analyzed the achievable diversity gains. We have presented Monte-Carlo simulation results for the error rate performance to confirm the analytical derivations and further

discussed the effect of imperfect channel estimation [45–48].

In Chapter 3, we have investigated the performance of a R2V cooperative communication system in which roadside access points use cooperating vehicles as relaying terminals. We proposed and studied two scenarios, the single relay and the best relay-selection from relays scenarios. For the doubly-selective vehicular channel under consideration, we have employed a precoded cooperative transmission technique to extract the underlying rich multipath-Doppler-spatial diversity. We came out with closed-forms expressions for the error performance and diversity analysis. Through the derivation of PEP as well as the numerical simulation results, we have demonstrated significant performance gains through cooperation and proper precoding [49].

In Chapter 4, we have investigated the performance of a multi-hop V2V system over frequency-time and time-selective fading channels using DF relaying. Through the derivation of PEP, we have shown that full temporal and multipath diversity can be obtained via precoding. Furthermore, we studied the ability to extract extra diversity gains by deploying a best-relay selection technique, where we choose the best relaying vehicle at each relaying hop based on the maximum SNR [50].

5.2 Future work

The spectral efficiency of the proposed cooperative IVC schemes can be improved by deploying a two-way relaying rather than the one-way relaying mode considered here. Two-way relaying mode is gaining much research attention recently [86–94]. It is a spectrally efficient two-phase communication, where one or multiple relaying vehicles establish a bidirectional communication between another two communicating vehicles. In the first phase, the two

communicating vehicles transmit their message to the relaying vehicles. In the second phase, the relays broadcast a composition of the two messages they received. The communicating terminals subtract the signal it already sent in the first phase from the broadcasted composition it received in the second phase. Performance analysis of cooperative vehicular communication with two-way relaying is an open problem to pursue.

Another open area is MIMO deployment. In Chapter 2 of this dissertation, we have considered the deployment of Alamouti-based MIMO scheme. In vehicular networks, spacing is not a problem and more antennas can be considered. The optimum number and arrangement of antennas, the possibility to modify/introduce specific space-time codes for vehicular channels, the scalability of relaying vehicles, etc., are other open problems.

Appendices

Appendix A

Effect of Imperfect Channel State Information

In this Appendix, we analyze the effect of channel estimation of the PEP expression given by (2.9). For the ease of illustration, we consider only the SISO case and suburban/highway scenario. Let $\mathbf{e}_{sd}$ and $\mathbf{e}_{srd}$ denote the estimation error vectors for the associated links. Therefore, we can write

$$\underbrace{\begin{bmatrix} \hat{\mathbf{h}}_{sd} & \hat{\mathbf{h}}_{srd} \end{bmatrix}^{\mathrm{H}}}_{\hat{\mathbf{h}}} = \underbrace{\begin{bmatrix} \mathbf{h}_{sd} & \mathbf{h}_{srd} \end{bmatrix}^{\mathrm{H}}}_{\mathbf{h}} - \underbrace{\begin{bmatrix} \mathbf{e}_{sd} & \mathbf{e}_{srd} \end{bmatrix}^{\mathrm{H}}}_{\mathbf{e}} \tag{A.1}$$

In the case of imperfect channel estimation, the output of the ML detector at the destination terminal can be expressed as

$$\mathbf{Y}_C = \hat{\mathbf{h}}_Q^{\mathrm{H}} \mathbf{Y} = \sqrt{E_s} \hat{\mathbf{h}}_Q^{\mathrm{H}} \mathbf{h}_Q \mathbf{S} + \hat{\mathbf{h}}_Q^{\mathrm{H}} \mathbf{n} \tag{A.2}$$

where $\mathbf{h}_Q = \sum_{q=0}^{Q} \mathrm{diag}[\mathbf{D}\left(w_q\right), \mathbf{D}\left(w_q\right)] \times \mathrm{diag}[\mathbf{H}_{sd,q}^{(0)}, \mathbf{H}_{srd,q}^{(0)}]$ and $\hat{\mathbf{h}}_Q$ is its estimate related to each other through $\mathbf{h}_Q = \hat{\mathbf{h}}_Q + \mathbf{e}_Q$. The estimate can be further rewritten as

$$\hat{\mathbf{h}}_Q^{\mathrm{H}} = \underbrace{\mathrm{diag}\left[\left(\sum_{q=0}^{Q} \hat{\mathbf{H}}_{sd,q}^{(0)}\right)^{\mathrm{H}}, \left(\sum_{q_3=0}^{Q} \hat{\mathbf{H}}_{srd,q_3}^{(0)}\right)^{\mathrm{H}}\right]}_{\text{Channel matrix}} \times \underbrace{\mathrm{diag}\left[\left(\mathbf{D}\left(w_q\right)\right)^{\mathrm{H}}, \left(\mathbf{D}\left(w_{q_3}\right)\right)^{\mathrm{H}}\right]}_{\text{Doppler spread matrix}} \tag{A.3}$$

where $[\mathbf{H}_{sd,q}^{(0)}(n)]_{k,m} = h_{rd,q}\left(n;\ k-m\right)$ and $[\mathbf{H}_{srd,q}^{(0)}(n)]_{k,m} = h_{sr}\left(n\right) h_{rd,q}\left(n, k-m\right)\ k, m \in [0, N_t - 1]$. Since the Doppler spread matrix is calculated with respect to a known velocity, estimation is needed only over the channel matrix. Noting $\mathbf{e}_Q = \sum_{q=0}^{Q} \mathrm{diag}[\mathbf{D}(w_q), \mathbf{D}(w_q)] \times \mathrm{diag}[\mathbf{e}_{h_{sd},q}, \mathbf{e}_{h_{srd},q}]$ where $\mathbf{e}_{h_{sd},q}$ and $\mathbf{e}_{h_{srd},q}$ are the estimation errors for channel matrices $\hat{\mathbf{H}}_{sd,q}^{(0)}$ and $\mathbf{H}_{srd,q}^{(0)}$, respectively, we have

$$\mathbf{Y}_C = \sqrt{E_s}\hat{\mathbf{h}}_Q^{\mathrm{H}}\hat{\mathbf{h}}_Q\mathbf{S} + \hat{\mathbf{h}}_Q^{\mathrm{H}}\left(\sqrt{E_s}\mathbf{e}_Q\mathbf{S} + \mathbf{n}\right) \tag{A.4}$$

The second term includes the effect of both noise and imperfect estimation and is zero-mean complex Gaussian with the variance of $E_s\sigma_{\mathbf{e}_Q}^2 + N_0$. The average of effective SNR ($\hat{\gamma}$) including the effect of both noise and imperfect estimation is then given by

$$\mathbb{E}\left(\hat{\gamma}\right) = \frac{\gamma\left|\sigma_{\mathbf{h}_Q}^2 + \sigma_{\mathbf{e}_Q}^2 - \mathbb{E}\left(\mathbf{h}_Q\mathbf{e}_Q\right)\right|}{\gamma\sigma_{\mathbf{e}_Q}^2 + 1} \tag{A.5}$$

where the estimation error variance vector $\sigma_{\mathbf{e}_Q}^2$ is

$$\sigma_{\mathbf{e}_Q}^2 = \gamma\sigma_{\mathbf{h}_Q}^2 - \mathbf{w}_c^{\mathrm{H}}\mathbf{R}_c^{-1}\mathbf{w}_c \tag{A.6}$$

Using [95], we can rewrite (A.6) as

$$\sigma^2_{\mathbf{e}_Q} = \left(\left(\frac{\gamma c}{|E_p|^2} \mathbf{1} \right)^{-1} + |E_p|^2 \tilde{\mathbf{R}}^{\mathrm{H}} \mathbf{I}^{-1} \tilde{\mathbf{R}} \right)^{-1} \tag{A.7}$$

The Chernoff bound on the conditional PEP in (2.9) can be therefore revised as

$$P\left(\mathbf{S} \to \hat{\mathbf{S}} \middle| \hat{\mathbf{h}} \right) \leq \exp\left(- \left(\hat{\mathbf{h}}^{\mathrm{H}}_{sd} \boldsymbol{\chi}_1 \hat{\mathbf{h}}_{sd} + K^2 \hat{\mathbf{h}}^{\mathrm{H}}_{srd} \boldsymbol{\chi}_2 \hat{\mathbf{h}}_{srd} \right) \frac{\gamma}{4\left(\gamma \sigma^2_{\mathbf{e}_Q} + 1 \right)} \right) \tag{A.8}$$

For sufficiently high SNR, we have

$$\lim_{\gamma \to \infty} P\left(\mathbf{S} \to \hat{\mathbf{S}} \middle| \hat{\mathbf{h}} \right) \leq \exp\left(- \left(\hat{\mathbf{h}}^{\mathrm{H}}_{sd} \boldsymbol{\chi}_1 \hat{\mathbf{h}}_{sd} + K^2 \hat{\mathbf{h}}^{\mathrm{H}}_{srd} \boldsymbol{\chi}_2 \hat{\mathbf{h}}_{srd} \right) \right) \tag{A.9}$$

which becomes independent of γ and indicates the presence of an error floor.

Bibliography

[1] F. Qu, F. Wang, and L. Yang, "Intelligent transportation spaces: vehicles, traffic, communications, and beyond," *IEEE Commun. Mag.*, vol. 48, no. 11, pp. 136–142, Nov. 2010. 1

[2] M. Jerbi, S. Senouci, Y. Ghamri-Doudane, and M. Cherif, *Handbook of research on next generation mobile networks and ubiquitous computing*, 2012, ch. Vehicular communications networks: current trends and challenges, pp. 50–58. 1, 2

[3] K. Dar, M. Bakhouya, J. Gaber, M. Wack, and P. Lorenz, "Wireless communication technologies for its applications [topics in automotive networking]," *IEEE Commun. Mag.*, vol. 48, no. 5, pp. 156–162, May 2010. 2

[4] V. Khairnar and S. Pradhan, "Comparative study of simulation for vehicular ad-hoc network," *Int. J. of Comput. Applicat. IJCA*, vol. 4, no. 10, pp. 15–18, Aug. 2010. 2

[5] I. Jawhar, N. Mohamed, and L. Zhang, "Inter-vehicular communication systems, protocols and middleware," in *IEEE 5th Int. Conf. on Networking, Architecture, and Storage*, 2010, pp. 282–287. 2

[6] F. Martinez, C. Toh, J. Cano, C. Calafate, and P. Manzoni, "Emergency services in future intelligent transportation systems based on vehicular communication networks," *IEEE Intell. Transp. Syst. Mag.*, vol. 2, no. 2, pp. 6–20, Summer 2010. 2

[7] D. Jiang and L. Delgrossi, "IEEE 802.11 p: Towards an international standard for wireless access in vehicular environments," in *IEEE Veh. Technol. Conf., (VTC)*, Spring 2008, pp. 2036–2040. 2, 78

[8] Y. Liu, F. Dion, and S. Biswas, "Dedicated short-range wireless communications for intelligent transportation system applications: State of the art," *Transp. Research Record: J. of the Transp. Research Board*, vol. 1910, pp. 29–37, 2005. 2

[9] M. Dohler and Y. Li, *Cooperative communications: hardware, channel and PHY*. Wiley, 2010. 2

[10] V. Tarokh, N. Seshadri, and A. Calderbank, "Space-time codes for high data rate wireless communication: Performance criterion and code construction," *IEEE Trans. Inf. Theory*, vol. 44, no. 2, pp. 744–765, Mar. 1998. 3, 33

[11] S. M. Alamouti, "A simple transmit diversity technique for wireless communications," *IEEE J. Sel. Areas Commun.*, vol. 16, no. 8, pp. 1451–1458, Oct. 1998. 3, 28

[12] D. Gesbert, M. Shafi, D. Shiu, P. Smith, and A. Naguib, "From theory to practice: an overview of MIMO space-time coded wireless systems," *IEEE J. Sel. Areas Commun.*, vol. 21, no. 3, pp. 281–302, Apr. 2003. 3

[13] S. Vishwanath, N. Jindal, and A. Goldsmith, "Duality, achievable rates, and sum-rate capacity of gaussian MIMO broadcast channels," *IEEE Trans. Inf. Theory*, vol. 49, no. 10, pp. 2658–2668, Oct. 2003. 3

[14] J. Kermoal, L. Schumacher, K. Pedersen, P. Mogensen, and F. Frederiksen, "A stochastic MIMO radio channel model with experimental validation," *IEEE J. Sel. Areas Commun.*, vol. 20, no. 6, pp. 1211–1226, Aug. 2002. 3

[15] B. Hochwald, T. Marzetta, and V. Tarokh, "Multiple-antenna channel hardening and its implications for rate feedback and scheduling," *IEEE Trans. Inf. Theory*, vol. 50, no. 9, pp. 1893–1909, Sept. 2004. 3

[16] F. H. P. Fitzek and M. D. Katz, *Cooperation in wireless networks: principles and applications; real egoistic behavior is to cooperate!* Springer Verlag, 2006. 3

[17] J. N. Laneman, D. N. C. Tse, and G. W. Wornell, "Cooperative diversity in wireless networks: Efficient protocols and outage behavior," *IEEE Trans. Inf. Theory*, vol. 50, no. 12, pp. 3062–3080, Dec. 2004. 3, 4, 23, 55

[18] J. N. Laneman and G. W. Wornell, "Distributed space-time-coded protocols for exploiting cooperative diversity in wireless networks," *IEEE Trans. Inf. Theory*, vol. 49, no. 10, pp. 2415–2425, Oct. 2003. 3

[19] A. Sendonaris, E. Erkip, B. Aazhang, Q. Inc, and C. A. Campbell, "User cooperation diversity. part I. system description," *IEEE Trans. Commun.*, vol. 51, no. 11, pp. 1927–1938, Nov. 2003. 3

[20] ——, "User cooperation diversity. part II. implementation aspects and performance analysis," *IEEE Trans. Commun.*, vol. 51, no. 11, pp. 1939–1948, Nov. 2003. 3

[21] J. G. Proakis, *Digital communication.* McGraw-Hill, 2001. 5, 6, 7

[22] W. C. Jakes, *Microwave mobile communications.* Wiley-IEEE Press, 1994. 6, 7

[23] C. Patel, G. L. Stuber, and T. G. Pratt, "Simulation of Rayleigh-faded mobile-to-mobile communication channels," *IEEE Trans. Commun.*, vol. 53, no. 11, pp. 1876–1884, Nov. 2005. 6, 9, 10, 13

[24] D. Matolak, "Channel modeling for vehicle-to-vehicle communications," *IEEE Commun. Mag.*, vol. 46, no. 5, pp. 76–83, May 2008. 7, 16

[25] I. Sen and D. W. Matolak, "Vehicle-vehicle channel models for the 5-GHz band," *IEEE Trans. Intell. Transp. Syst.*, vol. 9, no. 2, pp. 235–245, June 2008. 7, 16

[26] A. Akki and F. Haber, "A statistical model of mobile-to-mobile land communication channel," *IEEE Trans. Veh. Technol.*, vol. 35, no. 1, pp. 2–7, Feb. 1986. 9, 12, 13

[27] B. Talha and M. Patzold, "Channel models for mobile-to-mobile cooperative communication systems: A state of the art review," *IEEE Veh. Technol. Mag.*, vol. 6, no. 2, pp. 33 –43, June 2011. 11, 12, 14

[28] J. Salo, H. El-Sallabi, and P. Vainikainen, "Statistical analysis of the multiple scattering radio channel," *IEEE Trans. Antennas Propag.*, vol. 54, no. 11, pp. 3114–3124, Nov. 2006. 11

[29] J. Andersen, T. Rappaport, and S. Yoshida, "Propagation measurements and models for wireless communications channels," *IEEE Commun. Mag.*, vol. 33, no. 1, pp. 42–49, Jan. 1995. 11, 12, 36, 77, 84, 95

[30] A. Coulson, A. Williamson, and R. Vaughan, "A statistical basis for lognormal shadowing effects in multipath fading channels," *IEEE Trans. Commun.*, vol. 46, no. 4, pp. 494–502, Apr. 1998. 11

[31] V. Erceg, S. Fortune, J. Ling, A. Rustako Jr, and R. Valenzuela, "Comparisons of a computer-based propagation prediction tool with experimental data collected in urban microcellular environments," *IEEE J. Sel. Areas Commun.*, vol. 15, no. 4, pp. 677–684, May 1997. 11

[32] D. Caveney, "Cooperative vehicular safety applications," *IEEE Control Syst. Mag.*, vol. 30, no. 4, pp. 38–53, Aug. 2010. 15

[33] F. Dressler, F. Kargl, J. Ott, O. K. Tonguz, and L. Wischof, "Research challenges in intervehicular communication: Lessons of the 2010 dagstuhl seminar," *IEEE Commun. Mag.*, vol. 49, no. 5, pp. 158–164, May 2011. 15

[34] M. Sepulcre, J. Gozalvez, J. Harri, and H. Hartenstein, "Contextual communications congestion control for cooperative vehicular networks," *IEEE Trans. Wireless Commun.*, vol. 10, no. 2, pp. 385–389, Feb. 2011. 15

[35] M. Sepulcre, J. Mittag, P. Santi, H. Hartenstein, and J. Gozalvez, "Congestion and awareness control in cooperative vehicular systems," *Proc. IEEE*, vol. 99, no. 7, pp. 1260–1279, Jul 2011. 15

[36] Y. Hao, Y. Cheng, C. Zhou, and W. Song, "A distributed key management framework with cooperative message authentication in VANETs," *IEEE J. Sel. Areas Commun.*, vol. 29, no. 3, pp. 616–629, Mar. 2011. 15

[37] M. Li, Z. Yang, and W. Lou, "Codeon: Cooperative popular content distribution for vehicular networks using symbol level network coding," *IEEE J. Sel. Areas Commun.*, vol. 29, no. 1, pp. 223–235, Jan. 2011. 15

[38] S. Ahmed and S. S. Kanhere, "VANETCODE: network coding to enhance cooperative downloading in vehicular ad-hoc networks," in *Int. Conf. Wireless Commun. and Mobile Comput. (IWCMC)*, 2006, pp. 527–532. 15

[39] H. Ilhan, M. Uysal, and Ã. Altunbas, "Cooperative diversity for intervehicular communication: Performance analysis and optimization," *IEEE Trans. Veh. Technol.*, vol. 58, no. 7, pp. 3301–3310, Sept. 2009. 15

[40] H. Ilhan, I. Altunbas, and M. Uysal, "Cooperative diversity for relay-assisted intervehicular communication," in *IEEE Veh. Technol. Conf. (VTC)*, Spring, 2008, pp. 605–609. 15

[41] X. Xiaojian, M. Qingmin, and H. Hanying, "A novel two-relay collaborative multihop inter-vehicle communication systems," in *IEEE 1st Int. Conf. Innovative Comput., Inform. and Control (ICICIC'06)*, vol. 2, 2006, pp. 445–448. 15

[42] L. Weixin, W. Ning, L. Shaoqian, and J. Na, "The differential detection OFDM cooperative diversity system in vehicle-to-vehicle communications," in *IEEE 6th Int. Conf. Telecommun. (ITS)*, 2006, pp. 1118–1121. 15

[43] J. Nuckelt, M. Schack, and T. Kürner, "Deterministic and stochastic channel models implemented in a physical layer simulator for car-to-x communications," *Advances in Radio Science*, vol. 9, pp. 165–171, 2011. 15, 16

[44] I. Sen and D. Matolak, "V2V channels and performance of multi-user spread spectrum modulation," in *IEEE 66th Veh. Technol. Conf. (VTC)*, 2007, pp. 2139–2143. 16, 23, 47, 95

[45] S. S. Ikki, M. F. Feteiha, and M. Uysal, "Performance analysis of cooperative diversity networks with imperfect channel estimation over rician fading channels," in *IEEE 17th Int. Conf. Telecommun. (ICT)*, 2010, pp. 160–165. 16, 103

[46] M. Feteiha and M. Uysal, "Multipath-doppler diversity for broadband cooperative vehicular communications," in *IEEE Int. Conf. Commun. (ICC)*, 2011, pp. 1–6. 16, 103

[47] M. F. Feteiha, M. Uysal, and A. Ahmad, "Cooperative inter-vehicular communications in highway traffic," in *IEEE 24th Canadian Conf. Elect. and Comput. Eng. (CCECE)*, 2011, pp. 000 460–000 465. 16, 103

[48] M. Feteiha and M. Uysal, "Cooperative transmission for broadband vehicular networks over doubly-selective fading channels," *IEEE Trans. Veh. Technol.*, Submitted Sept. 2011. 16, 103

[49] M. F. Feteiha and M. Uysal, "Infrastructure-to-vehicle cooperative communications with decode-and-forward relaying," in *IEEE 22nd Annu. Int. Symp. Personal, Indoor and Mobile Radio Communic. (PIMRC)*, 2011. 17, 103

[50] M. Feteiha and M. Uysal, "Performance analysis of decode-and-forward multi-hop transmission for vehicular networks," in *IEEE Consum. Commun. and Netw. Conf. (CCNC)*, 2012. 18, 103

[51] X. Ma and G. Giannakis, "Maximum-diversity transmissions over doubly selective wireless channels," *IEEE Trans. Inf. Theory*, vol. 49, no. 7, pp. 1832–1840, Jul. 2003. 19, 23, 24, 78

[52] W. Kozek, "On the transfer function calculus for underspread LTV channels," *IEEE Trans. Signal Process.*, vol. 45, no. 1, pp. 219–223, Jan. 1997. 23

[53] A. Kannu and P. Schniter, "On the spectral efficiency of noncoherent doubly selective block-fading channels," *IEEE Trans. Inf. Theory*, vol. 56, no. 6, pp. 2829–2844, June 2010. 23

[54] G. Durisi, U. Schuster, H. Bolcskei, and S. Shamai, "Noncoherent capacity of underspread fading channels," *IEEE Trans. Inf. Theory*, vol. 56, no. 1, pp. 367–395, Jan. 2010. 23

[55] R. U. Nabar, H. Bolcskei, and F. W. Kneubuhler, "Fading relay channels: Performance limits and space-time signal design," *IEEE J. Sel. Areas Commun.*, vol. 22, no. 6, pp. 1099–1109, Aug. 2004. 26

[56] A. M. Sayeed and B. Aazhang, "Joint multipath-doppler diversity in mobile wireless communications," *IEEE Trans. Commun.*, vol. 47, no. 1, pp. 123–132, Jan. 1999. 27

[57] H. Mheidat and M. Uysal, "Non-coherent and mismatched-coherent receivers for distributed stbcs with amplify-and-forward relaying," *IEEE Trans. Wireless Commun.*, vol. 6, no. 11, pp. 4060–4070, Nov. 2007. 27

[58] J. K. Cavers, "An analysis of pilot symbol assisted modulation for Rayleigh fading channels [mobile radio]," *IEEE Trans. Veh. Technol.*, vol. 40, no. 4, pp. 686–693, Nov. 1991. 27, 45

[59] L. Tong, B. Sadler, and M. Dong, "Pilot-assisted wireless transmissions: general model, design criteria, and signal processing," *IEEE Signal Process. Mag.*, vol. 21, no. 6, pp. 12–25, 2004. 27

[60] A. Lozano, "Interplay of spectral efficiency, power and doppler spectrum for reference-signal-assisted wireless communication," *IEEE Trans. Wireless Commun.*, vol. 7, no. 12, pp. 5020–5029, 2008. 27, 28

[61] J. Zhang, Y. Zheng, C. Xiao, and K. Ben Letaief, "Channel equalization and symbol detection for single-carrier MIMO systems in the presence of multiple carrier frequency offsets," *IEEE Trans. Veh. Technol.*, vol. 59, no. 4, pp. 2021–2030, 2010. 27

[62] J. Hua, L. Meng, X. Xu, D. Wang, and X. You, "Novel scheme for joint estimation of SNR, doppler, and carrier frequency offset in double-selective wireless channels," *IEEE Trans. Veh. Technol.*, vol. 58, no. 3, pp. 1204–1217, 2009. 27

[63] C. Mecklenbräuker, A. Molisch, J. Karedal, F. Tufvesson, A. Paier, L. Bernadó, T. Zemen, O. Klemp, and N. Czink, "Vehicular channel characterization and its implications for wireless system design and performance," *Proc. IEEE*, no. 99, pp. 1–24, 2011. 27

[64] O. Damen, A. Chkeif, and J. Belfiore, "Lattice code decoder for space-time codes," *IEEE Commun. Lett.*, vol. 4, no. 5, pp. 161–163, May 2000. 28, 79

[65] X. Ma, G. Leus, and G. Giannakis, "Space-time-doppler block coding for correlated time-selective fading channels," *IEEE Trans. Signal Process.*, vol. 53, no. 6, pp. 2167–2181, June 2005. 28

[66] A. Abdi, C. Tepedelenlioglu, M. Kaveh, and G. Giannakis, "On the estimation of the k parameter for the rice fading distribution," *IEEE Commun. Letters*, vol. 5, no. 3, pp. 92–94, 2001. 34

[67] R. Meireles, M. Boban, P. Steenkiste, O. Tonguz, and J. Barros, "Experimental study on the impact of vehicular obstructions in vanets," in *IEEE Veh. Networking Conf. (VNC2010)*, 2010, pp. 338–345. 36, 84

[68] J. Otto, F. Bustamante, and R. Berry, "Down the block and around the corner the impact of radio propagation on inter-vehicle wireless communication," in *IEEE Int. 29th Distributed Computing Systems Conf. (ICDCS'09)*, 2009, pp. 605–614. 36, 84

[69] T. Fernández-Caramés, M. González-López, and L. Castedo, "Mobile wimax for vehicular applications: Performance evaluation and comparison against ieee 802.11 p/a," *Computer Networks*, 2011. 36, 47, 84, 96

[70] L. Cheng, B. Henty, D. Stancil, F. Bai, and P. Mudalige, "Mobile vehicle-to-vehicle narrow-band channel measurement and characterization of the 5.9 ghz dedicated short range communication (dsrc) frequency band," *IEEE J. Sel. Areas Commun.*, vol. 25, no. 8, pp. 1501–1516, 2007. 36, 84

[71] A. Paier, J. Karedal, N. Czink, C. Dumard, T. Zemen, F. Tufvesson, A. Molisch, and C. Mecklenbräuker, "Comparison of lund'07 vehicular channel measurements with the ieee 802.11 p channel model," *COST2100, Wroclaw (Poland)*, Feb. 2008. 36, 84

[72] S. M. Ross, *Introduction to probability and statistics for engineers and scientists*, 3rd ed. Elsevier Academic Press, 2004. 37, 64, 66, 90

[73] M. Ulrey, "Formulas for the distribution of sums of independent exponential random variables," *IEEE Trans. Rel.*, vol. 52, no. 2, pp. 154 –161, June 2003. 37, 64, 90

[74] H. Muhaidat and M. Uysal, "Cooperative diversity with multiple-antenna nodes in fading relay channels," *IEEE Trans. Wireless Commun.*, vol. 7, no. 8, pp. 3036–3046, Aug. 2008. 39

[75] O. Amin, B. Gedik, and M. Uysal, "Channel estimation for amplify-and-forward relaying: Cascaded against disintegrated estimators," *IET Commun.*, vol. 4, no. 10, pp. 1207–1216, Jul. 2010. 45

[76] W. Cho, S. Kim, H. kyun Choi, H. Oh, and D. Kwak, "Performance evaluation of V2V/V2I communications: the effect of midamble insertion," in *IEEE 1st Int. Conf. on Wireless Commun. Soc., Veh. technol., Inform. Theory and Aerosp. & Electron. Syst. Technol. (VITAE)*, 2009, pp. 793–797. 47, 95

[77] Y. Ma, N. Yi, and R. Tafazolli, "Bit and power loading for OFDM-based three-node relaying communications," *IEEE Trans. Signal Process.*, vol. 56, pp. 3236–3247, Jul. 2008. 57, 59, 79

[78] S. Benedetto and E. Biglieri, *Principles of digital transmission: with wireless applications*. Kluwer academic publishers, 1999. 59

[79] H. Shao and N. Beaulieu, "Block coding for impulsive Laplacian noise," in *IEEE Int. Conf. Commun. (ICC)*, 2010, pp. 1–6. 64, 89

[80] C. Liu, "The essence of the generalized Newton binomial theorem," *Commun. Nonlinear Sci. and Numerical Simulation*, vol. 15, no. 10, pp. 2766–2768, 2010. 66, 92

[81] S. S. Ikki and M. H. Ahmed, "Multi-branch decode-and-forward cooperative diversity networks performance analysis over Nakagami-m fading channels," *IET commun.*, vol. 5, no. 6, pp. 872–877, Apr. 2011. 68, 92

[82] J. Kenney, "Dedicated short-range communications (DSRC) standards in the united states," *Proc. IEEE*, vol. 99, no. 7, pp. 1162–1182, 2011. 78

[83] R. . Schwarz, *WLAN 802.11p Measurements for Vehicle to Vehicle (V2V), DSRC*, ser. Application Note, March 2009. 78

[84] J. Boyer, D. Falconer, and H. Yanikomeroglu, "Multihop diversity in wireless relaying channels," *IEEE Trans. Commun.*, vol. 52, no. 10, pp. 1820–1830, Oct. 2004. 81, 87

[85] N. Tam, T. Tran-Thien, T. Do-Hong, and V. Bao, "Performance analysis of decode-and-forward relaying for multi-hop Alamouti transmission over Rayleigh fading channels," in *IEEE Int. Conf. Adv. Technol. Commun. (ATC)*, 2010, pp. 195–200. 87

[86] B. Rankov and A. Wittneben, "Achievable rate regions for the two-way relay channel," in *IEEE Int. Symp. Inform. Theory.* IEEE, 2006, pp. 1668–1672. 103

[87] C. Hausl and J. Hagenauer, "Iterative network and channel decoding for the two-way relay channel," in *IEEE Int. Conf. Commun. (ICC)*, vol. 4, 2006, pp. 1568–1573. 103

[88] R. Wyrembelski, I. Bjelakovic, T. Oechtering, and H. Boche, "On the capacity of bidirectional broadcast channels under channel uncertainty," in *IEEE Int. Conf. Commun. (ICC)*, 2009, pp. 1–5. 103

[89] S. Cui, A. Goldsmith, and A. Bahai, "Energy-constrained modulation optimization," *IEEE Trans. Wireless Commun.*, vol. 4, no. 5, pp. 2349–2360, Sept. 2005. 103

[90] I. J. Baik and S. Y. Chung, "Network coding for two-way relay channels using lattices," in *IEEE Int. Conf. Commun. (ICC)*, 2008, pp. 3898–3902. 103

[91] W. Nam, S. Chung, and Y. Lee, "Capacity of the Gaussian two-way relay channel to within 1*over*2 bit," *IEEE Trans. Inf. Theory*, vol. 56, no. 11, pp. 5488–5494, Nov. 2010. 103

[92] Y. Jia and A. Vosoughi, "Two-way relaying for energy constrained systems: Joint transmit power optimization," in *IEEE Int. Conf. Acoust. Speech and Signal Process. (ICASSP)*, 2010, pp. 3026–3029. 103

[93] F. Li, G. Zhu, G. Su, and X. Ke, "An optimal transmission scheme for two-way relaying networks with power constraint," in *19th Ann. Wireless and Optical Commun. Conf. (WOCC)*, 2010, pp. 1–4. 103

[94] S. Shahbazpanahi and M. Dong, "Achievable rate region and sum-rate maximization for network beamforming for bi-directional relay networks," in *IEEE Int. Conf. Acoust. Speech and Signal Process. (ICASSP)*, 2010, pp. 2510–2513. 103

[95] S. M. Kay, *Fundamentals of statistical signal processing: Estimation theory.* PTR Prentice Hall, 1993. 108